ALMA MATER STUDIORUM
UNIVERSITÀ DI BOLOGNA

DIPARTIMENTO DI INGEGNERIA INDUSTRIALE

**CORSO DI LAUREA MAGISTRALE IN
INGEGNERIA ENERGETICA**

ANALYSIS OF THE START-UP PHASE OF AN INVERTER-DRIVEN DUAL-SOURCE HEAT PUMP AND DEVELOPMENT OF A SIMULATION MODEL BASED ON EXPERIMENTAL DATA

Tesi di laurea magistrale in Progettazione di Impianti a Pompa di Calore

Relatrice

Prof.ssa Claudia Naldi

Presentata da

Davide Lauria

Correlatori

Prof. Tobias Schrag

M.Eng. Tobias Reum

Sessione marzo 2026

Anno Accademico 2024/2025

Index

Abstract

Abstract in English

The present thesis analyzes the start-up phenomenon (start-up transient) of a prototype of a dual-source (air–ground) heat pump, manufactured by ratiotherm GmbH & Co. KG and installed at the Technische Hochschule Ingolstadt.
The study has a dual objective: to analyze the start-up of the prototype and to develop a simulation model capable of predicting its operation.
A total of 41 experiments were carried out: 36 using air as the source and 5 using the ground as the source. Several key parameters were selected based on the available literature, and each experiment was conducted by varying one of these parameters.
By analyzing the experimental results, it becomes evident that the Proportional–Integral–Derivative (PID) controller of the expansion valve plays a fundamental role in the start-up, causing the obtained results to deviate from the expected ones.
Three different simulation models were then developed and compared with each other. The first model is based on the penalty concept, the second was developed using polynomial equations, and the third using transfer functions.
Among the three models, the most reliable are the one based on the penalty concept and the one based on transfer functions. Between the two, the first is the simplest and therefore easily implementable, whereas the second, although more complex, generates a function that directly approximates the entire start-up transient.
In conclusion, the PID of the expansion valve plays an important role in the start-up phenomenon. In the analyzed prototype, several improvements must be made to the PID in order to reduce the start-up time of the machine and increase its performance. The start-up simulation model based on transfer functions proves to be the best, thanks to its reliability and its ability to accurately approximate the start-up transient.

Abstract in Italiano

La presente tesi analizza il fenomeno dello start-up (transitorio di avviamento) di un prototipo di una pompa di calore a doppia sorgente (aria-terreno), prodotto da ratiotherm GmbH & Co. KG e installato presso la Technische Hochschule Ingolstadt.
Lo studio ha un duplice scopo: analizzare lo start-up del prototipo, e sviluppare un modello di simulazione capace di prevederne il funzionamento.
Sono stati condotti in totale 41 esperimenti: 36 utilizzando l'aria come sorgente e 5 utilizzando il terreno come sorgente. Sono stati selezionati alcuni parametri chiave, sulla base della letteratura disponibile, ed ogni esperimento è stato condotto variando uno di questi parametri.
Analizzando i risultati degli esperimenti risulta evidente che il controllore Proporzionale–Integrale–Derivativo (PID) della valvola di espansione gioca un ruolo fondamentale nello start-up, facendo discostare i risultati ottenuti da quelli attesi.
Sono stati poi sviluppati tre differenti modelli di simulazione e confrontati fra di loro. Il primo modello si basa sul concetto di penalità, il secondo è stato sviluppato mediante equazioni polinomiali ed il terzo mediante funzioni di trasferimento.
Tra i tre modelli, i più affidabili risultano essere quello basato sul concetto di penalità e quello basato sulle funzioni di trasferimento. Fra i due, il primo risulta essere il più semplice e quindi facilmente realizzabile, mentre il secondo, pur se più complesso, genera una funzione che approssima direttamente tutto il transitorio di avviamento.
In definitiva, il PID della valvola di espansione gioca un ruolo importante nel fenomeno dello start-up. Nel prototipo analizzato, devono essere effettuate diverse migliorie sul PID per ridurre i tempi di avviamento della macchina ed aumentarne le prestazioni. Il modello di simulazione

dello start-up mediante funzioni di trasferimento risulta essere il migliore, grazie alla sua affidabilità ed alla capacità di approssimare bene il transitorio di avviamento.

List of Abbreviations

Abbreviation:	Meaning:
A	*Air*
ASHP	*Air-Source Heat Pump*
ASHX	*Air-Source Heat Exchanger*
ASO	*Air-Source Operation*
B	*Ground*
C1	*Compressor 1*
C2	*Compressor 2*
CO_2	*Carbon Dioxide*
COP	*Coefficient of Performance*
COP_{drop}	*Coefficient of Performance Drop*
COP_{ss}	*Coefficient of Performance during Steady-State*
COP_{su}	*Average Coefficient of Performance during Start-Up*
COP_{th}	*Theoretical Coefficient of Performance*
DSHP	*Dual-Source Heat Pump*
EU	*European Union*
EV1	*Valve 1*
EV2	*Valve 2*
F-Gases	*Fluorinated Greenhouse Gases*
GSHP	*Ground-Source Heat Pump*
GSHX	*Ground-Source Heat Exchanger*
GSO	*Ground-Source Operation*
GWP	*Global Warming Potential*
HFC	*Hydrofluorocarbons*
HP	*Heat Pump*
HSHX	*Heating System Heat Exchanger*
PFC	*Perfluorocarbons*
PO	*Parallel Operation*
S_{gen}	*Generation of entropy*
ssf	*Steady-State Frequency*
T_{ext}	*External Temperature*
THI	*Technische Hochschule Ingolstadt*
t_{stop}	*Shutdown Time // Stop Time*
t_{su}	*Start-Up Time*
W	*Water*

Chapter 1:
Introduction and case study description

1.1 Introduction

«The Commission has, in its communication of 11 December 2019 entitled 'The European Green Deal', set out a new growth strategy that aims to transform the Union into a fair and prosperous society, with a modern, resource-efficient and competitive economy, where there are no net emissions of greenhouse gases in 2050 and where economic growth is decoupled from resource use. The European Green Deal also aims to protect, conserve and enhance the Union's natural capital, and protect the health and well-being of citizens from environment-related risks and impacts.» [1]

In 2021, the European Union (EU) adopted its first European Climate Law, establishing legally binding targets to achieve climate neutrality by 2050. The Regulation also sets an intermediate objective of a 55% reduction in greenhouse gas emissions by 2030 compared to 1990 levels. In accordance with the provisions of the Climate Law, the European Commission further recommended, in February 2024, an additional intermediate target of a 90% reduction in emissions by 2040, thereby reinforcing the EU's trajectory towards long-term climate neutrality [2].
In 2023, total greenhouse gas emissions in the European Union (including land-use, land-use change, forestry, and indirect CO_2, and excluding international aviation and international navigation) were 37% lower than in 1990, corresponding to a reduction of 1,728 million tons of CO_2 equivalent[1]. Between 2022 and 2023, emissions decreased by 8.9%, corresponding to a reduction of 285 million tons of CO_2 equivalent.
From 1990 to 2023 there has been a marked decoupling between gross domestic product and emissions: while gross domestic product grew by 70%, greenhouse gas emissions declined by 37%. This overall trend reflects a combination of factors, including a rising share of renewable energy, the gradual substitution of coal with less carbon-intensive fossil fuels, improvements in energy efficiency, and broader structural changes in the economy.
Greenhouse gas emissions decreased in the majority of sectors between 1990 and 2023, with the notable exception of transport, refrigeration and air conditioning, where emissions increased, and forest land, where net removals decreased and the negative trend accelerated in the past few years [2].

In the case of refrigeration and air conditioning, the increase is associated with direct emissions of hydrofluorocarbons (HFCs), released from leaks of refrigerant fluids in heat pumps, air conditioners, and refrigeration equipment.
For these applications, two distinct effects should be considered:

- **Direct emissions:** caused by refrigerant leaks.
- **Indirect emissions**: resulting from the consumption of electrical energy.

The indirect emissions depend on the type of energy source used for electricity production, on the efficiency of energy production and transport, and on the efficiency of the heat pump or refrigeration system. In the Annual European Union Greenhouse Gas Inventory, only direct emissions are considered, while indirect emissions are allocated to other sectors, such as

[1] CO_2 equivalent is a measure that expresses the global warming impact of a given amount of a greenhouse gas relative to the same amount of carbon dioxide (CO_2).

emissions in the residential sector (where emissions also represented one of the largest reductions, thanks to the energy efficiency improvements from better insulation standards in buildings and a less carbon-intensive fuel mix).
The data of the Annual European Union Greenhouse Gas Inventory [3] show that, from 1990 to 2023, while indirect emissions were decreasing, direct emissions were increasing. This resulted from the introduction of the HFCs in the EU market at the end of 1990, as alternatives to ozone-depleting substances which are phased out under the Montreal Protocol[2]. Their use increased strongly over the next two decades and due to their high global warming potential[3], HFC emissions became significant with growing use.
The Fluorinated Greenhouse Gases (F-Gases), which include hydrofluorocarbons (HFCs) and perfluorocarbons (PFCs), account for about 2% of total greenhouse gas emissions in the European Union in 2023, where 90% come from refrigeration and air conditioning.
In 2023, HFCs emissions from refrigeration and air conditioning enormously increased since 1990 in the EU, but decreased by 5% compared to 2022 which is due to the measures of the EU F-gas Regulation, which introduces a stepwise phase-out of HFCs, starting in 2015 and aiming at a complete termination of use by 2050, supported by complementary measures such as bans for specific applications, recovery obligations, and personnel training requirements [3].

In order to reduce emissions from refrigeration and air conditioning, according to the plans of the European Union, it is necessary to reduce both direct and indirect emissions.
This study focuses on reducing indirect emissions by analyzing the start-up phenomenon in a dual-source heat pump and developing a simulation model based on the collected data.
The start-up is the initial operating phase of the heat pump during which the system transitions from rest to steady-state conditions and during this phase, for a certain time, there is a transient: that means that during the start-up time the normal operating conditions are altered and that leads to a decrease in the efficiency of the heat pump.
A dual-source heat pump is a heat pump able to use two different sources (air and ground in the case analyzed).

The present study is structured into four chapters:

- **Chapter 1** includes this introduction and provides a general overview of the analyzed dual-source heat pump and of the start-up phenomena.
- **Chapter 2** describes the experimental methodology and presents the experimental results and their discussion.
- **Chapter 3** focuses on the development of a simulation model based on the data collected and presented in Chapter 2. This model is able to simulate the dual-source heat pump, including the start-up phenomena. The chapter includes both the methodology adopted to build the model and the results and discussion obtained from its execution.
- **Chapter 4** summarizes the main conclusions of the study.

[2] The Montreal Protocol is an international treaty aimed at reducing the production and use of substances that deplete the ozone layer, particularly chlorofluorocarbons (CFCs).
[3] The Global Warming Potential (GWP) is a relative measure of how much heat a given mass of a greenhouse gas traps in the atmosphere, compared to the heat trapped by the same mass of CO_2 over a specific time horizon (typically 100 years). This index is therefore based on a relative scale, comparing the gas under consideration to an equal mass of CO_2, whose GWP is, by definition, equal to 1.

1.2 Dual-source heat pump description

A heat pump (HP) is a thermal machine that can absorb heat from the external ambient at a low temperature and release heat in an internal ambient at a higher temperature. This is possible by supplying work to the heat pump, in accordance with the second law of thermodynamics, which states that heat cannot flow spontaneously from a colder to a hotter reservoir. Figure 1.1 shows a functional scheme of a generic heat pump:

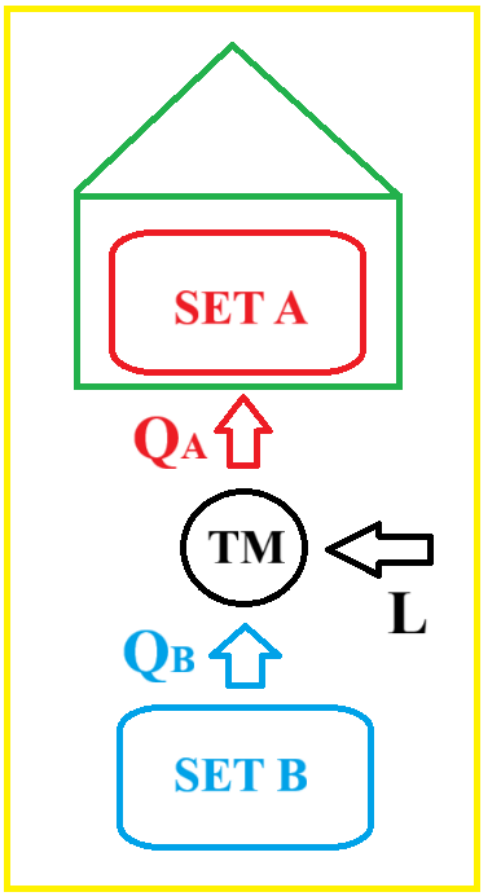

Figure 1.1 - Functional scheme of a generic heat pump

SET A is the higher temperature source and SET B is the lower temperature source. The thermal machine TM extracts energy Q_B from SET B and sends energy Q_A to SET A. This process required energy L because of the inversion of natural heat flow. When the HP operates in heating mode, SET A is the internal sink while SET B is the external sink.
The coefficient of performance COP[4] of the HP could be obtained as follows:

$$COP = \frac{Q_A}{L} \tag{1}$$

A heat pump can use different types of energy sources. As an external cold source, air (A), water (W), or ground (B) can be used, while as an internal hot source, either air or water can be used. The source temperatures play an important role in the COP.
Doing an energy balance on the system reported in Figure 1.1, it is possible to obtain:

$$L = Q_A - Q_B$$

[4] The COP defined as the ratio of energies is a performance factor related to an extended period of operation. The COP can also be defined as the ratio of powers when referring to instantaneous performance.

$$COP = \frac{Q_A}{Q_A - Q_B}$$

According to the second law of thermodynamics:

$$S_{gen} = \frac{Q_A}{T_A} - \frac{Q_B}{T_B} \geq 0$$

where S_{gen} is the generation of entropy, T_A the temperature of SET A and T_B the temperature of SET B. Assuming the thermal machine is reversible, it is possible to obtain:

$$S_{gen} = \frac{Q_A}{T_A} - \frac{Q_B}{T_B} = 0$$

$$\frac{Q_B}{Q_A} = \frac{T_B}{T_A}$$

$$COP_{th} = \frac{T_A}{T_A - T_B} \quad (2)$$

where the (2) is the theoretical COP, or COP of Carnot. The (2) could also be written as:

$$COP_{th} = \frac{1}{1 - \frac{T_B}{T_A}} \quad (3)$$

From the (3) it is possible to observe that if the external temperature T_B increases then the COP_{th} increases, while if the internal temperature T_A increases then the COP_{th} decreases:

$$T_B \uparrow\downarrow \; COP_{th} \uparrow\downarrow$$
$$T_A \uparrow\downarrow \; COP_{th} \downarrow\uparrow$$

For this reason, for a HP in heating mode it is important that the external temperature is not too low and that the internal temperature is not too high. [4]

A HP is made up of an evaporator, a compressor, a condenser and an expansion valve, as shown in Figure 1.2:

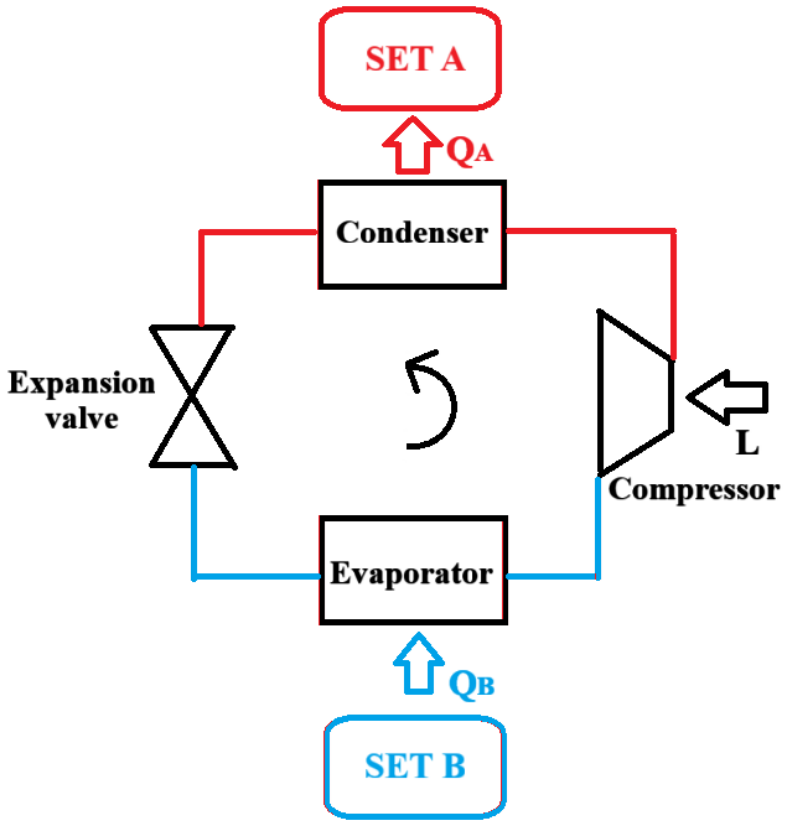

Figure 1.2 – Scheme of a HP with its components

A HP operates through a closed cycle using a refrigerant that continuously changes its phase to transfer heat from a cold to a warm source. The refrigerant absorbs heat and evaporates in the evaporator, is then compressed to raise its pressure and temperature, releases heat and condenses in the condenser and is finally expanded to restart the cycle. With this process, a small input of work moves a larger amount of heat. In Figure 1.2, the blue lines represent the low-pressure/temperature sections of the circuit while the red lines indicate the high-pressure/temperature sections. [5]
A heat pump with air as the external source is called an air-source heat pump (ASHP), while a heat pump with the ground as the external source is called a ground-source heat pump (GSHP). The advantages of the ASHP are the low cost of investment and the high air availability; the disadvantage is that the external temperature is not constant, and if T_B decreases then also the COP decreases.
The advantage of the GSHP is that the temperature in the ground is almost constant during the year and this means that the COP of a GSHP is more predictable than the one of the ASHP and it does not change when the temperature of the external air decreases; the disadvantage is that the GSHPs costs more than the ASHPs because it is necessary to drill the ground to install the heat exchanger.
To combine the advantages of both ASHP and GSHP, a dual-source heat pump (DSHP) has been investigated at the Technische Hochschule Ingolstadt – THI by Reum et al. [6]. The cycle scheme is presented in Figure 1.3:

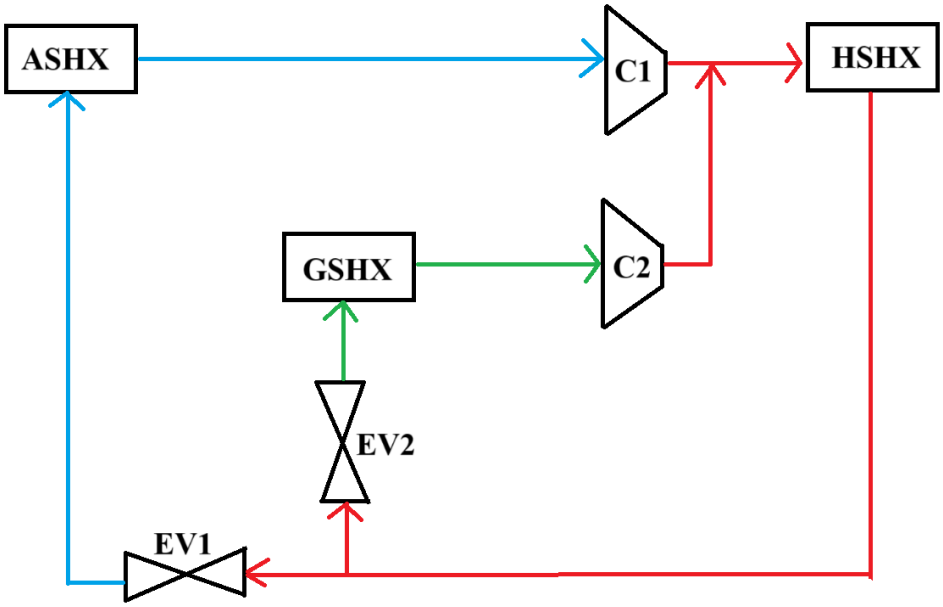

Figure 1.3 - Scheme of the DSHP and its components

The differences between a classic HP and this DSHP are that in this one there are two compressors, two expansion valves and two evaporators, instead of one. In Figure 1.3 the two compressors are called C1 and C2, the two valves EV1 and EV2, the two evaporators ASHX (air-source heat exchanger) and GSHX (ground-source heat exchanger), and the condenser is called HSHX (heating system heat exchanger). The low-pressure part of the circuit is in blue, the medium-pressure part is in green and the high-pressure part is in red. The medium-pressure part corresponds to the ground-source, which is at a higher temperature level than the air-source (when ambient temperature is very low), so the evaporation pressure is also higher.
This DSHP can use air, ground, or both sources in parallel operation (PO); in PO mode both compressors are active. The technical details of the DSHP and of its components are reported in Section 1.3.

The DSHP investigated at THI, although based on pre-developed and non-optimized components, demonstrated promising performance. In air-source operation it outperformed comparable market systems, mainly due to the large ASHX, while ground-source operation showed lower efficiency than similar single-source units. Parallel operation with two compressors proved stable, with COP values lying between air-source and ground-source operation [7].
Prototype testing demonstrated the reliable performance of the DSHP and showed that smaller ASHX and GSHX sizes are feasible. DSHPs combine the advantages of air and ground systems while mitigating their respective limitations, requiring less demanding geological conditions than conventional GSHX systems and achieving higher efficiencies than standard air systems. Parallel operation of both heat sources improves efficiency compared to air operation and allows peak heating loads to be covered without relying on electric heaters, reducing operating costs. Although efficiency and heating power are slightly lower than in ground operation, the thermal load on ASHX and GSHX is significantly reduced, enabling a smaller GSHX (up to 50% smaller) without sacrificing overall performance and the reduction of ASHX load allows lower fan speeds, which decreases noise emissions. Combining both sources also increases flexibility, improves equipment longevity, reduces defrost cycles and allows better heat source management [8].
An analysis of the seasonal and annual energy performance of an innovative DSHP able to use both ground and outdoor air as external heat sources was conducted at the University of Bologna by Grossi et al. [9]. They demonstrated that a DSHP allows for reducing the ground temperature drift, especially in the presence of buildings with unbalanced loads, and to stabilize the HP performance over the years. Determining the right switching temperature to switch from air-source to ground-source (and vice versa) is possible to maximize the annual energy performance and preserve the ground-source functionality during the whole operative life of the thermal plant.
A research by Natale et al. [10] reports that, in order to recharge the ground, it can be convenient for a DSHP providing only space heating and cooling to operate only in ground-source mode during summer, if coupled to a building with strongly unbalanced heat loads (higher winter loads).
A GSHX undersized also of 70% can be used in a DSHP to supply the thermal demand of a building also in the most severe part of the season, thanks to the possibility to switch to an air-source, and its efficiency can be kept high recharging the ground during the air-source mode [11].
An undersized GSHX also allows for limiting the ground temperature drift over time, and for this reason the recharging process is easier and faster than a well or oversized GSHX [12].

1.3 Technical details of the DSHP

The DSHP investigated in this research is located at Technische Hochschule Ingolstadt – THI and it was manufactured by the industry partner ratiotherm GmbH & Co. KG. The DSHP is a prototype based on pre-developed components and therefore not optimized. The DSHP operates with a dual-compressor refrigerant cycle, where both compressors are rolling-piston technology. The HP can operate with only one of the two compressors active in single-source operations or with both compressors active in dual-source operations. In the case of single-source operations it can work only with the ASHX, for air-source operation (ASO), or only with the GSHX, for ground-source operation (GSO). In the case of dual-source operation, it can work with both ASHX and GSHX in PO. C1 and V1 are used for ASO, C2 and V2 are used for GSO, and for PO, both C1 and C2, as well as both EV1 and EV2, are used.

The compressors are inverter-driven, allowing variable-speed operations, but there is no automatic control of the frequency; this means that during the tests the frequency was changed manually. Additionally, the control of the defrosting is not included.
The refrigerant is R454B, a blend of 68.9% of R32[5] and 31.1% of R1234yf[6], with a global warming potential (GWP) of 466 and with an A2L[7] safety classification. Although most of the components were designed for R410A or R32, R454B is close thermodynamically to these two refrigerants [7].

The main components of the DSHP are listed in Table 1.1:

Table 1.1 – Main components of the DSHP

Component abbreviation	Used component	Details
C1	GMCCKTN150D42UFZ	Displacement: 14.9 cm³
C2	GMCC KTN110D42UFZ	Displacement: 11.1 cm³
EV1	DunAn DPF B1.65C-101	Max orifice: 1.65 mm
EV2	DunAn DPF B1.3C-103	Max orifice: 1.3 mm
GSHX	Danfoss D62-E-36	No. of plates: 36
HSHX	Swep B25–30	No. of plates: 30
Inverters	Bonfiglioli ACS402–19 2 FA	Max capacity: 5.5 kW

1.4 Start-up

The start-up is the initial operating phase of the heat pump during which the system transitions from rest to steady-state conditions. During the start-up of a HP, for a certain time, there is a transient. That means that during the start-up time t_{su} the normal operating conditions are altered. The transient operation of a HP affects the response of the sensible and the latent capacities, the efficiency and the seasonal efficiency. Major influences on the transient losses are the refrigerant dynamics, the thermal mass of the heat exchangers and the expansion device. It has been proven, in a study conducted by S. Katipamula [13], that the transient performance during the start-up of a HP A/A (air to air) operating in cooling depends on:

1. indoor dry-bulb temperature
2. outdoor dry-bulb temperature
3. indoor relative humidity
4. cycling rate
5. percent ON-time

The results obtained by this research are:

- The duration of the thermal transient is longer than the duration of the electrical transient.
- The t_{su} decreases if the indoor dry-bulb temperature increases.
- The t_{su} remains almost constant when the outdoor dry-bulb temperature changes.

[5] Belonging to the family of hydrofluorocarbons (HFCs).
[6] Belonging to the family of hydrofluoroolefins (HFOs), these refrigerants represent a new generation characterized by a low GWP, due to their short atmospheric lifetime.
[7] A2L refrigerants are characterized by low toxicity and mild flammability.

Figure 1.4 summarizes the main result obtained by Katipamula, showing that the start-up time of a refrigeration system decreases with increasing internal temperature, and that the electrical start-up time is consistently shorter than the cooling capacity start-up time.

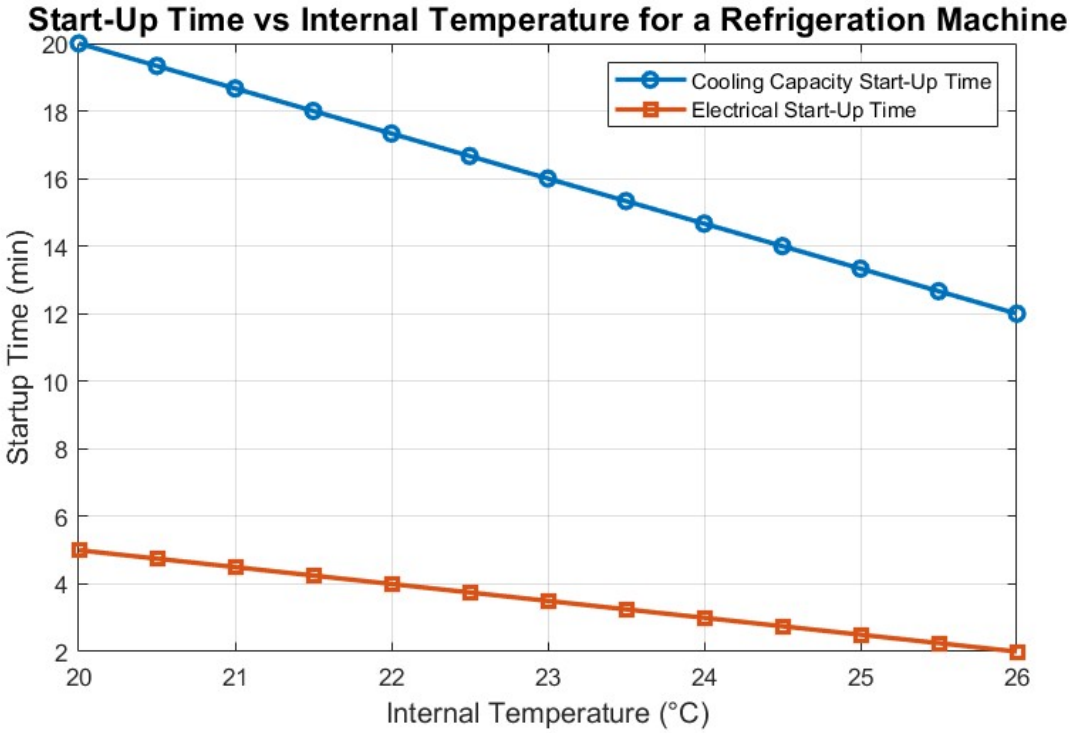

Figure 1.4 - Schematic trend of electrical and cooling start-up times vs. indoor temperature

Murphy and Goldschmidt (1984) reported that the migration of refrigerant from the condenser to the evaporator caused noticeable power differences and capacity losses immediately after start-up, and some of these occurred due to a direct exchange of heat between the condenser and the evaporator. Tanaka, et al. (1982) and Mulroy and Didion (1985), investigated the distribution of refrigerant and variation of temperature and pressure for steady- state and start-up conditions. The test results in the cooling mode indicated that, at start-up, more than half of the refrigerant was in the evaporator and almost all of it was liquid. The study showed that it takes almost 10 minutes to achieve steady-state. The large amount of time to reach steady-state was due to unequal refrigerant distribution in the heat pump coupled with larger heat inertia (due to the mass of the heat exchanger coils). In conclusion, the efficiency of an air-source heat pump was reduced in transient mode.

The result obtained that the t_{su} decreases if the indoor dry-bulb temperature increases probably depends on the migration of refrigerant from the condenser to the evaporator. In cooling mode, the evaporator is located indoors, and its performance during start-up is influenced by the indoor dry-bulb temperature. When the indoor temperature increases, the pressure gradient between the condenser and the evaporator becomes lower, resulting in lower refrigerant migration from the condenser to the evaporator when the cooling machine is off. Furthermore, the higher indoor temperature allows the refrigerant to evaporate more quickly. As a result, the start-up time decreases with higher indoor temperatures, even though the total cooling load may be greater. For this reason it is expected that, in heating mode, the start-up time decreases as the outdoor temperature increases, because in heating mode the evaporator is outside.

This was demonstrated in a study conducted by Zhaowei Xu et al. [14], in which the start-up of a heat pump in heating mode was tested under varying outdoor temperatures. The results showed that an increase in outdoor temperature led to a reduction in start-up time. Furthermore,

it was demonstrated that start-up losses decrease as ambient temperature rises. This occurs because part of the power consumption during start-up is required to establish the refrigerant pressure difference between the condenser and the evaporator. When the external temperature decreases, while the internal temperature is kept constant, the resulting increase in pressure difference leads to higher power consumption during the start-up process.
The research by Uhlmann and Bertsch [15] suggests a clear correlation between the off-time duration of a heat pump and the COP observed during start-up. This happens because, when the heat pump is off, the refrigerant slowly moves from the condenser to the evaporator to equalize pressure levels. The longer the heat pump remains off, the more refrigerant accumulates in the evaporator, cools down and becomes (partly) liquid. As a result, upon start-up, the system requires more time and energy to recompress and reheat the refrigerant, which delays the return to optimal operating conditions and reduces the initial COP. The study links this behavior to the concept of duty cycle, defined as the ratio between the active time of the heat pump and the total cycle time, expressed as a percentage. In the case of an air-source heat pump, the research shows that short run times (low duty cycles) lead to performance losses of about 2–5%. These losses are due to heat dissipation during off-time and the energy required to re-establish pressure and temperature conditions. However, when the run time exceeds 10–15 minutes, the performance degradation becomes minimal.
For geothermal heat pumps, the behavior is notably different. The study demonstrates that lower duty cycles can improve COP. This improvement is not directly related to the start-up phase, which remains penalising for the refrigeration cycle; however, during the off-time, the borehole thermally regenerates, allowing the system to restart with a higher source temperature. This leads to efficiency gains of up to 5% in dry boreholes, and potentially more in wet boreholes due to faster thermal recovery.
Roccatello et al. [16] studied the drop of the COP and the t_{su} during the transient; the COP drop is defined as follows:

$$COP_{drop} = \frac{COP_{su} - COP_{ss}}{COP_{ss}} \qquad (4)$$

where COP_{su} is the average COP during the start-up and the COP_{ss} is the COP in the steady-state. They studied the COP_{drop} and the t_{su} as functions of the steady-state frequency (ssf) and of the difference between the temperature of the water at the setpoint and the temperature of the water at time 0 in the sink system $\Delta T_{sink} = T_{w,setpoint} - T_{w,0}$. The influence of the initial temperature $T_{w,0}$ is limited, as shown by experimental data results, but it is used to calculate the ΔT_{sink}. Experimental data show that the HP under some conditions can take up to 20 min before it comes up to capacity, and during this time the COP degrades to about 15% from the nominal COP. Furthermore, the t_{su} increases with the rise of the ssf at frequencies below 30 Hz, while it decreases with the increase of the ssf at frequencies above 30 Hz. Finally, the COP_{drop} is more affected by ΔT_{sink} for low frequencies than for high frequencies.
Dongellini and Morini [17] calculated the seasonal efficiency of a heating system for three reversible air-to-water heat pumps having equivalent thermal performance at full load but different power modulation capacity: a single-stage heat pump, a multi-stage heat pump and an inverter-driven heat pump. The results highlight that, considering the single-stage heat pump as a reference case, the seasonal coefficient of performance SCOP can be increased by about 4.7% and 18.3% respectively from the multi-stage and the inverter-driven heat pump, and the annual number of cycles can be decreased respectively by about 2.2% and 66.9%. That means that the modulating units are less influenced by the cycling penalization than the single-stage units, as expected, because of the fewer on-off cycles.

As seen by start-up literature, it is expected that COP_{su} and t_{su} for an inverter-driven heat pump (in heating mode) are functions of:

$$COP_{su} = f\left(T_{ext,}ssf, t_{stop}, \Delta T_{sink}\right) \quad (5)$$

$$t_{su} = f\left(T_{ext}, ssf, t_{stop}, \Delta T_{sink}\right) \quad (6)$$

where $T_{ext,}$ is the external temperature, ssf is the frequency of the inverter at the steady-state, t_{stop} is the duration time of the shutdown of the HP and ΔT_{sink} is the difference between the temperature of the water at the setpoint and the temperature of the water at time 0 in the sink system.

Chapter 2:
Development and description of the start-up experiments

2.1 Experimental methodology

This section presents the experimental methodology adopted in this study. It provides a description of the experimental setup, including the main components of the system and the measurement instrumentation. The test procedures followed for both the ASO and GSO experiments are then described, highlighting the operating conditions and control variables considered in each case. Finally, the section introduces the data processing procedure adopted for the analysis of the experimental datasets.

2.1.1 Experimental setup

The experimental setup consisted of a hydraulic test bench and a climate chamber to generate suitable ambient conditions.
The hydraulic part of the test bench consists of a heat source and a heat sink. The heat source circuit is fed by a 28 kW electric heater with a 2000 l water storage tank. The circuit can control the feed temperature and the volume flow into the test device. A substance separation with a heat exchanger allows brine to be used as the flow medium to the test devices, thus allowing temperatures below 0°C without freezing. The test rig is capable of setting flow rates up to 1500 l/h, although the actual achievable values depend on the brine viscosity, operating temperature, and the hydraulic resistance of the connected test devices. The heat sink circuit is designed in a similar way, enabling control of both the return temperature to the test device and the corresponding volume flow. This side is powered by a 75 kW chiller in combination with two water storage tanks of 1000 l each. Since the sink generally operates at higher temperatures than typical ambient conditions, water is used as the heat transfer medium. As with the source circuit, flow rates up to 2000 l/h can be established, although the actual limit depends on the hydraulic resistance of the device under test. A dedicated control system manages both the hydraulic loops and the test units. Supply and return temperature sensors, together with a volumetric flow meter, allow accurate determination of the heat flows during operation.
The climate chamber housed the outdoor unit of the DSHP, including the ASHX with its electronic expansion valve (EV1). Measuring 2280 × 2330 × 3680 mm, it was supplied by an air conditioning unit capable of setting inlet air temperatures between −5 °C and 30 °C and airflow rates from 1000 to 4000 m^3/h. Air was evenly distributed by four dispensers, while an outlet fan ensured pressure balance through a flow-through design. Since the ASHX extracts heat from the chamber, the setpoints of the air conditioning system had to be adjusted to maintain stable conditions [7].
Operations were managed by a LabVIEW-based control system connected to data loggers, which handled data acquisition and PID regulation of pumps and valves for temperature and flow control. Specifically, the volume flow is controlled by a PID loop adjusting the flow control valve, while the return temperature is regulated by a PID-controlled mixing valve comparing the measured return temperature to the setpoint [7].
All measurement data are continuously recorded by the LabVIEW program and the DSHP monitoring system, allowing for subsequent processing and analysis using MATLAB [6].

A simplified scheme of the experimental setup is reported in Figure 2.1:

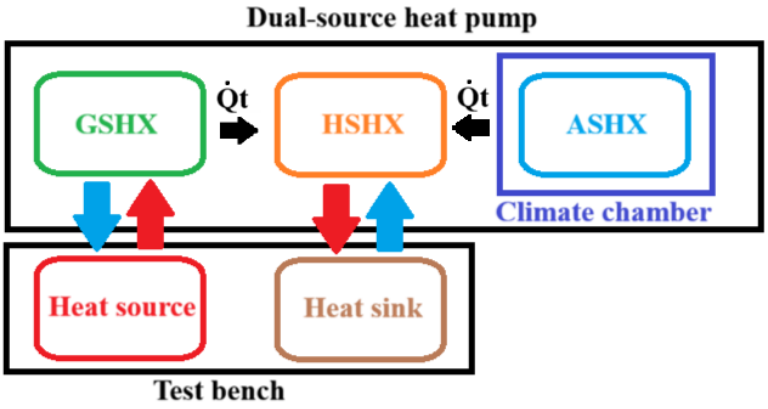

Figure 2.1 – Scheme of the experimental setup

In Figure 2.1, the dual-source heat pump and the test bench are highlighted in black. The test bench consists of the heat source (red) and the heat sink (brown). The climate chamber is shown in blue. Red arrows indicate the flow of hot water/brine, while light blue arrows represent the cold return flow.
The GSHX extracts energy (Qt) from the hot brine heated by the heat source using electrical energy, and after which the cooled brine returns to the heat source to be reheated by an electric resistance heater. The heat source can therefore simulate ground conditions, with the extracted energy being transferred to the HSHX. In parallel, the ASHX extracts heat from the air (Qt) and also delivers it to the HSHX.
Within the HSHX, water is heated and subsequently sent to the heat sink, which simulates space heating or domestic hot water demand by cooling the water before it returns to the HSHX to be reheated.

2.1.2 Test procedure

This section describes the test procedure based on the literature reviewed in Section 1.4. As observed, the start-up of an inverter-driven heat pump (in heating mode) depends on $T_{ext,}$ ssf, t_{stop} and ΔT_{sink}.
This research focuses on an inverter-driven dual-source heat pump (in heating mode) on air-source operation and ground-source operation.

2.1.2.1 ASO test procedure

For air-source operation (ASO), it is expected that ΔT_{sink} varies with t_{stop} and with ssf, but its influence is not particularly relevant, especially at high ssf, as reported by Roccatello et al. For this reason, the main tests focused only on $T_{ext,}$ ssf and t_{stop}.
The approach is to select three values for each of $T_{ext,}$ ssf and t_{stop}, leading to 27 start-ups of the DSHP and subsequent data analysis. The three values are reported in Table 2.1:

Table 2.1 – Values assumed by the control variables for ASO

Control variables	Value 1	Value 2	Value 3
$T_{ext,}$	20 °C	7 °C	2 °C
ssf	25%	50%	75%
t_{stop}	60 min	10 min	2 min

A large range of $T_{ext,}$ is chosen to get a better view of the phenomenon. In addition, 20 °C is the room temperature, which makes the experiment easier because it was not necessary to

refrigerate the climate chamber, while 7 °C and 2 °C are two temperatures previously studied for this DSHP in steady-state conditions. Negative temperatures are not considered because defrosting is not optimized for this DSHP.
Regarding the ssf, the three chosen values have already been studied for this DSHP during start-up and are therefore predictable.
Concerning t_{stop}, 60 minutes is a reasonable duration to expect that most of the refrigerant has moved from the condenser to the evaporator generating a loss of efficiency, while 10 and 2 minutes are included to study what happens with more frequent start-ups: 10 minutes represents cycling operation, 2 minutes represent losses e.g. during defrosting cycles.
By combining these three control variables, 27 combinations can be obtained, which provide a good approximation of what happens to important parameters for different external temperatures, different start-up frequencies, and different shutdown durations. Some of the important parameters are the COP during the start-up, the duration time of the start-up t_{su}, and the average thermal and electrical powers during start-up. In Table 2.2 are reported all the 27 combinations of the 3 variables.

Table 2.2 – Main experiments with all 27 combinations of the 3 control variables for ASO

TEST N°	ssf [%]	$T_{ext,}$ [°C]	t_{stop} [min]	Volume flow heat sink [l/h]	$T_{out,sink}$ [°C]
TEST 1	25%	20	60	950	30
TEST 2	25%	20	10	950	30
TEST 3	25%	20	2	950	30
TEST 4	50%	20	60	950	30
TEST 5	50%	20	10	950	30
TEST 6	50%	20	2	950	30
TEST 7	75%	20	60	950	30
TEST 8	75%	20	10	950	30
TEST 9	75%	20	2	950	30
TEST 10	25%	7	60	950	30
TEST 11	25%	7	10	950	30
TEST 12	25%	7	2	950	30
TEST 13	50%	7	60	950	30
TEST 14	50%	7	10	950	30
TEST 15	50%	7	2	950	30
TEST 16	75%	7	60	950	30
TEST 17	75%	7	10	950	30
TEST 18	75%	7	2	950	30
TEST 19	25%	2	60	950	30
TEST 20	25%	2	10	950	30
TEST 21	25%	2	2	950	30
TEST 22	50%	2	60	950	30
TEST 23	50%	2	10	950	30
TEST 24	50%	2	2	950	30
TEST 25	75%	2	60	950	30
TEST 26	75%	2	10	950	30
TEST 27	75%	2	2	950	30

Before each test, the heat pump is turned on and allowed to operate for 1 h. This operating period ensures a standard starting condition. After this time, the heat pump is switched off for the duration of the shutdown prescribed by the experiment. Once the heat pump is turned on again, it is allowed to run for 1 h to give enough time for the start-up to complete and for fluctuations to stabilize. In this way, it is also possible to perform a new test immediately after the previous one (since the system returns to the standard condition) by turning the heat pump off again and letting it rest for the shutdown duration required for the subsequent test.
The volume flow of the heat sink is kept constant at $950\frac{l}{h}$ and the inlet water's temperature inside the HSHX is kept constant at 30°C; for this reason, the temperature difference ΔT between the water inlet and outlet of the HP is not constant across all experiments.

In addition to these 27 experiments, another 9 experiments were conducted to investigate the effects of longer t_{stop} and higher ΔT_{sink}. Table 2.3 reports the additional 5 experiments for longer t_{stop}, while Table 2.4 reports the additional 4 experiments for higher ΔT_{sink}. The higher ΔT_{sink} was obtained by varying $T_{w,0}$ and $T_{out,sink}$, which are respectively the temperature of the water at time 0 in the sink system and the inlet water temperature in the HSHX. It is important to remember that $\Delta T_{sink} = T_{w,setpoint} - T_{w,0}$, where $T_{w,setpoint}$ can be obtained by experimental data and corresponds to the outlet water temperature of the HSHX, which is always higher than $T_{out,sink}$.

Table 2.3 - Additional 5 experiments for longer t_{stop} for ASO

TEST N°	ssf [%]	T_{ext}, [°C]	t_{stop} [min]	Volume flow heat sink [l/h]	$T_{out,sink}$ [°C]
TEST 28	50%	20	180	950	30
TEST 29	25%	20	3600	950	30
TEST 30	50%	20	3600	950	30
TEST 31	50%	20	3600	950	30
TEST 32	75%	20	3600	950	30

Table 2.4 – Additional 4 experiments for higher ΔT_{sink} for ASO

TEST N°	ssf [%]	T_{ext}, [°C]	t_{stop} [min]	Volume flow heat sink [l/h]	$T_{out,sink}$ [°C]	$T_{w,0}$ [°C]
TEST 33	50%	7	60	950	30	20
TEST 34	50%	7	60	950	50	20
TEST 35	50%	20	60	950	50	20
TEST 36	50%	20	60	950	30	20

2.1.2.2 GSO test procedure

For ground-source operation (GSO), as reported by Uhlmann and Bertsch [15], the efficiency of a ground-source heat pump is expected to increase with increasing t_{stop}, since a longer stop time allows the ground to thermally recharge. However, this effect cannot be measured in the present DSHP, because the ground-source is simulated by the test bench rather than a real borehole. In these experimental series, the ground temperature is considered almost constant throughout the year, and therefore it is not considered as a variable. Dynamic simulations would be necessary to capture these effects, not conducted in this study.

For this reason, in GSO the stop time t_{stop} is fixed at 10 minutes and the ground temperature is fixed at 5 °C, and only two parameters are analyzed: ssf and ΔT_{sink}. Five tests are carried out, as reported in Table 2.5:

Table 2.5 – Five experiments carried out for GSO

TEST N°	ssf [%]	$T_{ext,}$ [°C]	t_{stop} [min]	Volume flow heat sink [l/h]	$T_{out,sink}$ [°C]	$T_{w,0}$ [°C]
TEST 37	50%	5	10	950	30	28
TEST 38	25%	5	10	950	30	28
TEST 39	75%	5	10	950	30	28
TEST 40	50%	5	10	950	30	18
TEST 41	50%	5	10	950	50	18

2.1.3 Data analysis

During the experiments, data loggers recorded all measurements every 10 seconds. The data are in .txt and .csv formats, but a MATLAB script provided by THI allows converting them into a timetable in MATLAB. The timetable contains many parameters, such as heating power, electrical power, COP, and others.
In order to extract and analyze these data, it is necessary to develop a MATLAB script which allows the extraction from the timetable of the heating power, the electrical power and the COP, calculating the start-up time for each of them as well as the average value during this time.
Developing the script can be challenging due to the possible fluctuations of the expansion valve during ASO. As described by Reum et al. [6], during air-source operation measurements, significant fluctuations in both the COP and the heating power were observed. These fluctuations were caused by variations in the evaporation pressure, which in turn resulted from fluctuating superheating temperatures due to unstable expansion valve opening. The expansion valve was not properly controlled; the most likely cause is inappropriate PID parameters within the DSHP software. As a consequence of the fluctuating expansion valve [7], the superheating temperature at the compressor inlet did not consistently reach the desired values.
Obviously, these fluctuations make the development of the MATLAB code more difficult. Under normal conditions, the thermal and electrical power are expected to increase logarithmically until the steady-state value is reached. However, due to the fluctuations of the expansion valve, which lead to variations in both the COP and the thermal power, developing a code capable of correctly identifying the start-up time despite these fluctuations can be challenging.
The most appropriate approach is therefore to first collect all the experimental data and only then attempt to develop a code that performs well across the entire dataset. This will be discussed in Section 2.2.1, where different codes capable of determining the start-up time will be implemented and compared.

2.2 Experimental results and discussion

The results of the experiments are presented and discussed in this section. Three MATLAB codes for the analysis of the thermal start-up (Code A, B, and C) are introduced and tested on all experiments carried out in the ASO case. Afterwards, the three codes are compared, and the most suitable one is selected to obtain the results, which are then analyzed and discussed.

2.2.1 Start-up time evaluation code

The following describes the procedures used to determine the start-up times of the electrical power and the thermal power, respectively.

The **electrical power**, in all experiments, shows a behavior similar to a logarithmic function, as shown in Figure 2.2.

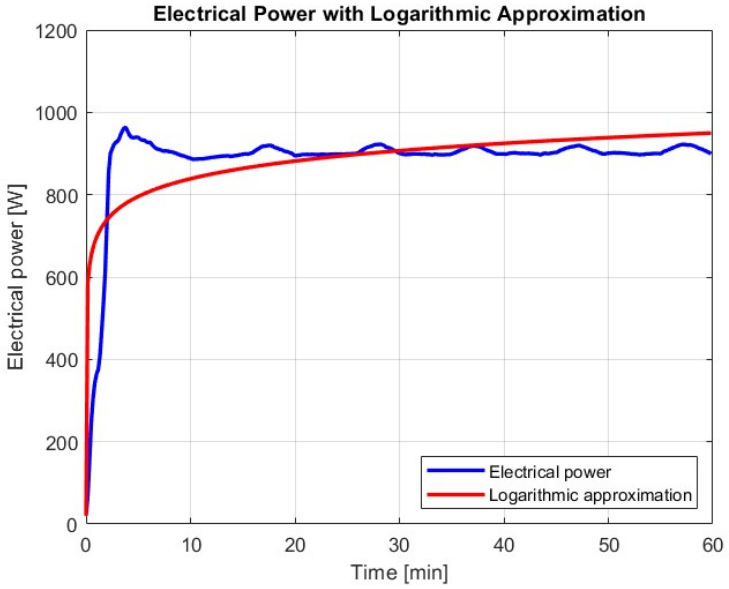

Figure 2.2 – Electrical power as a function of time (Test 15)

To determine the electrical start-up time, it is first necessary to reduce the noise in the data, which can be done using a moving average. At this point, the steady-state electrical power can be defined as the average value of the smoothed electrical power over the last 10 minutes, where the system is considered to have reached steady-state.
Knowing the steady-state power, it is possible to identify the point at which the start-up ends, defined as the point where the electrical power reaches at least 95% of its steady-state value.
The moving average is calculated over 5 minutes, as this is the minimum duration that sufficiently smooths the functions in all cases, preventing evaluation errors. Larger values were not considered, as they would excessively slow down the function approaching the asymptote.
In Figure 2.3, the electrical power is shown in blue and the smoothed electrical power in red; the orange rectangle indicates the region where the steady-state is defined, while the green dashed line shows where the code identifies the end of the start-up.

The **thermal power**, unlike the electrical power, can assume different forms, as shown in Figure 2.4. This is caused by the expansion valve: when the expansion valve opens slowly, the thermal power start-up is longer and the function resembles a logarithmic trend (a), while when the expansion valve opens quickly, the thermal power function assumes a sinusoidal form (b) or an irregular oscillatory form (c). The irregular oscillatory form depends on the expansion valve acting in an anomalous way.
Determining the thermal start-up can be a big challenge because of the different possible functions. It is necessary that the MATLAB code recognize which case it is and then use a different approach depending on the case it is in. In order to do that, different codes are developed and compared, and they are discussed below.

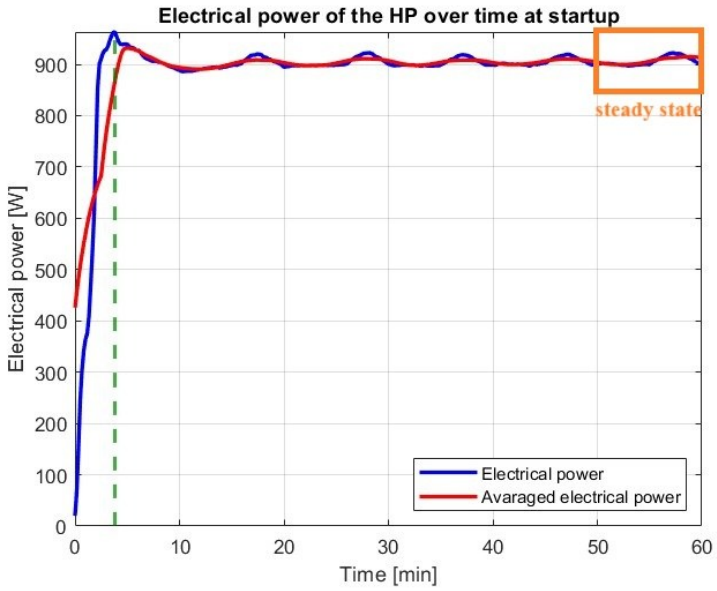

Figure 2.3 – Determination of the electrical start-up time (Test 15)

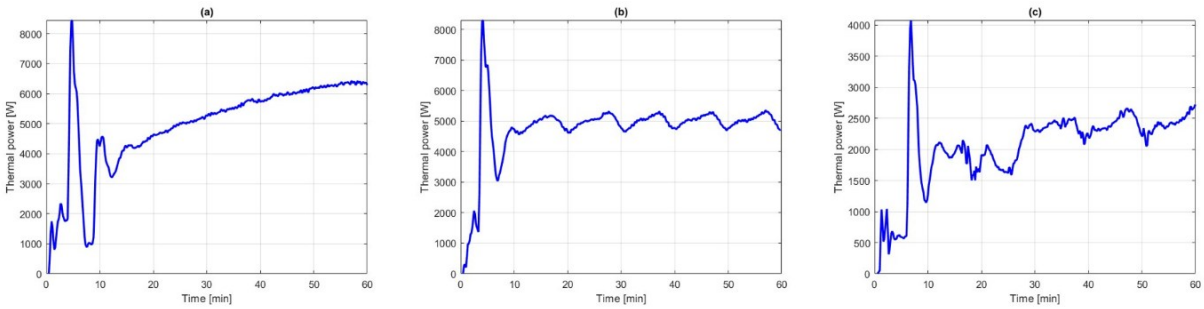

Figure 2.4 -Thermal power as a function of time for:
(a) logarithmic form - Test 28, (b) sinusoidal form - Test 15, (c) irregular oscillatory form - Test 10

2.2.1.1 Code A

To determine whether the function is logarithmic or oscillatory, the code calculates the maximum peak, the minimum peak, and the average thermal power, all over the last 10 minutes, where the thermal power is considered at steady-state. The peak that is farthest from the average thermal power over the last 10 minutes is then used to calculate the percent deviation from the mean of these last 10 minutes. For logarithmic forms, the percent deviation is less than 5%, while for oscillatory functions, where the oscillations are larger, the percent deviation exceeds 5%. An example of the application of this methodology is shown in Figure 2.5.
If the thermal power follows a logarithmic trend, the procedure is the same as for the electrical power. It is first necessary to reduce the noise in the data, which can be done using a moving average. At this point, the steady-state thermal power can be defined as the average value of the smoothed thermal power over the last 10 minutes, where the system is considered to have reached steady-state. Knowing the steady-state power, it is then possible to identify the point at which the thermal start-up ends, defined as the point where the thermal power reaches at least 95% of its steady-state value. The moving average is calculated over 5 minutes, in accordance with the value chosen for the electrical power, to ensure consistency between the two analyses. Larger values were not considered, as they would excessively flatten the function.

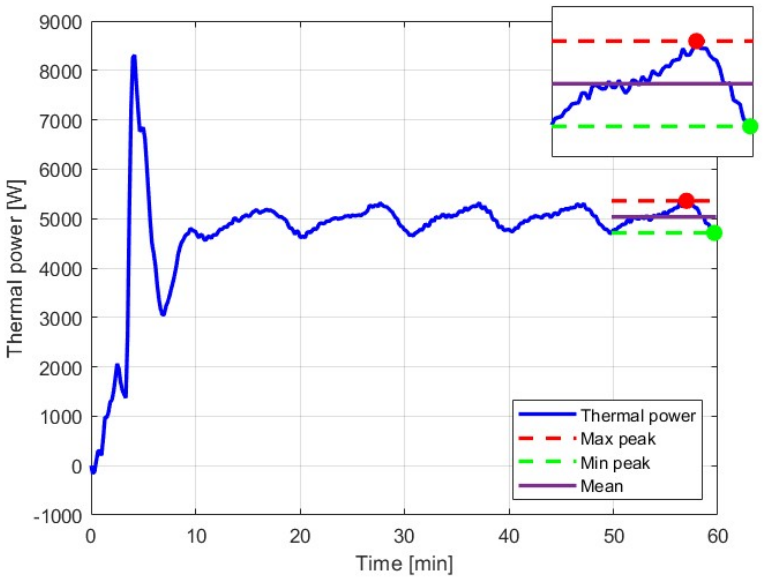

Figure 2.5 - Determination of the thermal power function shape (Test 15)

In Figure 2.6, the thermal power is shown in blue and the smoothed thermal power in red; the orange rectangle indicates the region where the steady-state is defined, while the green dashed line shows where the code identifies the end of the thermal start-up.

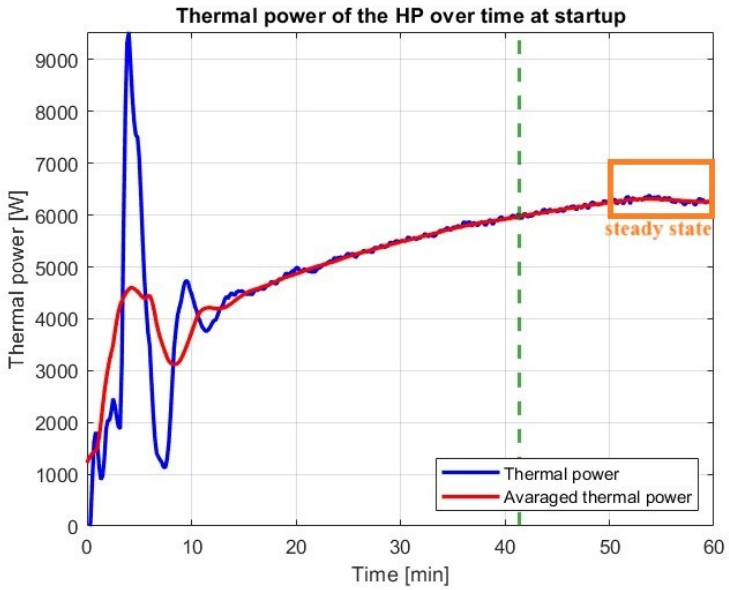

Figure 2.6 - Determination of the thermal start-up time for a logarithmic form (Test 4)

If the thermal power follows an oscillatory trend, a moving average of 2 minutes is applied to reduce the oscillations. After that, a backward loop is initialized to find the first value that is outside the range defined by the maximum and minimum peaks of the last 10 minutes; an example is shown in Figure 2.7.

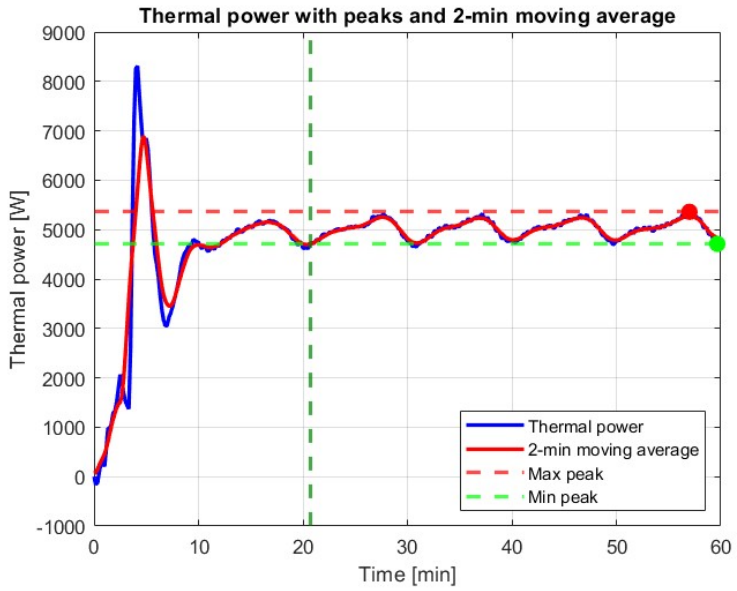

Figure 2.7 - Determination of the thermal start-up time for an oscillatory form using Code A (Test 15)

Figure 2.8 provides a schematic overview of the logic implemented in Code A for extracting the thermal start-up time from the experimental datasets.

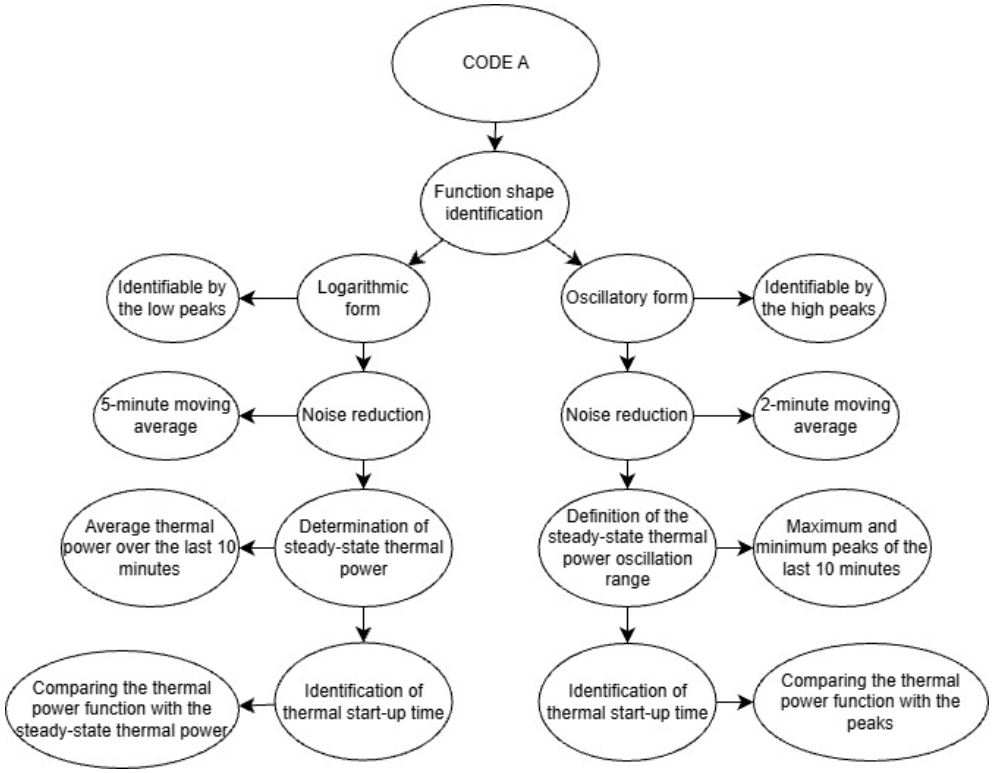

Figure 2.8 - Schematic representation of the MATLAB code A for the thermal start-up time determination

2.2.1.2 Code B

This code works in the same way as "Code A", with the only difference that the moving average for the oscillatory trend is 5 minutes instead of 2. The higher moving average smooths the thermal power more and helps the code avoid incorrect evaluations. Figure 2.9 shows the same example presented in Figure 2.7, but executed using Code B.

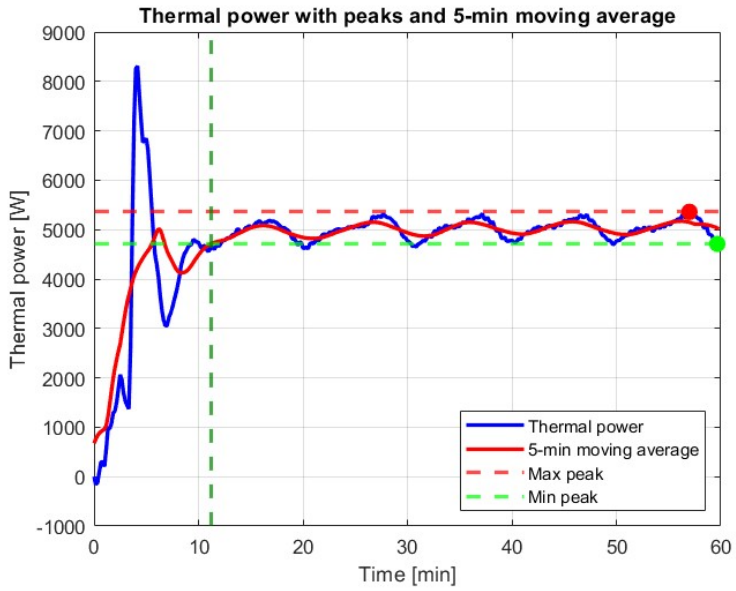

Figure 2.9 - Determination of the thermal start-up time for an oscillatory form using Code B (Test 15)

Figure 2.10 provides a schematic overview of the logic implemented in Code B for extracting the thermal start-up time from the experimental datasets.

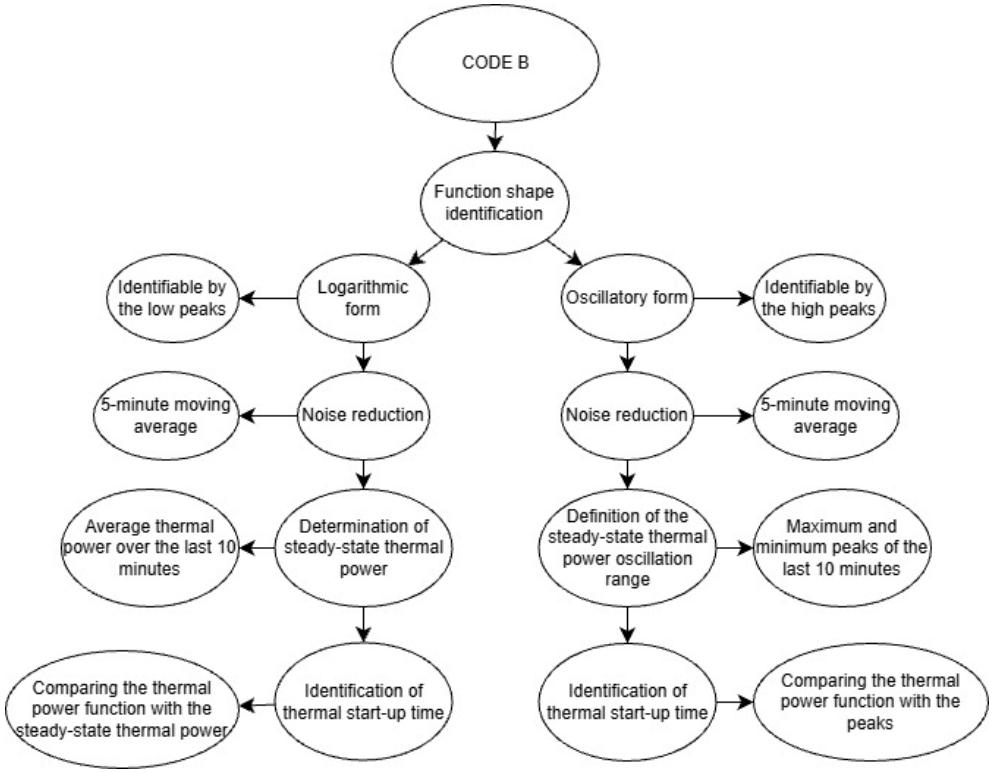

Figure 2.10 - Schematic representation of the MATLAB code B for the thermal start-up time determination

2.2.1.3 Code C

Codes A and B are not always able to identify consistent thermal start-up times because the thermal power function oscillates due to the behavior of the expansion valve. As a result, the thermal start-up is directly linked to the expansion valve: the system pressures only reach the required values once the valve has achieved the necessary opening. A practical solution to determine the thermal start-up time, therefore, is to consider the evaporation and condensation pressures, which indicate when the system has effectively stabilized.

First, a 10-minute moving average is applied to the pressure data to reduce noise. After this filtering, it is possible to identify both the evaporation and condensation pressures at steady-state, calculated as the mean value of the pressure over the last 10 minutes, as shown in Figure 2.11. These steady-state values are then used to determine the end of the start-up phase, defined as the first moment, counting backwards from the end of the measurement, when the moving average pressure differs by more than ±5% from the steady-state value. This backward analysis is necessary because, for example, the condensation pressure starts lower and gradually increases; if the search were performed from the beginning of the measurement, the code would detect the end of start-up at time zero instead of at the correct point. A 10-minute moving window is used for this comparison with the steady-state average to further reduce fluctuations in the data. Finally, between the two pressures (evaporation and condensation), the longer time is selected as the thermal start-up time to adopt a conservative approach. An example of the determination of the thermal start-up time for an oscillatory form using Code C is reported in Figure 2.12.

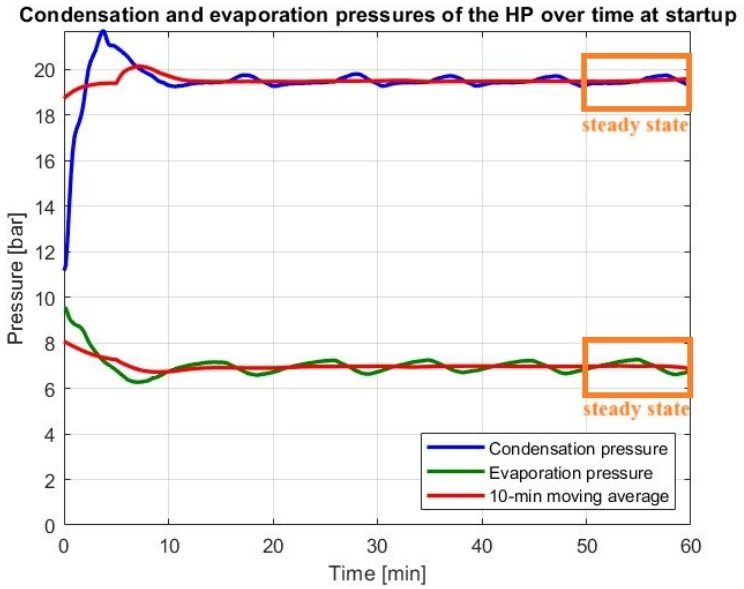

Figure 2.11 – Condensation and evaporation pressures over time (Test 15)

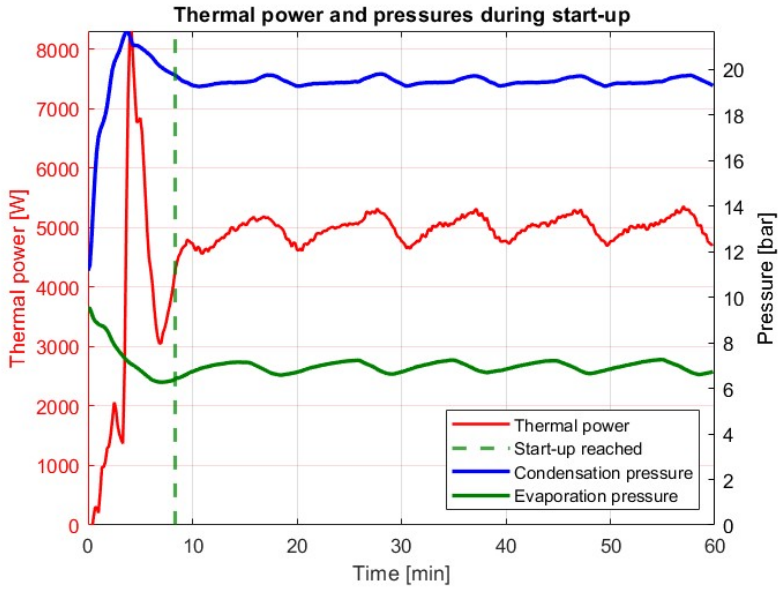

Figure 2.12 - Determination of the thermal start-up time for an oscillatory form using Code C (Test 15)

Figure 2.13 provides a schematic overview of the logic implemented in Code C for extracting the thermal start-up time from the experimental datasets.

Figure 2.13 - Schematic representation of the MATLAB code C for the thermal start-up time determination

2.2.1.4 Comparison between Code A, Code B and Code C

Code A performs particularly well when the thermal power follows a logarithmic trend. However, when the thermal power exhibits an oscillatory form, the code detects the start-up too early in Tests 1, 2, and 3, and too late in Tests 11, 13, 15, 20, 22, 23, 25, and 29.

Code B also performs well when the thermal power follows a logarithmic trend. When the thermal power is oscillatory, the code detects the start-up too early in Tests 1, 2, 3, 21, and 34, and too late in Test 20. It is evident that increasing the moving average reduces the number of tests in which the start-up is detected late, but increases the number of tests in which it is detected early.

Code C performs better than Codes A and B, avoiding the detection of the start-up either too early or too late. Figures 2.14 and 2.15 show the results of Tests 21 and 25, respectively, for the three different codes. It is evident that in Figure 2.14 Code B detects the start-up too early, while in Figure 2.15 Code A detects it too late. In both figures, Code C performs well, avoiding the incorrect detection of the start-up.

The main results obtained using Codes A and B are reported in Appendix A, while Code C is presented in its entirety in Appendix B.

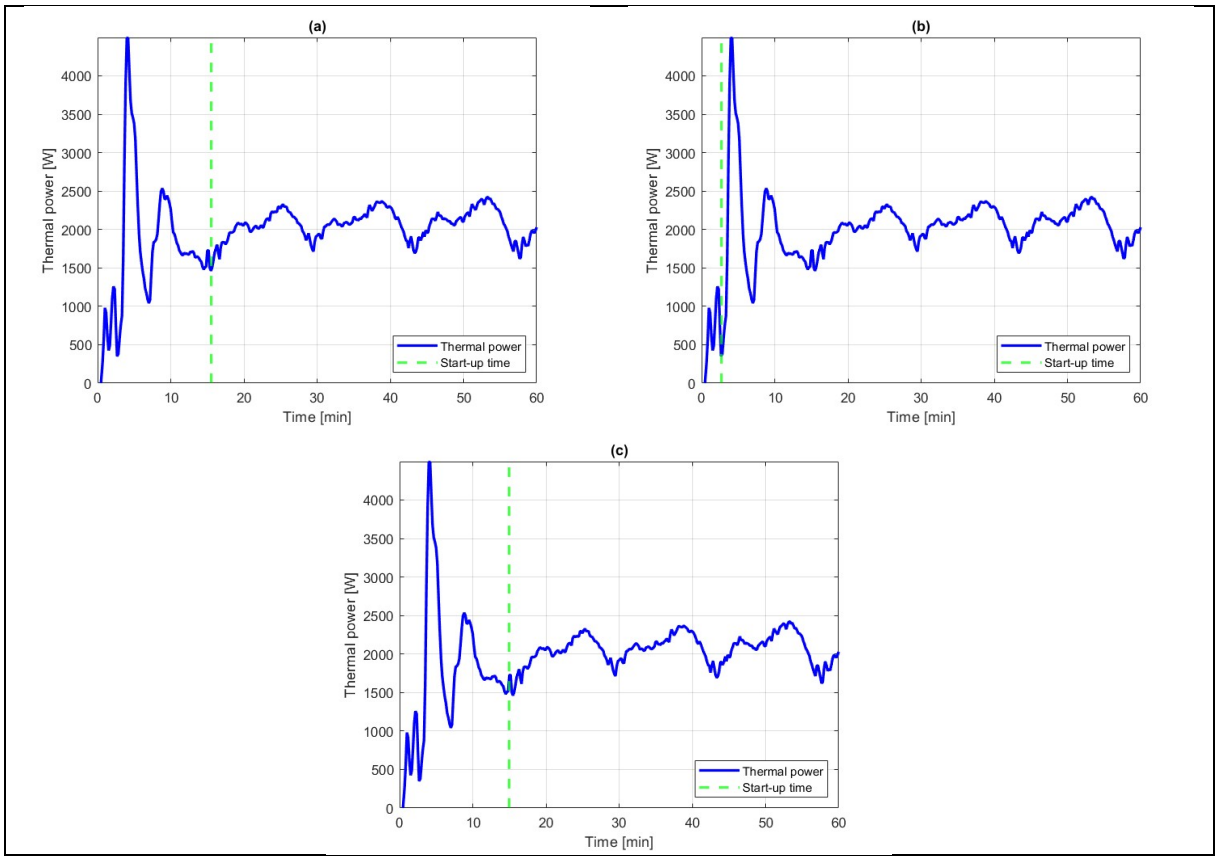

Figure 2.14 - Determination of the thermal start-up for Test 21 using:
(a) Code A, (b) Code B, and (c) Code C

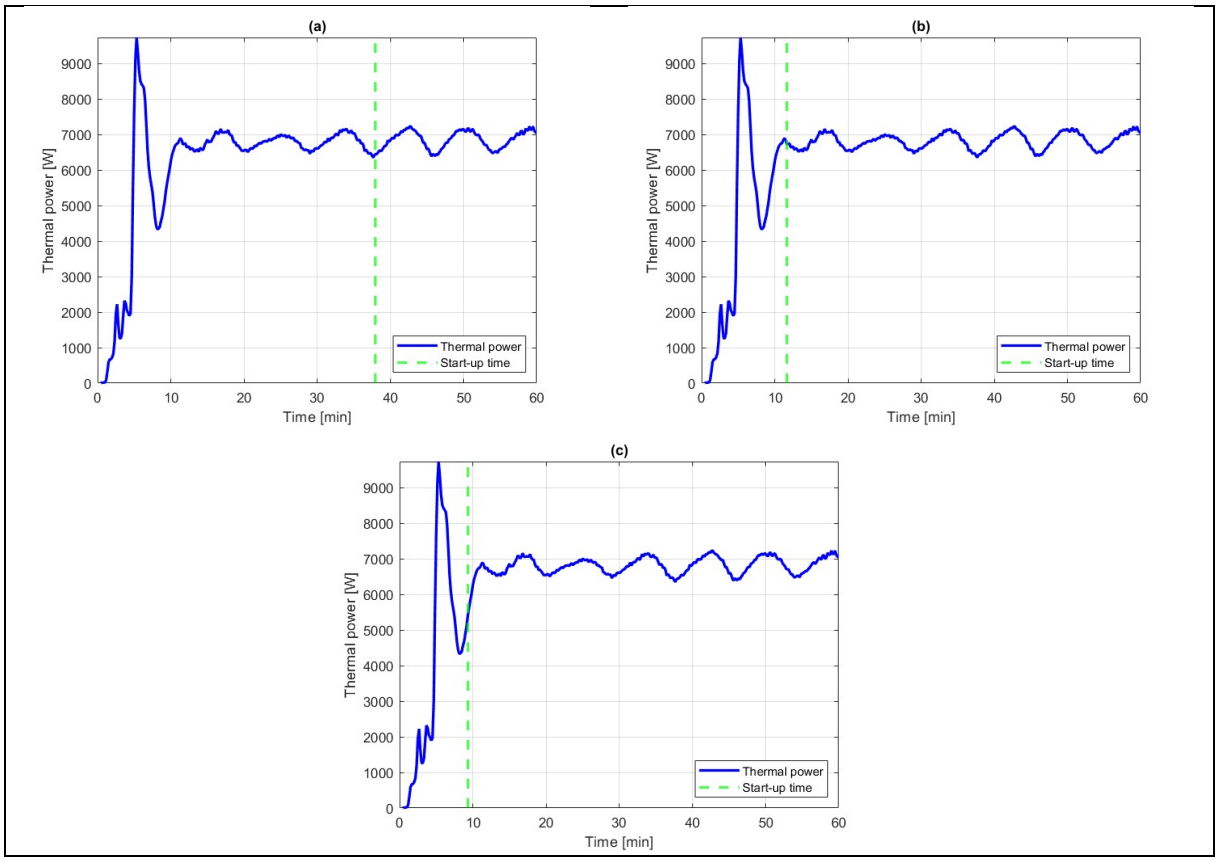

Figure 2.15 - Determination of the thermal start-up for Test 25 using:
(a) Code A, (b) Code B, and (c) Code C

Therefore, Code C was used to perform the analysis and obtain the results, both for ASO and GSO cases. In the GSO case, the code was slightly adapted to operate correctly, without altering the previously described logic.

2.2.2 Results

In this section, the results of the experiments are presented for both the ASO and GSO cases. Section 2.2.2.1 presents the results of the 27 main experiments and the 5 additional experiments with an extended t_{stop}. Section 2.2.2.2 presents the results of the experiments carried out at different ΔT_{sink}, while Section 2.2.2.3 presents the results of the 5 experiments performed under GSO conditions. Table 2.6 provides the legend of the tabulated data used in these three subsections.
Appendix C contains the complete set of experimental results, while Appendix D contains the thermal and electrical power profiles over time for each experiment.

Table 2.6 - Legend of the tabulated data

Data:	Meaning:
Δtsink [°C]	*Difference between the temperature of the water at the setpoint and the temperature of the water at time 0 in the sink system*
Electrical transient duration [min:sec]	*Duration of the electrical transient (electrical start-up time)*
ssf [%]	*Percentage of the frequency of the inverter*
TEST N°	*Number of the experiment*
$T_{ext,}$ [°C]	*Target temperature in the climate chamber during the experiment*
Thermal transient duration [min:sec]	*Duration of the thermal transient (thermal start-up time)*
T out Sink [°C]	*Inlet water temperature inside the HSHX*
t_{stop} [min]	*Time between the initial shutdown and the start of the experiment*
Tw,0 [°C]	*Water temperature at time 0 in the sink system*

2.2.2.1 ASO results for main and extended t_{stop} experiments

In this section, the results of the 27 main experiments and of the 5 additional experiments with longer t_{stop} are presented.
Table 2.7 reports the results of the 27 main experiments. The shutdown time t_{stop} has little impact on both the thermal and electrical start-up times, as shown in Figure 2.16, which reports the standard deviation of the start-up times for t_{stop} set at 2, 10, and 60 minutes for each combination of frequency and temperature. This standard deviation reflects the variability of the start-up time due to different shutdown durations, and the results show that this variability is generally negligible, never exceeding 5 minutes. It should also be noted that the start-up time does not always increase with longer shutdown periods; in some cases, it may even decrease. This behavior is in clear contrast with expectations, indicating that variations in start-up times are mostly due to measurement or evaluation errors rather than a direct effect of the shutdown duration.
This effect is even more evident for experiments with longer t_{stop}; for this reason, Table 2.8 compares Tests 28 to 32 (with extended t_{stop}) with Tests 1 to 9. As shown in Figure 2.17, also in this case the shutdown time t_{stop} has little impact on both the thermal and electrical start-up times. The graphs in the figure show the start-up times for each shutdown duration, and it is evident that these times do not necessarily increase with longer shutdown periods.

Table 2.7 - Thermal and electrical start-up times for the 27 main experiments

TEST N°	ssf [%]	Text [°C]	t_{stop} [min]	Thermal transient duration [min:sec]	Electrical transient duration [min:sec]
Air Source Operation					
TEST 1	25%	20	60	10:10	2:40
TEST 2	25%	20	10	9:50	2:40
TEST 3	25%	20	2	10:40	1:20
TEST 4	50%	20	60	45:50	3:50
TEST 5	50%	20	10	45:40	3:40
TEST 6	50%	20	2	40:30	3:30
TEST 7	75%	20	60	63:00	38:20
TEST 8	75%	20	10	63:10	38:00
TEST 9	75%	20	2	60:20	32:30
TEST 10	25%	7	60	24:20	3:00
TEST 11	25%	7	10	18:30	2:50
TEST 12	25%	7	2	27:00	2:50
TEST 13	50%	7	60	8:50	4:10
TEST 14	50%	7	10	6:20	3:50
TEST 15	50%	7	2	8:20	3:50
TEST 16	75%	7	60	26:30	5:00
TEST 17	75%	7	10	36:30	4:40
TEST 18	75%	7	2	31:50	4:30
TEST 19	25%	2	60	17:30	3:00
TEST 20	25%	2	10	23:20	2:40
TEST 21	25%	2	2	15:00	2:40
TEST 22	50%	2	60	14:10	4:20
TEST 23	50%	2	10	14:40	4:10
TEST 24	50%	2	2	13:20	4:00
TEST 25	75%	2	60	9:20	4:30
TEST 26	75%	2	10	9:30	4:20
TEST 27	75%	2	2	8:00	4:30

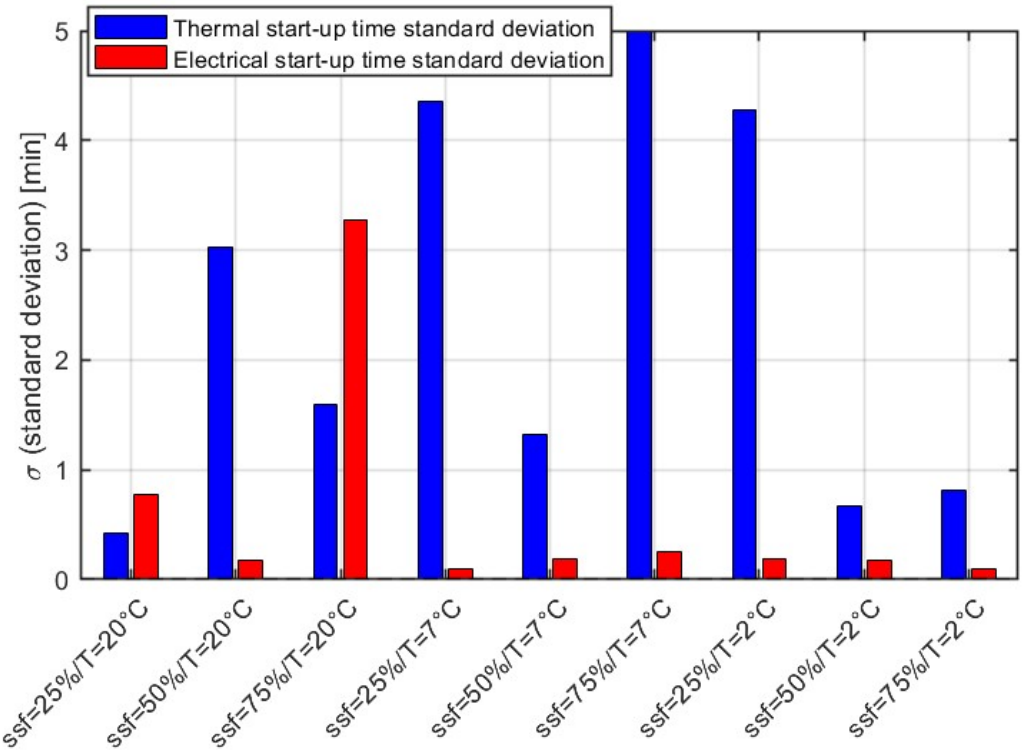

Figure 2.16 – Standard deviation of thermal and electrical start-up times for the three different shutdown times across the 27 main experiments

Table 2.8 - Thermal and electrical start-up times for different shutdown times

TEST N°	ssf [%]	Text [°C]	t_{stop} [min]	Thermal transient duration [min:sec]	Electrical transient duration [min:sec]
TEST 29	25%	20	3600	12:10	4:50
TEST 1	25%	20	60	10:10	2:40
TEST 2	25%	20	10	9:50	2:40
TEST 3	25%	20	2	10:40	1:20
TEST 30	50%	20	3600	47:30	5:00
TEST 31	50%	20	3600	51:00	5:50
TEST 28	50%	20	180	49:00	4:10
TEST 4	50%	20	60	45:50	3:50
TEST 5	50%	20	10	45:40	3:40
TEST 6	50%	20	2	40:30	3:30
TEST 32	75%	20	3600	63:00	38:50
TEST 7	75%	20	60	63:00	38:20
TEST 8	75%	20	10	63:10	38:00
TEST 9	75%	20	2	60:20	32:30

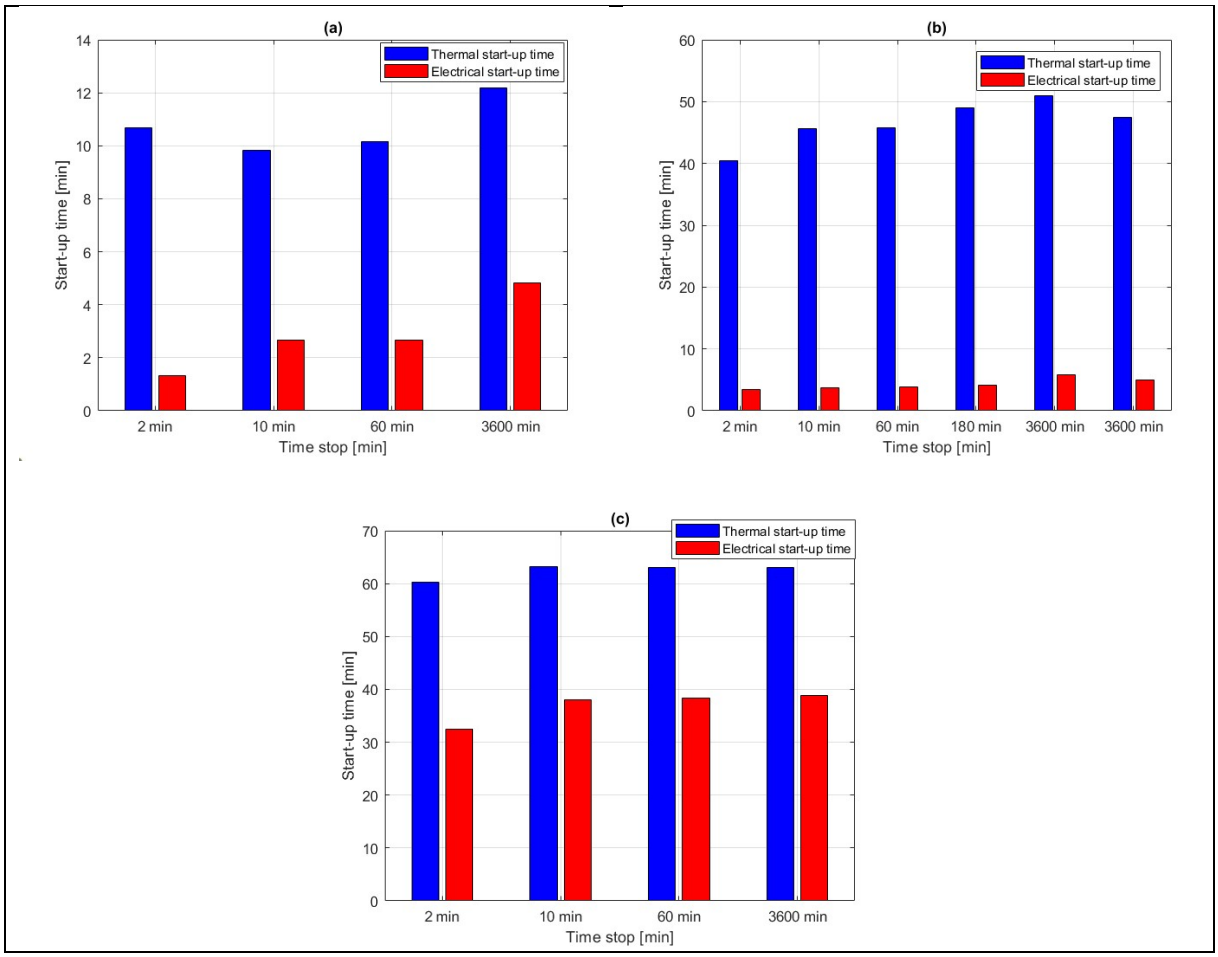

Figure 2.17 – Thermal and electrical start-up times: graphical representation of Table 2.8 results for T_{ext} = 20 °C and (a) ssf = 25%, (b) ssf = 50%, and (c) ssf = 75%

2.2.2.2 ASO results for different ΔT_{sink}

This section presents the results for different ΔT_{sink}. In Table 2.9, the effect of an increased ΔT_{sink} for ASO is shown by comparing Tests 4 and 13 with Tests 33 to 36, which were conducted at a higher ΔT_{sink}.

All tests were conducted at $ssf = 50\%$; Tests 4, 35, and 36 were performed at $T_{ext} = 20$ °C, while Tests 13, 33, and 34 were carried out at $T_{ext} = 7$ °C.

Table 2.9 - Comparison between tests at different ΔT_{sink} values

TEST N°	TEST 4	TEST 36	TEST 35	TEST 13	TEST 33	TEST 34
ssf [%]	50%	50%	50%	50%	50%	50%
Text [°C]	20	20	20	7	7	7
t_{stop} [min]	60	60	60	60	60	60
T out Sink [°C]	30	30	50	30	30	50
Tw,0 [°C]	26	20	20	26	20	20
Thermal transient duration [min:sec]	45:50	46:30	27:30	8:50	11:10	20:20
Electrical transient duration [min:sec]	3:50	4:30	12:50	4:10	5:20	12:50
Δtsink [°C]	9.68	15.56	34.98	8.41	14.26	33.84

Figure 2.18 graphically presents the results shown in Table 2.9:

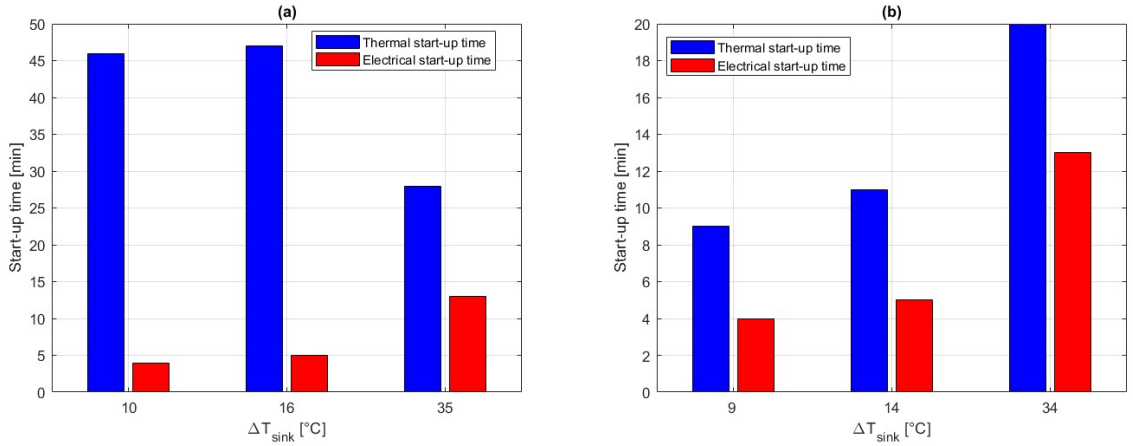

Figure 2.18 – Thermal and electrical start-up times: graphical representation of Table 2.9 results for ssf = 50% and (a) T_{ext} =20°C and (b) T_{ext} =7°C

2.2.2.3 GSO results

This section presents the results of the ground-source operation (GSO) tests. As described in Section 2.1.2.2, only the variation of ssf and ΔT_{sink} is analyzed, since t_{stop} and T_{ext} are fixed. The results of the five tests conducted are summarized in Table 2.10.

Table 2.10 - Thermal and electrical start-up times for five GSO experiments

TEST N°	TEST 37	TEST 38	TEST 39	TEST 40	TEST 41
ssf [%]	50%	25%	75%	50%	50%
Text [°C]	5	5	5	5	5
t_{stop} [min]	10	10	10	10	10
T out Sink [°C]	30	30	30	30	50
Tw,0 [°C]	28	28	28	18	18
Thermal transient duration [min:sec]	15:10	54:40	12:30	14:10	41:30
Electrical transient duration [min:sec]	3:40	7:10	3:30	6:30	16:40
Δtsink [°C]	4.78	3.29	6.36	15.43	34.77

Figure 2.19 graphically presents the results shown in Table 2.10:

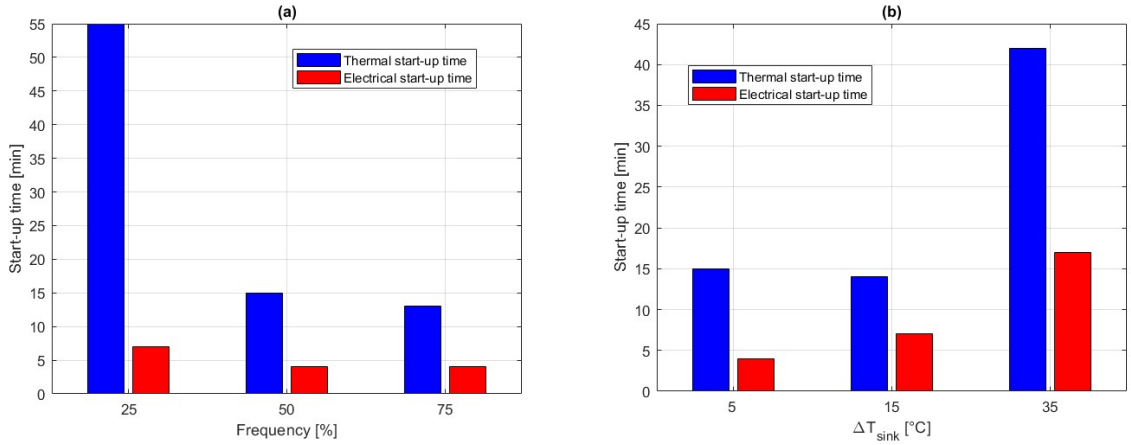

Figure 2.19 – Thermal and electrical start-up times: graphical representation of Table 2.10 results for (a) different ssf *and (b) different* ΔT_{sink}

2.2.3 Discussion

In this section, the results presented in Section 2.2.2 are discussed. First of all, it is important to make some clarifications: during the experiments T_{ext} oscillated because of the control system, and the same occurred for $T_{out,sink}$.

The heating power of the heat pump is obtained indirectly, through the outlet and inlet water temperatures of the HSHX.

The cooling power $\dot{Q}_{cool}$ is defined as the product of the water mass flow $\dot{m}_{H_2O}$, the specific heat of water c_p, and the temperature difference between the inlet water temperature of the sink $T_{in,sink}$ and the outlet water temperature of the sink $T_{out,sink}$, as displayed in Equation (7).

$$\dot{Q}_{cool} = \dot{m}_{H_2O} \cdot c_p \cdot (T_{in,sink} - T_{out,sink}) \qquad (7)$$

The heating power $\dot{Q}_{heat}$ is defined by Equation (8), where $T_{out,HSHX}$ and $T_{in,HSHX}$ are respectively the outlet and inlet water temperatures of the HSHX.

$$\dot{Q}_{heat} = \dot{m}_{H_2O} \cdot c_p \cdot (T_{out,HSHX} - T_{in,HSHX}) \qquad (8)$$

$T_{in,sink}$ and $T_{out,HSHX}$ represent the same temperature, as do $T_{out,sink}$ and $T_{in,HSHX}$. This means that $\dot{Q}_{heat}$ corresponds to the same power as $\dot{Q}_{cool}$ (9).

$$\dot{Q}_{cool} = \dot{Q}_{heat} \qquad (9)$$

Each experiment is characterized by a peak in thermal power. This peak is illustrated in Figure 2.20 and does not represent the real behavior of the thermal power; it is caused by a delay between the measurement of $T_{in,HSHX}$ and $T_{out,HSHX}$, due to the piping connecting the two points. As a result, the water enters the HSHX at a temperature lower than the setpoint, but while passing through the heat exchanger it warms up, and $T_{out,HSHX}$ exits the exchanger at a temperature higher than the setpoint. At this moment, the chiller must activate, rapidly cooling the water and creating a large ΔT and, consequently, a thermal power peak that does not correspond to the real system behavior. This phenomenon is illustrated more clearly in Figure 2.21.

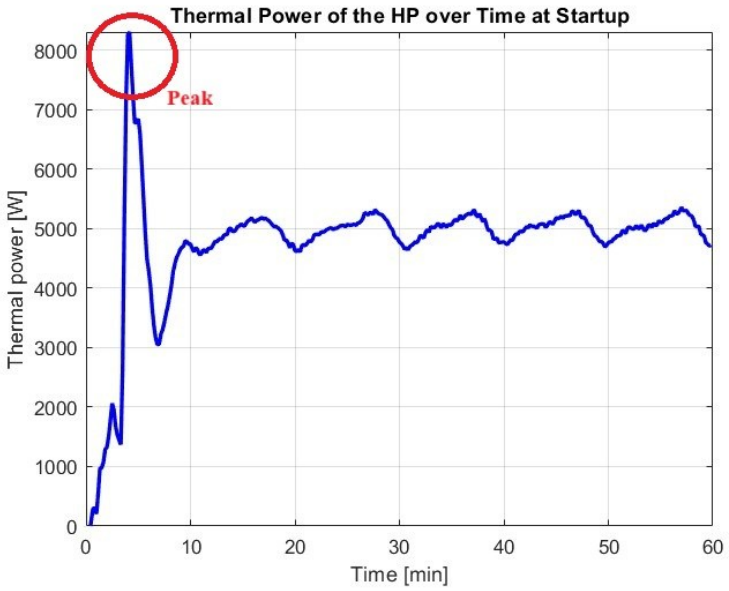

Figure 2.20 - Peak in measured heating power caused by chiller activation (Test 15)

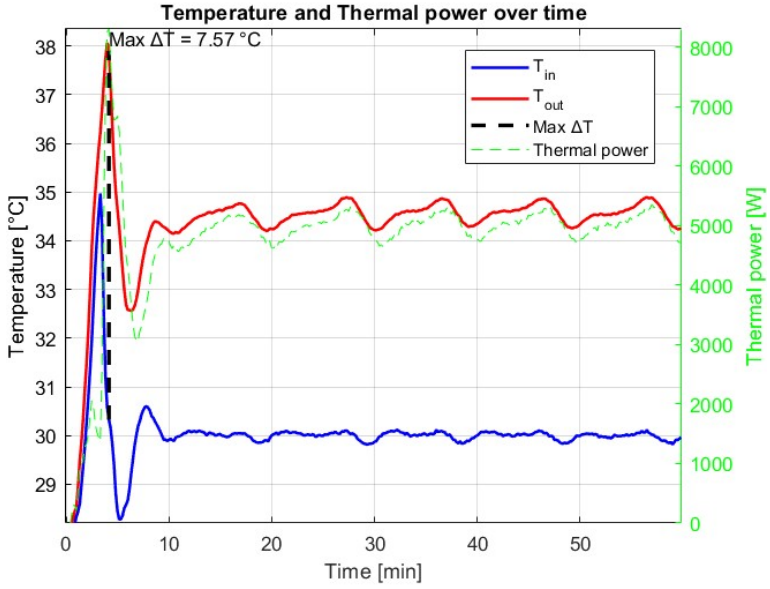

Figure 2.21 - $T_{in,HSHX}$, $T_{out,HSHX}$ and maximum ΔT responsible for the thermal power peak

2.2.3.1 ASO discussion for main and extended t_{stop} experiments

From the literature, an increase in the shutdown time was expected to lead to a longer start-up time, but, as shown in Figures 2.16 and 2.17, the effect of t_{stop} on t_{su} is negligible. This occurs because the expansion valve automatically fully opens when the heat pump is shutdown. This causes the pressure between the evaporator and condenser to equalize in less than 10 minutes, as the automatic opening allows the refrigerant to flow freely and rapidly between the two sides, making it impossible to observe an increase in the evaporation pressure or a decrease in the condensation pressure over time. If the valve remained closed after the shutdown of the heat pump, the pressure difference would be maintained. This means that some pressure losses would occur over time, and the lower the external temperature, the greater these losses would be, due to the larger pressure difference between condenser and evaporator (fixed $T_{w,setpoint}$).

Since the dependence on t_{stop} can be neglected, it is possible to reduce the number of control variables from three (T_{ext}, ssf, t_{stop}) to two (T_{ext}, ssf). In this way, the first 27 main experiments for ASO can be grouped into only 9 cases, since there are now only two variables, each with three values. The 9 cases are presented in Table 2.11: the thermal and electrical transient durations are calculated as the average of the transient durations measured for the three different t_{stop} values.

Table 2.11 - Results of the first 27 main experiments after reduction of control variables

Case N°	ssf [%]	Text [°C]	Thermal transient duration [min:sec]	Electrical transient duration [min:sec]
Case 1	25%	20	10:13	2:13
Case 2	25%	7	23:17	2:53
Case 3	25%	2	18:37	2:47
Case 4	50%	20	44:00	3:40
Case 5	50%	7	7:50	3:57
Case 6	50%	2	14:03	4:10
Case 7	75%	20	62:10	36:17
Case 8	75%	7	31:37	4:43
Case 9	75%	2	8:57	4:27

It was expected that t_{su} would decrease with increasing T_{ext} and ssf. This is because, on the one hand, a lower external temperature results in a higher pressure difference between the evaporator and condenser at a fixed water setpoint temperature $T_{w,setpoint}$, which requires more time to establish. On the other hand, a higher ssf reduces the time needed to reach $T_{w,setpoint}$.
What happens, instead, is that t_{su} depends mainly on the expansion valve, which does not operate correctly due to its PID control. For almost the first six minutes after start-up, the valve remains at its default opening of 18%; only afterward does it begin to increase its opening percentage.
Figure 2.22 shows the start-up behavior of the expansion valve and the compressor frequency (controlled by the inverter). The figure refers to Test 15, performed at $ssf = 50\%$, $T_{ext} = 7°C$, and $t_{stop} = 2$ min.

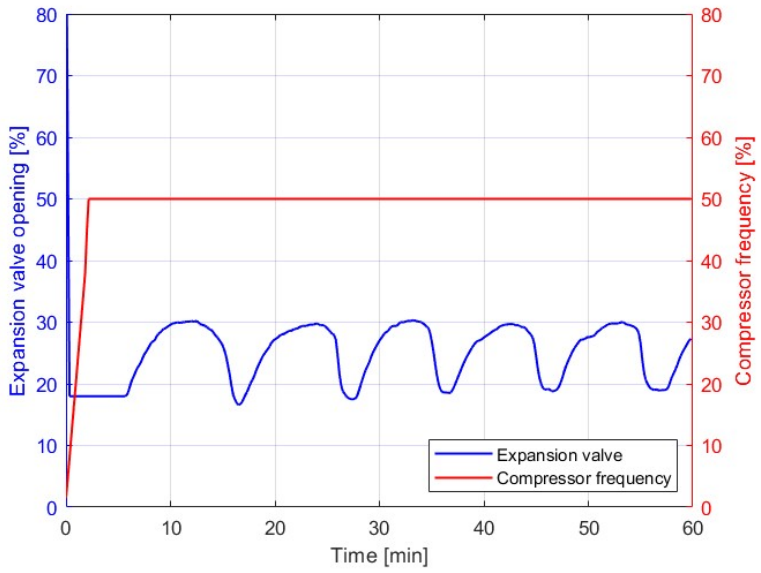

Figure 2.22 - Expansion valve opening and compressor frequency during start-up

It can be observed that the expansion valve is open at the beginning: as noted above, after the heat pump is shutdown the expansion valve automatically opens to rebalance the pressures, and after two minutes of shutdown time it is still open. When the heat pump is restarted, the valve

opening percentage reaches approximately 18% for about six minutes, after which normal regulation begins. The inverter frequency does not increase from 0% to 50% linearly, as suggested by the figure. In reality, ramps are applied by the controller to avoid sudden changes in compressor speed, so the frequency rises gradually, pauses, and then continues to increase only after reaching certain intermediate thresholds.

The expansion valve is expected to open less as the external temperature increases, due to the reduced pressure difference, while it should open more as the ssf increases, due to the higher refrigerant mass flow. It is difficult to predict which of these two effects will dominate. With the PID configured as it is, the valve tends to open faster at low temperatures, while achieving a larger opening percentage when the ssf increases. The combination of these two effects leads to longer start-up times in Tests 4 to 9, as presented in Table 2.7.

Since it was not possible to examine how the PID controller was programmed, its control logic is not entirely clear. To provide an idea of how it operates with varying T_{ext} and ssf, Figures 2.23 to 2.31 show the time evolution of the thermal power and the expansion valve opening percentage for the case $t_{stop} = 1$ h, with T_{ext} varying from 20°C to 2°C and ssf ranging from 25% to 75%.

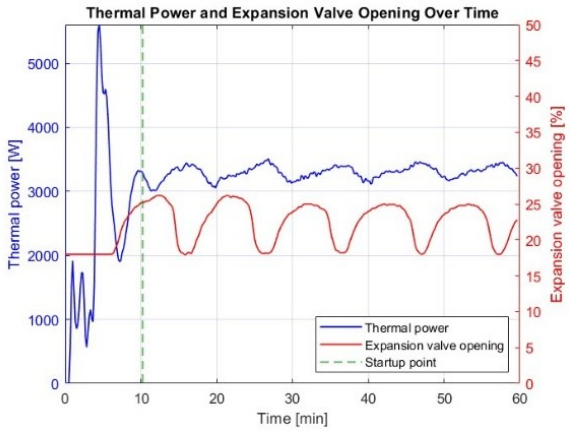

Figure 2.23 - Thermal power and the expansion valve opening percentage over time for $T_{ext} = 20°C$ and $ssf = 25\%$ (Test 1)

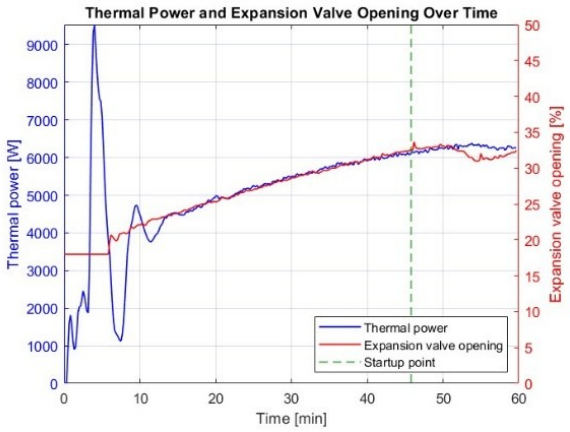

Figure 2.24 - Thermal power and the expansion valve opening percentage over time for $T_{ext} = 20°C$ and $ssf = 50\%$ (Test 4)

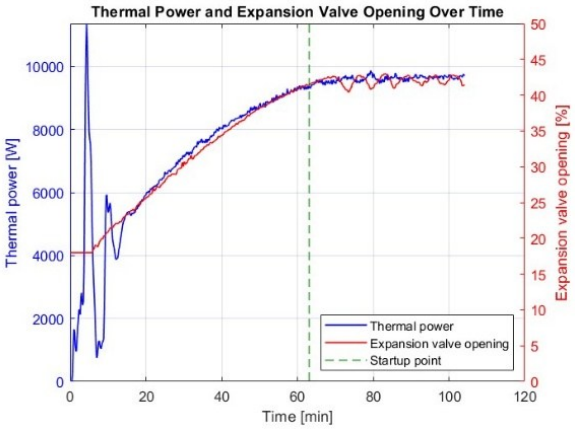

Figure 2.25 - Thermal power and the expansion valve opening percentage over time for $T_{ext} = 20°C$ and $ssf = 75\%$ (Test 7)

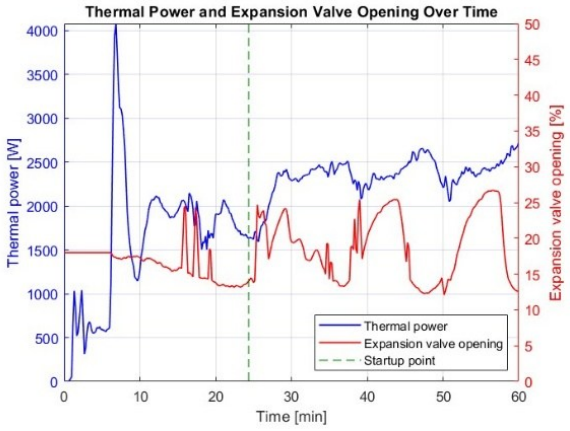

Figure 2.26 - Thermal power and the expansion valve opening percentage over time for $T_{ext} = 7°C$ and $ssf = 25\%$ (Test 10)

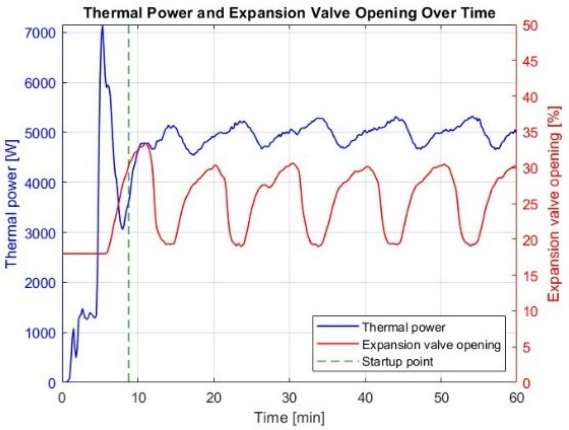

Figure 2.27 - Thermal power and the expansion valve opening percentage over time for $T_{ext} = 7°C$ and $ssf = 50\%$ (Test 13)

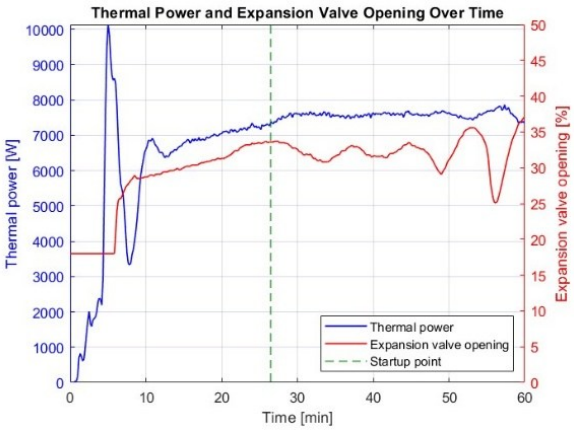

Figure 2.28 - Thermal power and the expansion valve opening percentage over time for $T_{ext} = 7°C$ and $ssf = 75\%$ (Test 16)

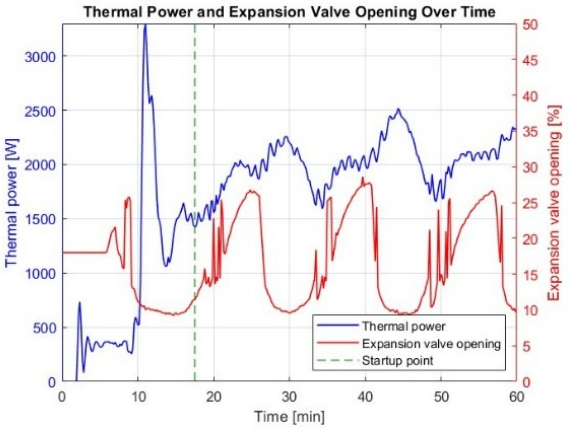

Figure 2.29 - Thermal power and the expansion valve opening percentage over time for $T_{ext} = 2°C$ and $ssf = 25\%$ (Test 19)

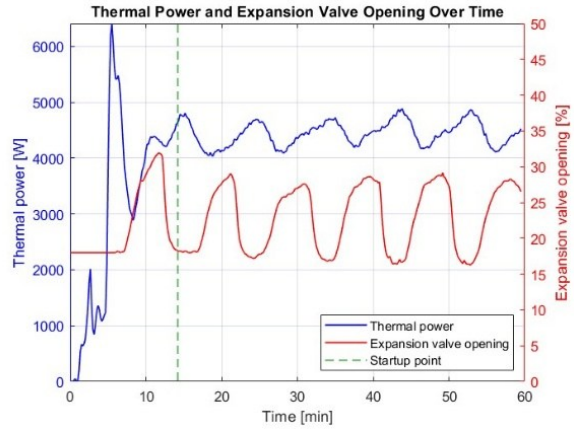

Figure 2.30 - Thermal power and the expansion valve opening percentage over time for $T_{ext} = 2°C$ and $ssf = 50\%$ (Test 22)

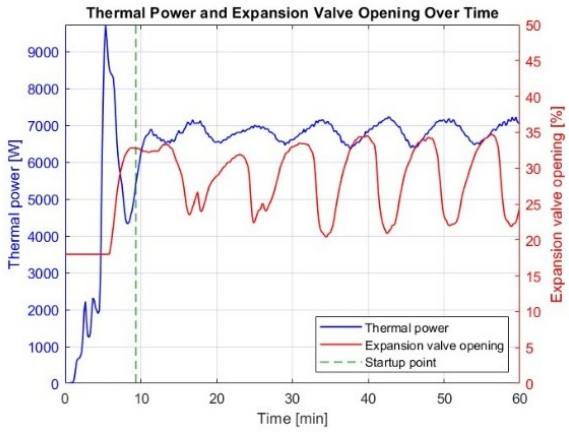

Figure 2.31 - Thermal power and the expansion valve opening percentage over time for $T_{ext} = 2°C$ and $ssf = 75\%$ (Test 25)

The behavior of the thermal start-up times as functions of frequency and temperature, with reference to Table 2.11, is shown in Figures 2.32 and 2.33.

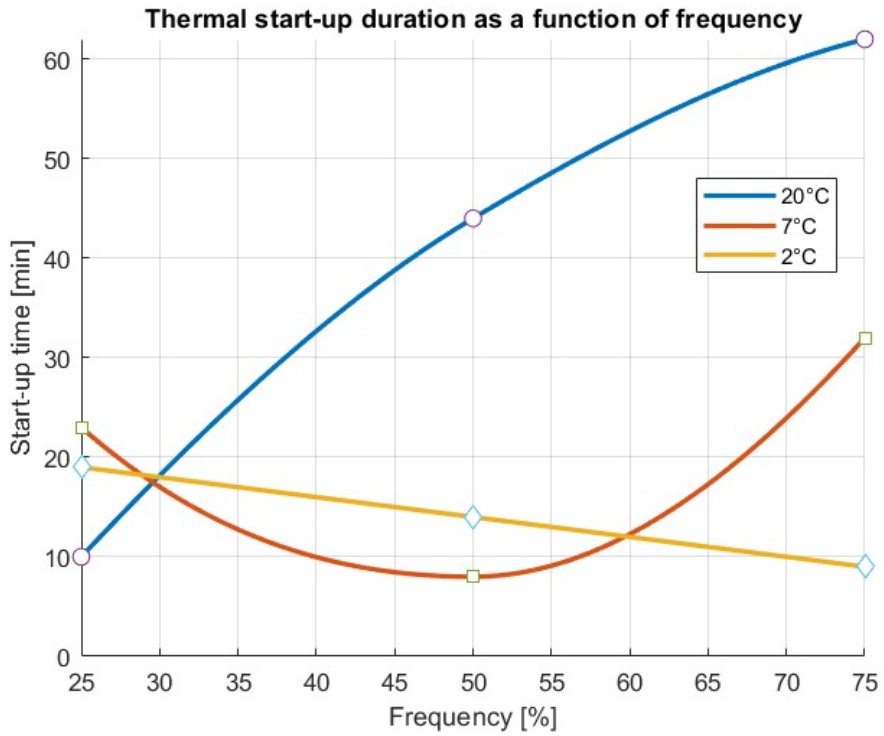

Figure 2.32 - Thermal start-up duration as a function of frequency (ASO)

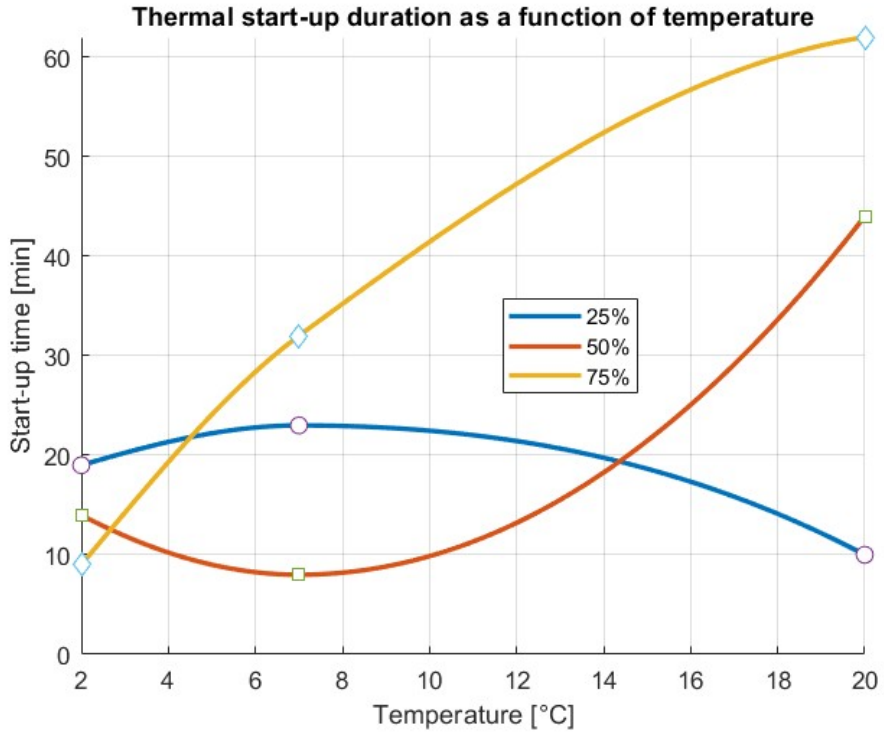

Figure 2.33 - Thermal start-up duration as a function of temperature (ASO)

Figure 2.32 shows the thermal start-up duration as a function of frequency, and it is evident that the effects described in the literature are combined with those of the expansion valve's PID. For $T_{ext} = 20°C$, the thermal start-up time increases with ssf because higher ssf values require larger steady-state valve openings. In addition, a high T_{ext} slows down the valve response due

to the PID controller configuration. The combination of these two effects delays the establishment of stable operating conditions.
For $T_{ext} = 7°C$, the thermal start-up time first decreases as ssf increases from 25% to 50%, but then increases at 75%, becoming higher than the value at 25%. This indicates that, at 7°C, the valve opens faster than at 20°C, but not fast enough to reduce t_{su} at $ssf = 75\%$.
For $T_{ext} = 2°C$, a higher ssf results in a lower t_{su}, in agreement with the literature presented in Section 1.4; this shows that the PID operates better at low temperatures, allowing the valve to open more quickly.
Figure 2.33 shows the thermal start-up duration as a function of temperature and, as in Figure 2.32, it is evident that the effects of T_{ext} and ssf are combined with those of the expansion valve's PID.
For $ssf = 25\%$, as T_{ext} increases, t_{su} first increases and then decreases. This behavior results from two opposing effects: on one hand, increasing the external temperature tends to reduce t_{su}; on the other hand, a higher T_{ext} slows down the expansion valve response due to the PID controller configuration, which increases the time required to reach steady operating conditions.
For $ssf = 50\%$, as T_{ext} increases, t_{su} first decreases and then increases. The decrease from $T_{ext} = 2°C$ to $T_{ext} = 7°C$ is caused by the MATLAB post-processing, which identifies t_{su} slightly earlier for Tests 13 to 15 because the steady-state pressure in the evaporator and condenser is reached faster.
For $ssf = 75\%$, as T_{ext} increases, t_{su} increases. This is due to the slower valve opening response at higher external temperatures.

According to the literature in Section 1.4, the electrical start-up time is always shorter than the thermal start-up time, as reported by S. Katipamula [13]. Regarding the electrical start-up time in the 27 main experiments, it ranges between 2 and 5 minutes, with a single exception for the case with $T_{ext} = 20°C$ and $ssf = 75\%$, where it reaches approximately 36 minutes. Figures 2.34 and 2.35 show the electrical start-up duration as a function of frequency and as a function of temperature, respectively, with reference to Table 2.11.

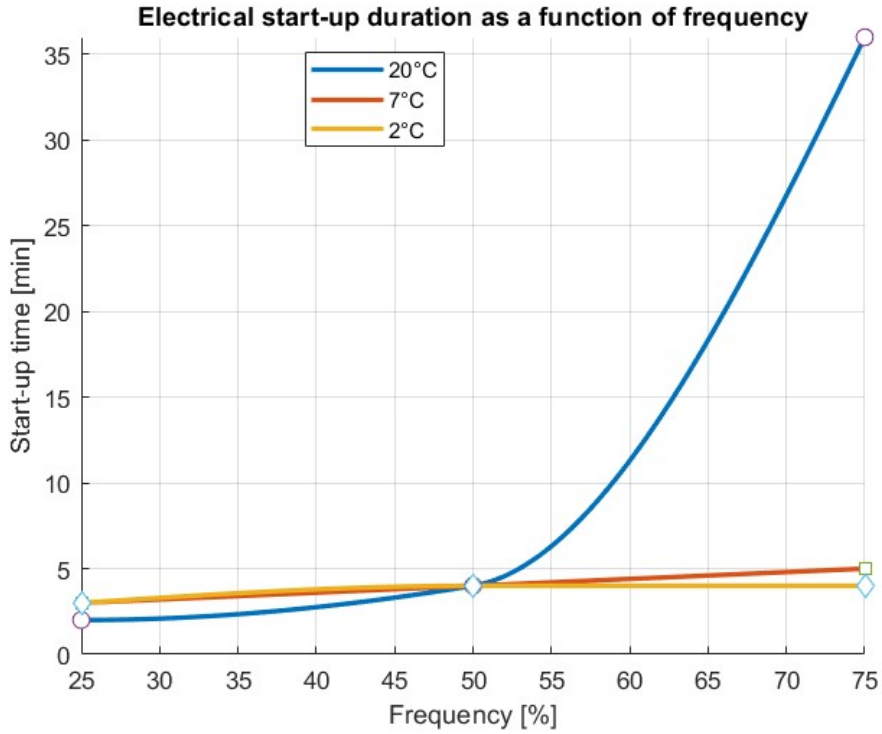

Figure 2.34 - Electrical start-up duration as a function of frequency (ASO)

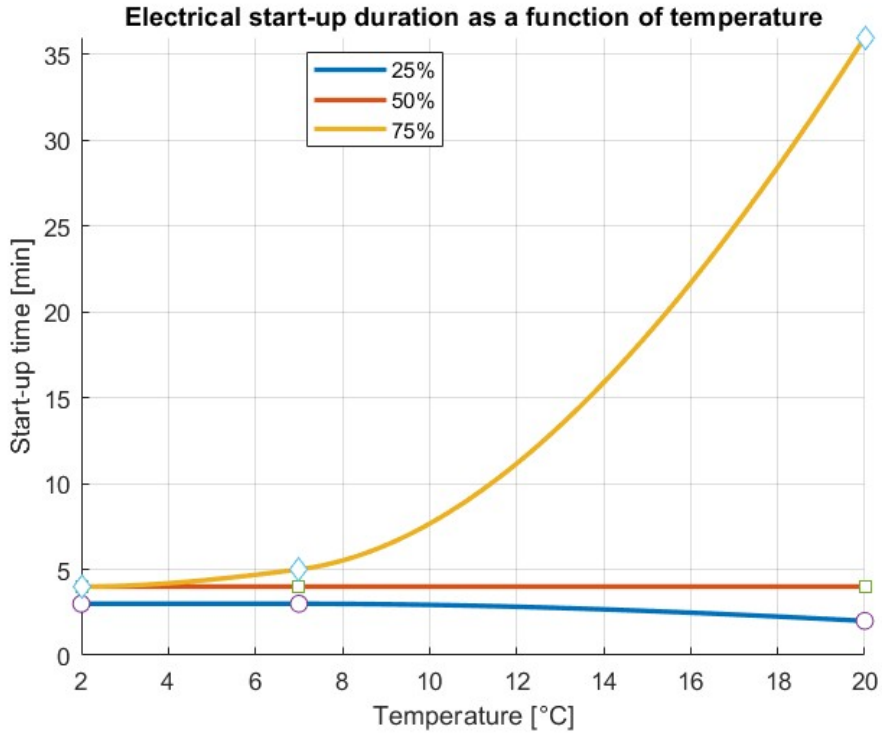

Figure 2.35 - Electrical start-up duration as a function of temperature (ASO)

In the case of $T_{ext} = 20°C$ and $ssf = 75\%$, the electrical start-up time is particularly long due to the behavior of the PID controller, which opens the expansion valve slowly. The slow opening of the expansion valve causes both the thermal and electrical start-up times to increase, since the valve reaches the required opening percentage only after almost one hour. Figure 2.36 shows the evolution of the electrical power and the expansion valve opening during the start-up phase.

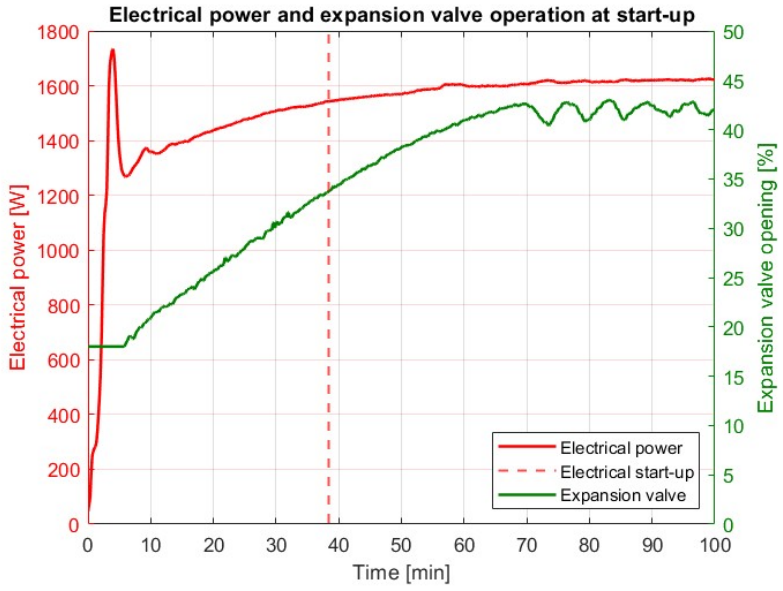

Figure 2.36 - Electrical power and expansion valve opening during start-up at $T_{ext} = 20°C$ and $ssf = 75\%$

Figure 2.17 shows that, for shutdown times longer than 1 hour, the electrical start-up time tends to increase, although not significantly.

2.2.3.2 ASO discussion for different ΔT_{sink}

Regarding the dependence on ΔT_{sink}, Figure 2.37 analyses the thermal start-up time as a function of ΔT_{sink}, with reference to Table 2.9.

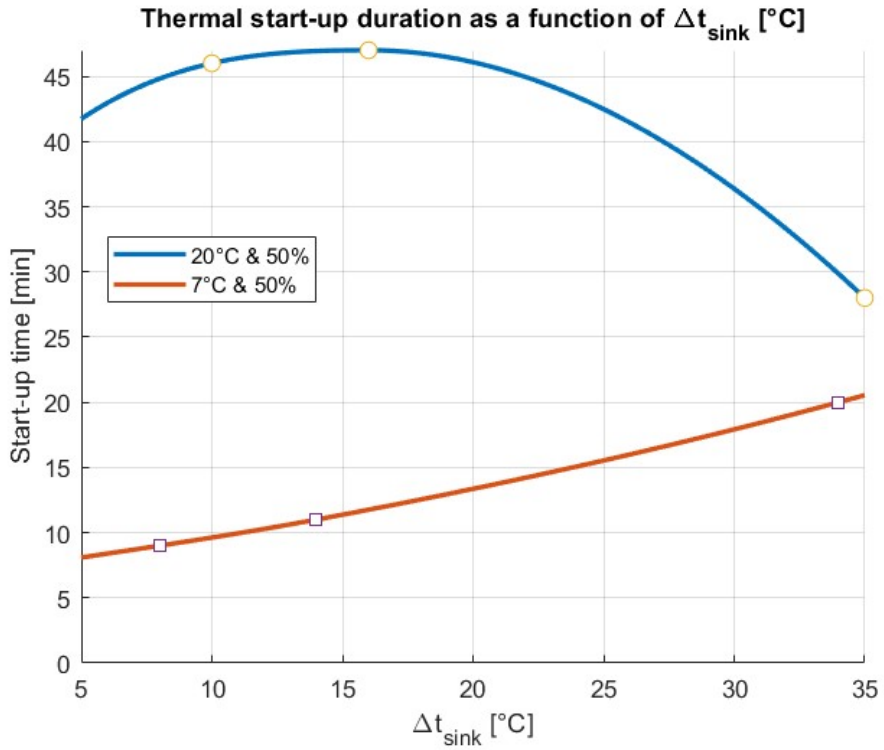

Figure 2.37 - Thermal start-up duration as a function of Δtsink [°C] (ASO)

It can be observed that an increase in ΔT_{sink} from approximately 8/10°C to 14/16°C leads to a slight increase in the thermal start-up time, although the effect is not particularly significant. When ΔT_{sink} becomes significantly higher (34/35°C), as in the case of domestic hot water production, the start-up time decreases for $T_{ext} = 20°C$ and $ssf = 50\%$, while it increases for $T_{ext} = 7°C$ and $ssf = 50$. This occurs because, the higher the temperature of the water to be produced, the more the expansion valve tends to stay less open. Producing domestic hot water requires a higher condenser temperature, which is achieved by increasing the condenser pressure, thereby reducing the opening of the expansion valve. This has a positive effect in the case of $T_{ext} = 20°C$, where the valve opening velocity is very low; a decrease in the steady-state valve opening percentage results in a faster start-up time. At lower T_{ext}, where the slow valve opening is no longer an issue, the time required to reach the set-point temperature becomes the more dominant factor.

Figures 2.38 and 2.39 show, respectively, the thermal powers and valve opening percentages for Tests 4 and 35, illustrating how the valve changes from an average steady-state opening of 32% in Test 4 ($T_{ext} = 20°C$, $ssf = 50\%$, $\Delta T_{sink} = 10°C$) to 25% in Test 35 ($T_{ext} = 20°C$, $ssf = 50\%$, $\Delta T_{sink} = 35°C$).

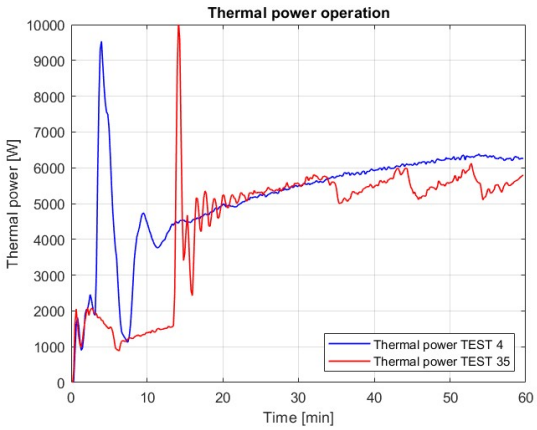

Figure 2.38 – Thermal power for Test 4 and Test 35

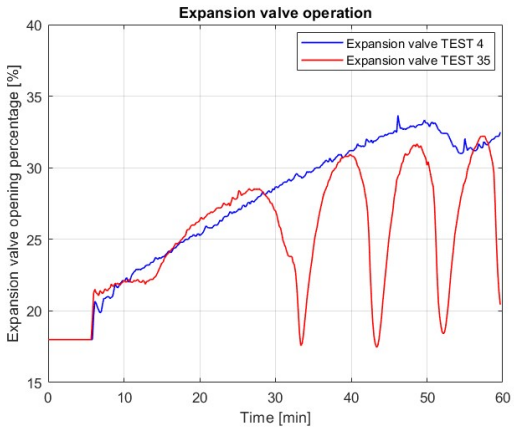

Figure 2.39 – Valve opening percentage for Test 4 and Test 35

Tests 33 to 36, conducted at higher ΔT_{sink}, show that the electrical start-up time increases with ΔT_{sink}, as reported in Table 2.9 and illustrated in Figure 2.40, rising from approximately 4 minutes for ΔT_{sink} below 10°C to around 13 minutes for ΔT_{sink} of 34-35°C.

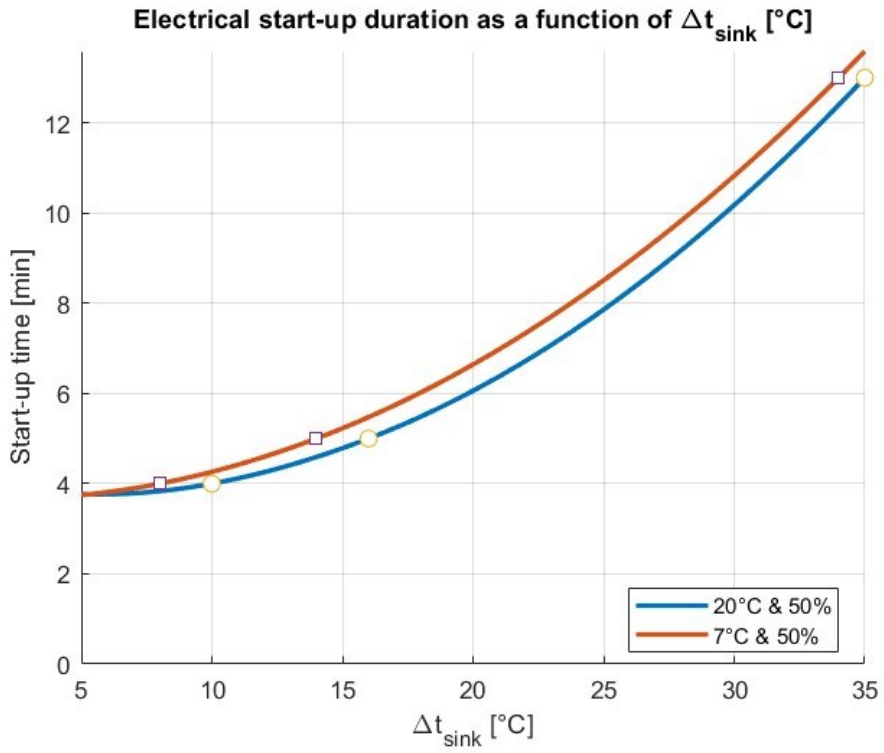

Figure 2.40 - Electrical start-up duration as a function of Δtsink [°C] (ASO)

2.2.3.3 GSO discussion

As reported in Section 2.1.2.2, for GSO the ground temperature is not considered as a variable and the shutdown time t_{stop} is fixed. The only two parameters analyzed are ssf and ΔT_{sink}, and the results are presented in Section 2.2.2.3 (Table 2.10).

Three tests are conducted at low ΔT_{sink}, varying only ssf, and two additional tests are conducted at high ΔT_{sink}, keeping $ssf = 50\%$ constant.

Figure 2.41 presents the results for the tests at low ΔT_{sink} (Tests 37, 38 and 39, corresponding to $ssf = 50\%$, $ssf = 25\%$ and $ssf = 75\%$, respectively); the figure shows the thermal and electrical start-up times as a function of frequency. In both cases, the results are consistent with

the literature presented in Section 1.4: the electrical start-up is shorter than the thermal start-up, as reported by S. Katipamula [13], and the start-up time decreases with increasing ssf, as observed by Roccatello et al. [16].

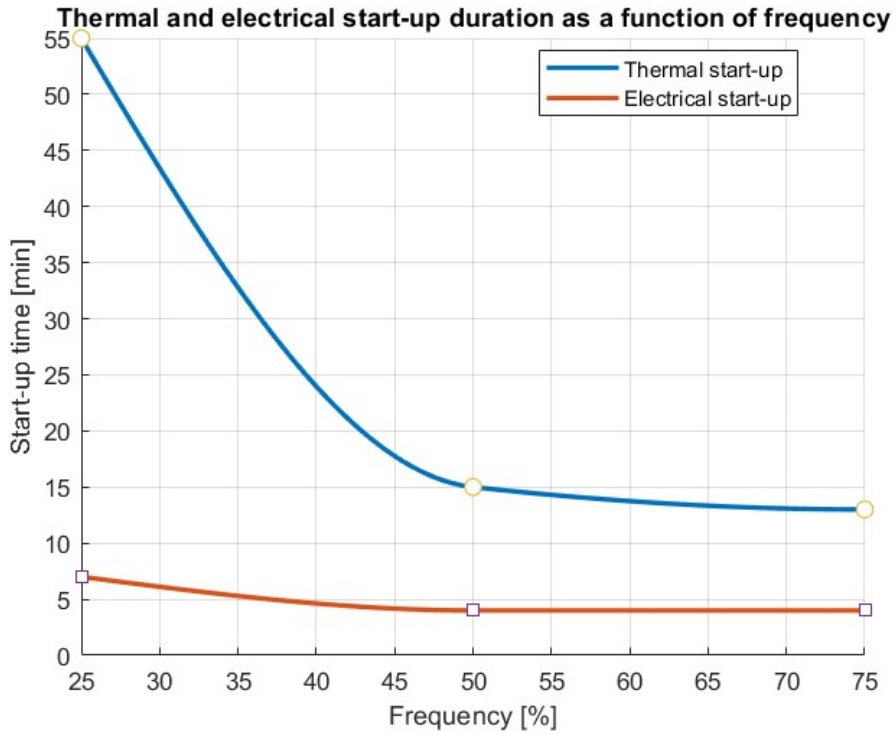

Figure 2.41 - Thermal and electrical start-up duration as a function of frequency (GSO)

Figure 2.42 shows the thermal and electrical start-up times as a function of ΔT_{sink}. It can be observed that an increase in ΔT_{sink} from approximately 5°C to 15°C does not vary the thermal start-up time significantly, while leading to a slight increase in the electrical start-up time. When ΔT_{sink} becomes significantly higher (35°C), as in the case of domestic hot water production, the start-up time increases significantly.

It is worth noting that for Tests 38 and 41, the start-up times are significantly longer than in the other cases; this is again due to the PID controller of the expansion valve, which does not operate correctly. Figures 2.43 and 2.44 show the behavior of the expansion valve and the superheating for Tests 38 and 41, respectively, highlighting an anomalously long initial ramp in the expansion valve opening percentage, which leads to an increase in the start-up times. The expansion valve is excessively open at the beginning due to the PID controller, resulting in the absence of superheating during the initial phase. Moreover, the valve closes too slowly, causing the superheating to stabilize only after a long period, when the correct valve opening is finally reached and proper superheating can be established.

Since it was not possible to examine how the PID controller was programmed, its control logic is not entirely clear. In any case, unlike the expansion valve in the ASO case, for the GSO case there is no default initial opening percentage fixed for a given duration, as shown in the figures.

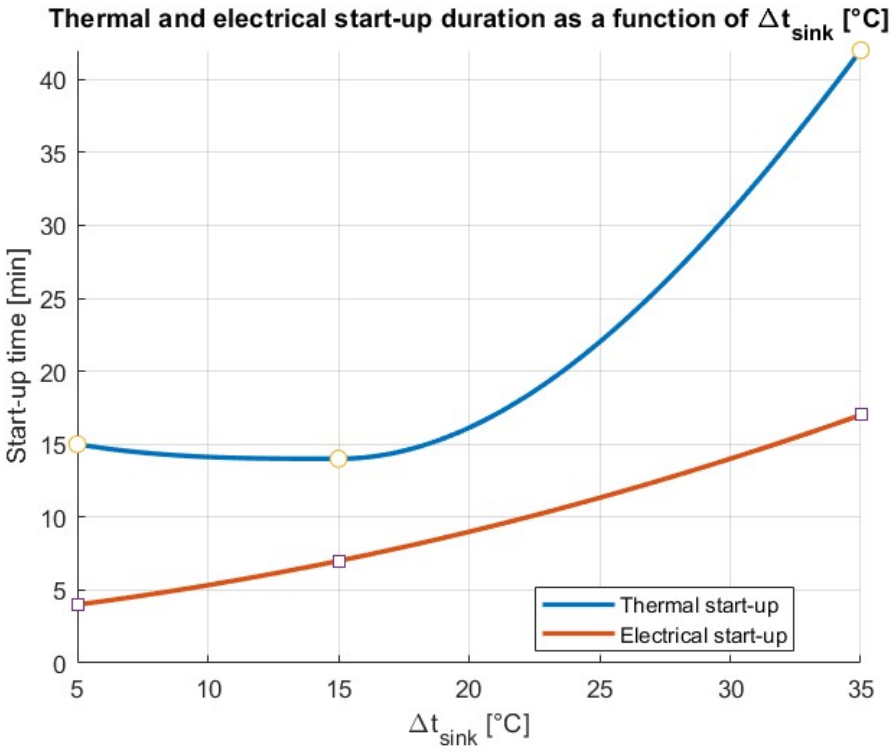

Figure 2.42 - Thermal and electrical start-up duration as a function of Δtsink [°C] (GSO)

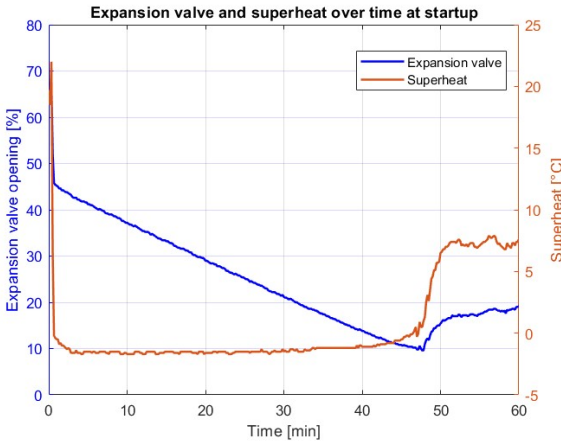

Figure 2.43 – Expansion valve opening percentage and superheating over time for Test 38

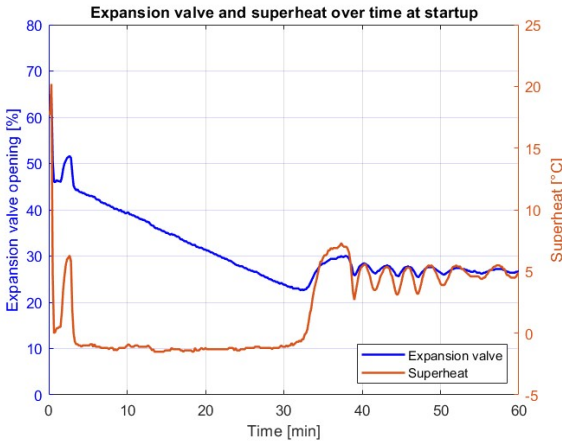

Figure 2.44 – Expansion valve opening percentage and superheating over time for Test 41

Chapter 3:
Development and description of the heat pump simulation model

3.1 Modelling methodology

In this chapter, three different heat pump models are developed in Simulink, including the start-up phase analyzed in the previous chapters. The models are then described and compared.
The following three approaches are presented, and Figure 3.1 provides a graphical representation of their conceptual idea.

1) **Penalty model:** this model calculates the thermal and electrical power during start-up using the penalty approach, incorporating interpolation[8] to predict the behavior in cases outside the experimental data. In this method, a certain percentage of the thermal and electrical power is subtracted to account for the reduced efficiency or limitations occurring during the start-up phase. Essentially, the "penalty" represents the portion of power that is not effectively delivered due to transient effects at the beginning of operation.
2) **Polynomial equation model:** the thermal and electrical power during start-up are calculated using a second-degree polynomial equation, which provides an approximation of the behavior observed during the start-up phase. This approach captures the general trend of the power variations while simplifying the modelling of transient effects.
3) **Transfer function model:** the thermal and electrical power during start-up are calculated using a transfer function, which provides an approximation of the behavior observed during the start-up phase. A transfer function represents the dynamic relationship between the input and output of a system and is commonly used to model system responses in the time domain through its transient behavior. This approach captures the general trend of the power variations while simplifying the modelling of transient effects, allowing the start-up dynamics to be represented without a full dynamic simulation.

Figure 3.1 shows the behavior of the three different models, each of which approximates the slope of the thermal and electrical power in a different way.
The penalty model generates a step function with a single vertical jump from the start-up power level to the steady-state power level, representing the two stages of power during the start-up phase.
The polynomial equation model generates a second-degree equation that reaches its maximum at the start-up time, after which a straight line represents the steady-state. This model provides a simple mathematical approximation given by the combination of two functions: a parabola and a straight line.

[8] An alternative approach to interpolation, based on a neural network, was also considered. In this case, a feedforward neural network was created using the MATLAB function fitnet, which defines a supervised learning model composed of interconnected layers of neurons trained to approximate a nonlinear relationship between inputs and outputs based on example data. However, this approach was ultimately abandoned, as the results were difficult to predict and, in some cases, physically inconsistent with the expected system behavior; therefore, it is not included in this study.

The transfer function model directly approximates the power behavior using a transfer function, capturing the dynamic response without explicitly separating start-up and steady-state.

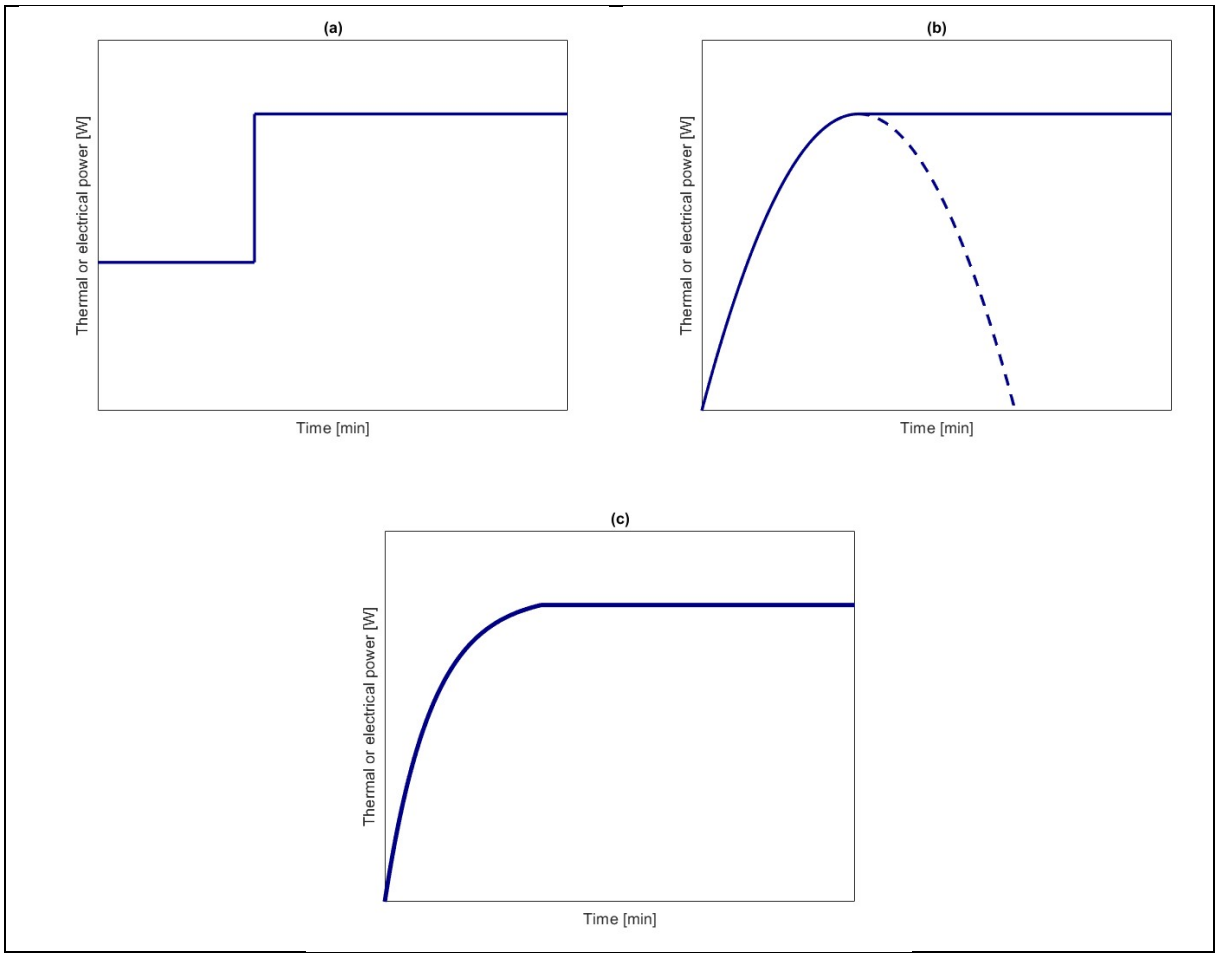

Figure 3.1 - Conceptual representation of the three start-up approximation models: (a) Penalty model, (b) Polynomial equation model, (c) Transfer function model

3.1.1 Penalty model

The model is divided into two subsystems: one for the ASO logic and one for the GSO logic. As shown in Figure 3.2, the inputs of the **ASO subsystem** are T_{ext}, ssf, the steady-state thermal and electrical power, and ΔT. In order to simplify the model, the shutdown time is not taken into account, and the cases of heating production and domestic hot water production are clearly distinguished.

Figure 3.2 - Interface of the penalty model for ASO with inputs on the left and outputs on the right

Figure 3.3 shows what is inside the subsystem:

- in blue, a Bus Creator, which groups all the inputs;
- in red, a Bus Selector, which extracts the required inputs;
- in green, two Enabled Subsystems, which are activated only when their input is equal to 1 (true);
- in yellow, two Relational blocks, which output 0 if the condition is not satisfied and 1 if it is satisfied;
- in orange, another Subsystem that selects the correct output.

The Bus Creator groups all the inputs, which can then be called by the Bus Selector. Using buses is not strictly necessary, but they make the model clearer. The two Enabled Subsystems analyze two different situations: heating production and domestic hot water production. Domestic hot water production is considered when the ΔT is higher than 30 °C, and this condition is set by the Relational blocks. Since the two Enabled Subsystems generate four possible outputs (two for electrical power and two for thermal power), another Subsystem is required to select the correct two outputs.

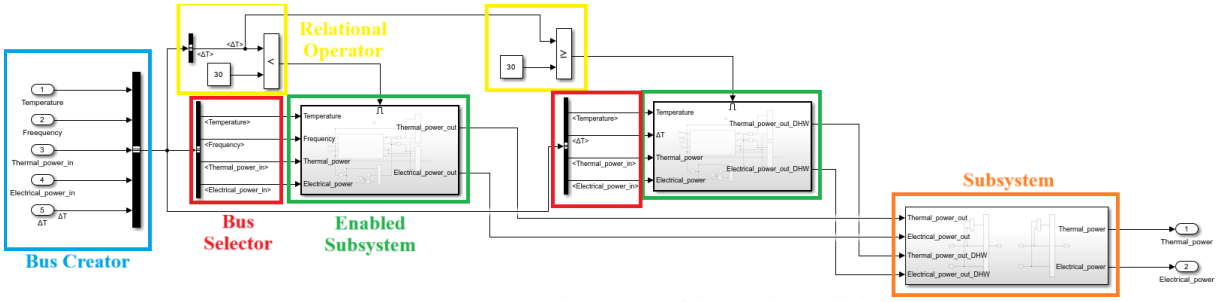

Figure 3.3 – Internal structure of the penalty model

The two Enabled Subsystems are very similar; the only differences lie in the inputs they use and in the interpolated data from which the outputs are derived.
In the first Enabled Subsystem ($\Delta T < 30$ °C), ΔT is not used as an input. In the second Enabled Subsystem ($\Delta T \geq 30$ °C), ΔT is considered as an input, while ssf is no longer taken into account. The internal structure of the Enabled Subsystems is shown in Figure 3.4, and the elements are as follows:

- in orange, a Subsystem that takes the inputs necessary for the interpolation and calculates the outputs; this is the core of the model.
- in red, a Compare to Zero block that allows the model to detect when the heat pump is activated, monitoring the electrical power; when electrical power is greater than zero, the model begins to count the start-up time.
- in yellow, a Discrete-Time Integrator block that counts the time elapsed after the heat pump is activated.
- in blue, the first Multiport Switch outputs the counted time when the heat pump is running (electrical power above zero and Compare to Zero outputs 1), and outputs infinity when the heat pump is off.
- in green, Relational Operator blocks compare the thermal and electrical start-up times with the output of the first Multiport Switch; they output 1 if the condition is satisfied, 0 otherwise.
- in blue, the other two Multiport Switches output the thermal and electrical power with the penalty when the relational operators output 1 (start-up time longer than counted

time), and steady-state thermal and electrical power when the Relational Operators output 0 (start-up finished or heat pump off).

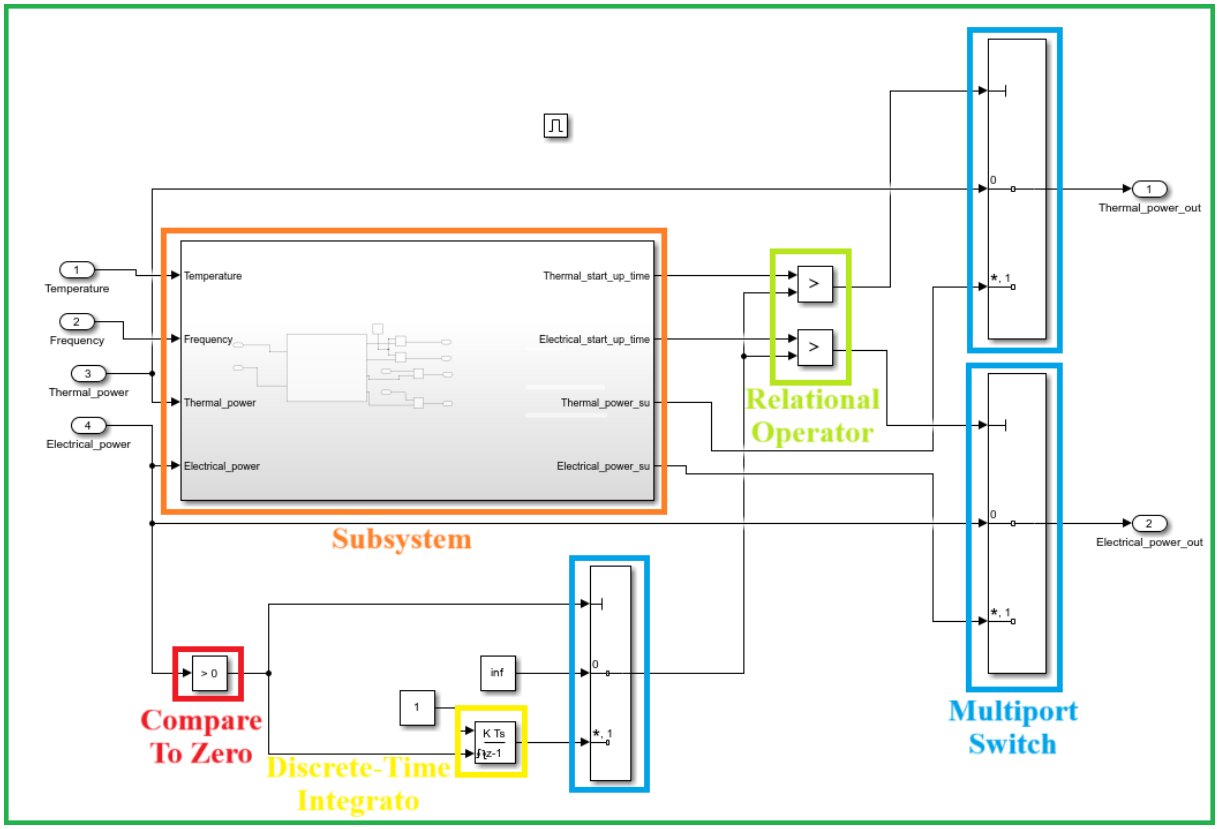

Figure 3.4 – Internal structure of the green Enabled Subsystems in Figure 3.3 (penalty model)

Inside the orange Subsystem, as shown in Figure 3.5:

- in green, a MATLAB Function block takes T_{ext} and ssf as inputs, performs interpolation, and returns the thermal and electrical start-up times (in minutes) and the corresponding reductions in power.
- in blue, Product blocks convert the start-up times to seconds and apply the penalty to the thermal and electrical power to generate the final outputs.

The MATLAB command "scatteredInterpolant" is used to construct an interpolant from scattered data, applying the linear method for interpolation and the nearest method for extrapolation (value of the closest point outside the data domain), returning a function that estimates values at any requested position. The command is described in more detail in Appendix E.

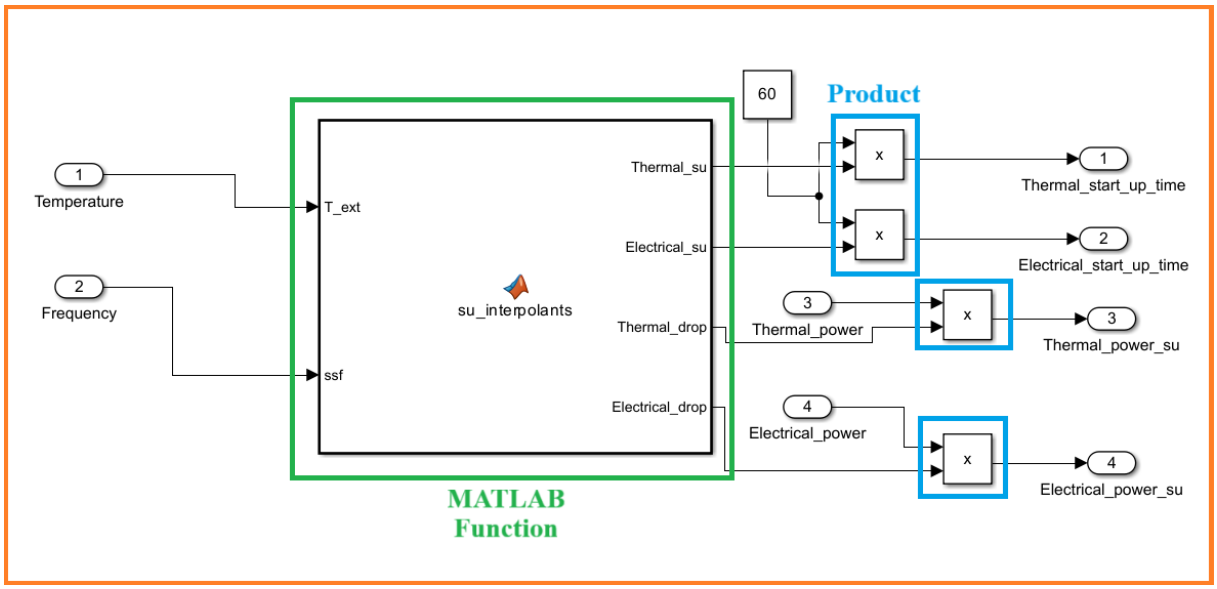

Figure 3.5 – Internal structure of the orange Subsystems in Figure 3.4

Referring to Figure 3.3, by opening the orange Subsystem it is possible to see how the correct output is selected; as shown in Figure 3.6, a Relational Operator compares the thermal and electrical power outputs from both Enabled Subsystems, and a Multiport Switch selects the higher value. This strategy works because when an Enabled Subsystem is not active, its output is zero; therefore, if both Enabled Subsystems are inactive, the output is zero, while if one of the two is active, the output corresponds to the Enabled Subsystem that is operating.

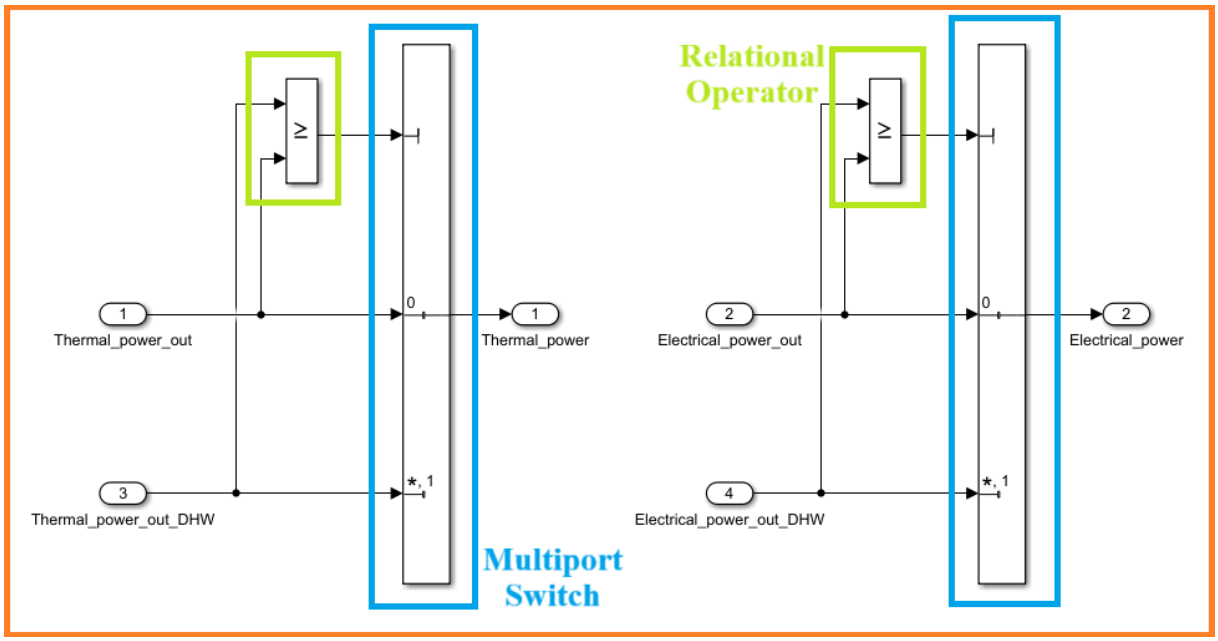

Figure 3.6 – Internal structure of the orange Subsystems in Figure 3.3

As shown in Figure 3.7, the inputs for the **GSO subsystem** are ssf, ΔT and the steady-state thermal and electrical power.

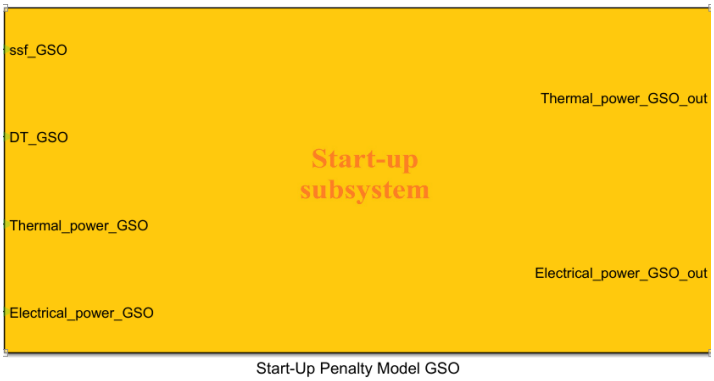

Figure 3.7 - Interface of the penalty model for GSO with inputs on the left and outputs on the right

The internal structure of this Subsystem is similar to that shown in Figures 3.4 and 3.5; only the inputs and the interpolated data change.

3.1.2 Polynomial equation model

The idea of this method is to approximate the thermal and electrical start-up power using a second-degree polynomial equation:

$$y = ax^2 + bx + c \tag{10}$$

In this way, it is possible to determine the coefficients a, b, and c to describe the behavior of the start-up. In Equation (10), y represents the power and x represents the time.
It is also possible to interpolate the coefficients to approximate the behavior when the initial conditions differ from those used in the experiments.
To determine the coefficients, some boundary conditions are established:

- The power is zero at time zero.
- The power reaches its maximum at the end of the start-up time.
- The derivative of the power with respect to time is zero at the end of the start-up time.

Convert the following into an equation:

$$\begin{cases} c = 0 \\ y_{max} = a{x_{su}}^2 + bx_{su} + c \\ \left.\dfrac{dy}{dx}\right|_{x=x_{su}} = 0 \end{cases} \tag{11}$$

where y_{max} is the power at steady-state and x_{su} is the start-up time. By solving the system, it is possible to obtain the coefficients a and b:

$$\begin{cases} y_{max} = a{x_{su}}^2 + bx_{su} \\ 2ax_{su} + b = 0 \end{cases}$$

$$\begin{cases} b = -2ax_{su} \\ y_{max} = a{x_{su}}^2 - 2a{x_{su}}^2 \end{cases}$$

$$\begin{cases} a = -\dfrac{y_{max}}{{x_{su}}^2} \\ b = \dfrac{2y_{max}}{x_{su}} \end{cases} \tag{12}$$

Using Equations (12), it is possible to determine the coefficients a and b for the different tests and interpolate them.

The model is divided into two subsystems: one for the ASO logic and one for the GSO logic. In this model, it is not necessary to provide the thermal and electrical power as inputs, as was required in the penalty method. Instead, the thermal and electrical power at steady-state are obtained directly, as they correspond to the maximum values of the parabola defined by the second-degree equation.
As shown in Figure 3.8, the inputs of the **ASO subsystem** are T_{ext}, ssf, t_{stop}, and ΔT. In order to simplify the model, only shutdown times of 2 and 60 minutes are used, and the cases of heating production and domestic hot water production are clearly distinguished.

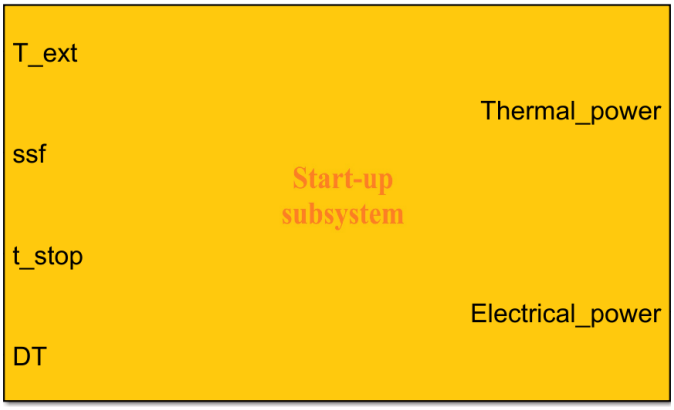

Figure 3.8 - Interface of the polynomial equation model for ASO with inputs on the left and outputs on the right

The model inside the Subsystem is similar to the one used for the penalty method in Figure 3.3: the only differences are the inputs and the internal structure of the Enabled Subsystem.
The two Enabled Subsystems are very similar; the only differences lie in the inputs they use and in the interpolated coefficients from which the outputs are derived.
In the first Enabled Subsystem ($\Delta T < 30$ °C), ΔT is not used as an input. In the second Enabled Subsystem ($\Delta T \geq 30$ °C), ΔT is considered as an input, while ssf and the shutdown time are no longer taken into account.
Opening the first Enabled Subsystem (the second is identical), there are two subsystems inside, as shown in Figure 3.9: the red Subsystem calculates the thermal power, while the green Subsystem calculates the electrical power.

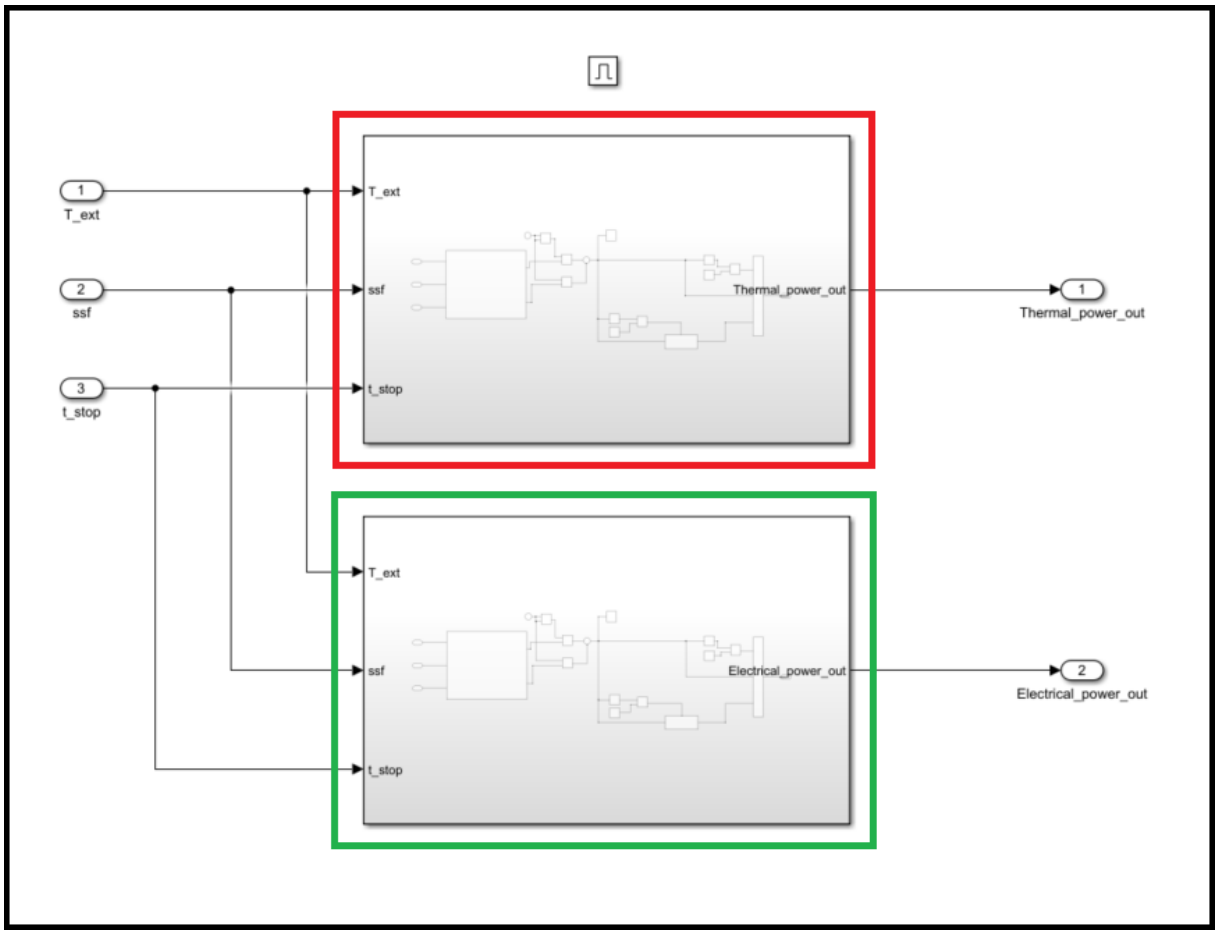

Figure 3.9 – Internal structure of the green Enabled Subsystems in Figure 3.3 (polynomial model)

Opening one of these two subsystems (they are identical, the only differences are the data inside), the core of the model can be seen, as shown in Figure 3.10:

- In green, the MATLAB Function block provides the interpolation and extrapolation of the coefficients a and b for different conditions.
- In orange, blue, and yellow, a Clock block, three Product blocks, and a Sum block implement Equation (10); the Clock block counts the time and represents x (time) in the equation.
- In brown, the two Relational Operators, combined with a Derivative block and a Constant block, analyse the slope of the parabola.
- In red, a Multiport Switch selects the correct power: if the slope is increasing, the power is described by Equation (10); if the slope is decreasing, the power is represented by a straight line equal to the maximum power.
- In grey, the Enabled Subsystem is empty (composed only of input and output) and is used to store the maximum power. It is active while the slope is increasing, and when the slope begins to decrease, it saves the last value, which corresponds to the maximum power.

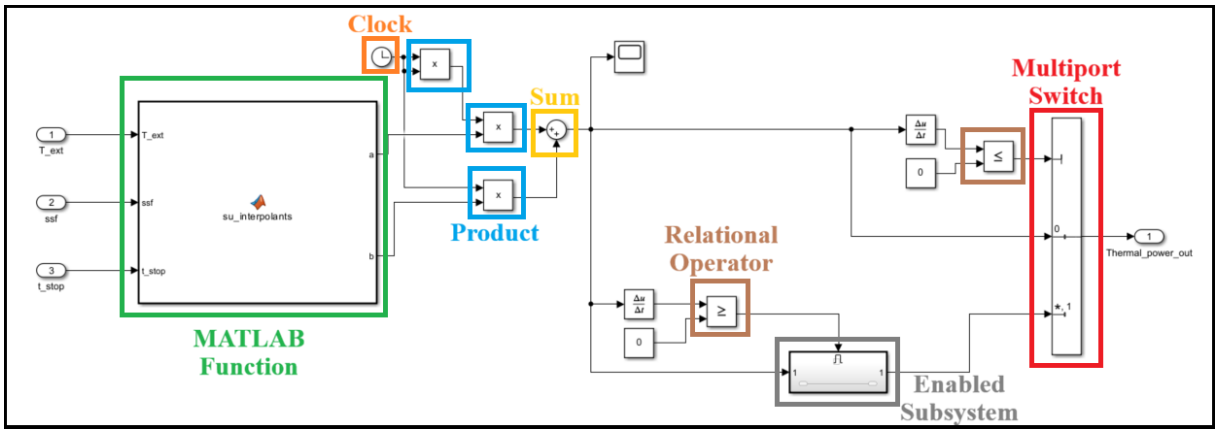

Figure 3.10 – Internal structure of the red Subsystems in Figure 3.9 (polynomial model)

As shown in Figure 3.11, the inputs for the **GSO subsystem** are ssf and ΔT:

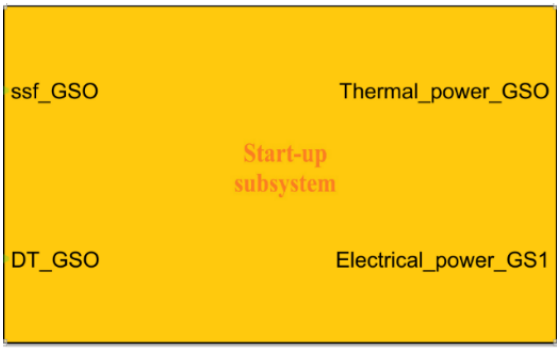

Figure 3.11 - Interface of the polynomial equation model for GSO with inputs on the left and outputs on the right

The internal structure of this Subsystem is similar to that shown in Figures 3.9 and 3.10; only the inputs and the interpolated data change.

3.1.3 Transfer function model

The transfer function model is introduced to describe the thermal and electrical power evolution during the start-up phase through a simplified dynamic representation of the system. The transfer function provides a mathematical framework that reproduces the gradual variation of thermal and electrical power over time, reflecting the physical response of the system without requiring a fully detailed dynamic simulation. As a result, the transfer function model provides a good compromise between computational simplicity and physical realism, making it suitable for applications where an accurate description of start-up behavior is required.
The idea is to provide a step function as input, which transitions from zero to the steady-state thermal and electrical power, and to use the transfer function to obtain an output that reproduces the experimental results.
The step function can be easily determined for each experiment, since the steady-state thermal and electrical power are known. The transfer function can be obtained using the "System Identification Toolbox", a MATLAB tool that allows a transfer function to be identified from experimental data by providing an input signal, in this case the step function. The System Identification Toolbox is described in more detail in Appendix E.

Since the System Identification Toolbox requires the experimental data as output to identify the transfer function, unlike the previous cases, this method necessitates knowledge of the entire evolution of the thermal and electrical power signals.

The following transfer function is implemented in the model:

$$u(t) = \int \left(\frac{a}{b} \cdot y(t) - \frac{c}{b} \cdot u(t)\right) dt \tag{13}$$

In Equation (13), the output (thermal or electrical power) is represented by $u(t)$ while the input (the step function) is represented by $y(t)$. The coefficients (a, b, c) are obtained from the System Identification Toolbox and define the transfer function. For each test, three coefficients can be identified, which define the transfer function for that specific experiment. Through interpolation, new coefficients can then be obtained, and consequently new transfer functions and step functions can be generated, allowing the power trends to be described also outside the experimental ranges. As in the other cases, linear interpolation was used for interpolation, while the nearest method was adopted for extrapolation in order to avoid estimation errors.

The model is divided into two subsystems: one for the ASO logic and one for the GSO logic. In this model, it is not necessary to provide the thermal and electrical power as inputs, as was required in the penalty method, because the transfer function directly approximates the entire behavior of both the thermal and electrical power.
As shown in Figure 3.12, the inputs of the **ASO subsystem** are T_{ext}, ssf, t_{stop}, and ΔT. In order to simplify the model, only shutdown times of 2 and 60 minutes are used, and the cases of heating production and domestic hot water production are clearly distinguished.

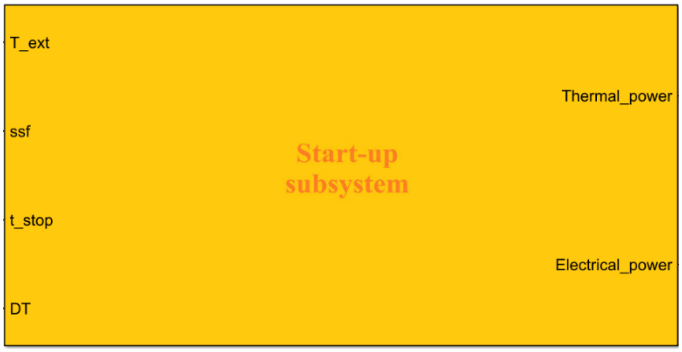

Figure 3.12 - Interface of the transfer function model for ASO with inputs on the left and outputs on the right

The model inside the Subsystem is similar to the one used for the penalty method in Figure 3.3. The two Enabled Subsystems are very similar; the only differences lie in the inputs they use and in the interpolated coefficients from which the outputs are derived.
In the first Enabled Subsystem ($\Delta T < 30$ °C), ΔT is not used as an input. In the second Enabled Subsystem ($\Delta T \geq 30$ °C), ΔT is considered as an input, while ssf and the shutdown time are no longer taken into account.
The internal structure of the green Enabled Subsystems is identical to that of the polynomial equation model shown in Figure 3.9.
There are two subsystems inside: the red Subsystem calculates the thermal power, while the green Subsystem calculates the electrical power.

Opening one of these two subsystems (they are identical, the only differences are the data inside), the core of the model can be seen, as shown in Figure 3.13:

- In green, the MATLAB Function blocks provide: the interpolation and extrapolation for different conditions of (1) the thermal (or electrical) power in steady-state, (2) the step function needed as input in the transfer function and the interpolation and extrapolation for different conditions of (3) the two coefficients that define the transfer function (three in total, however one of the three coefficients is always constant and equal to 1).
- In orange, a Clock block counts the time for generating the step function.
- In red, a Subsystem containing the transfer function. This Subsystem takes the step function and the coefficients as inputs and provides the thermal (or electrical) power signal as output.

Figure 3.14 shows the internal structure of the red Subsystem in Figure 3.13, which represents the transfer function. The Subsystem reproduces Equation (13) using:

- In green, two Product blocks.
- In yellow, a Sum block.
- In blue, an Integrator block.

Since one of the three coefficients is always equal to 1, Equation (13) can be rewritten as:

$$u(t) = \int (a \cdot y(t) - c \cdot u(t))dt \tag{14}$$

The two Product blocks together with the Sum block reproduce the integrand of Equation (14), while the Integrator block performs the integration to obtain $u(t)$.

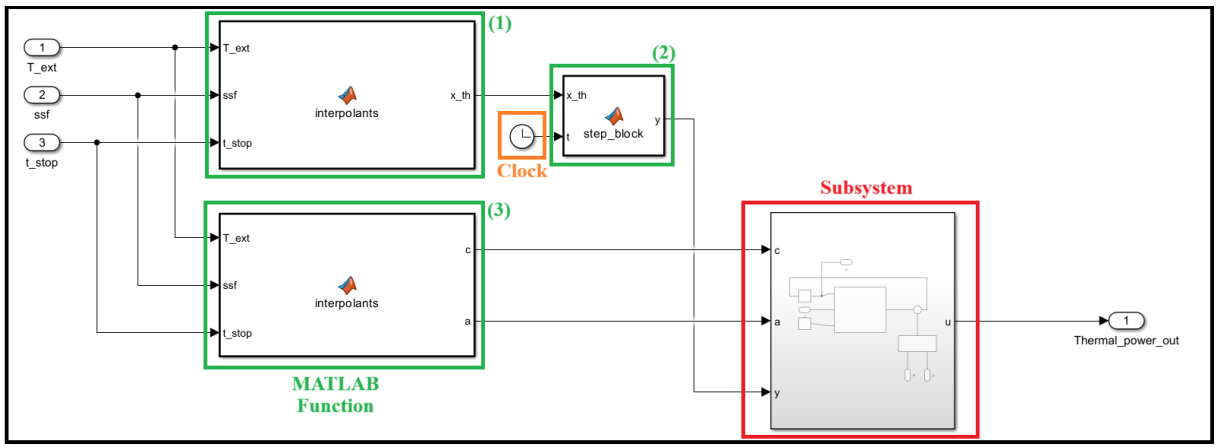

Figure 3.13 – Internal structure of the red Subsystems in Figure 3.9 (transfer function model)

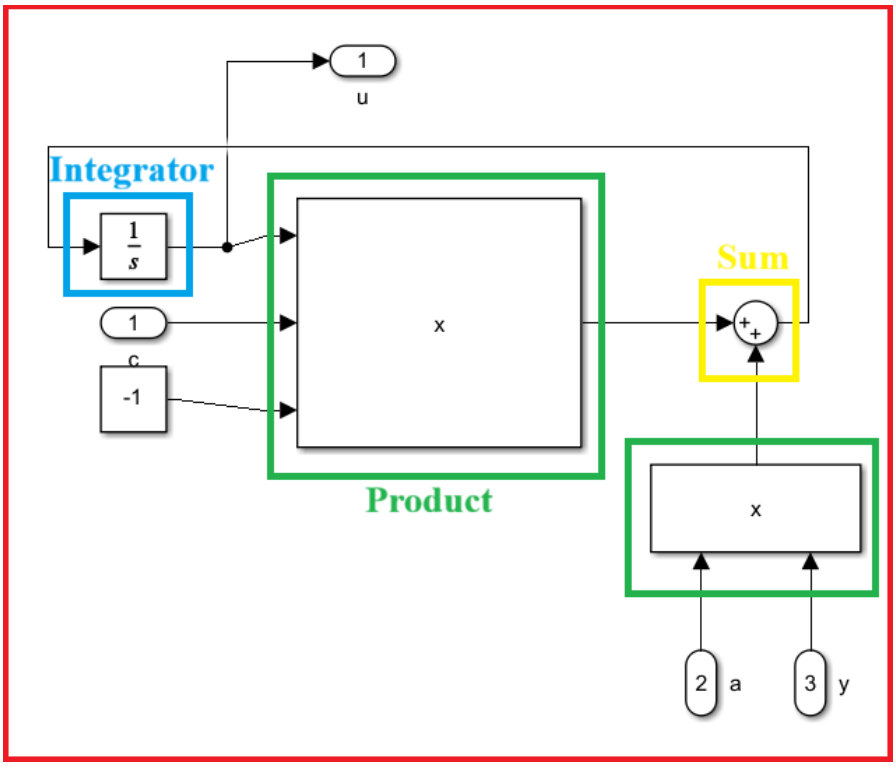

Figure 3.14 – Internal structure of the red Subsystems in Figure 3.13

As shown in Figure 3.15, the inputs for the **GSO subsystem** are ssf and ΔT:

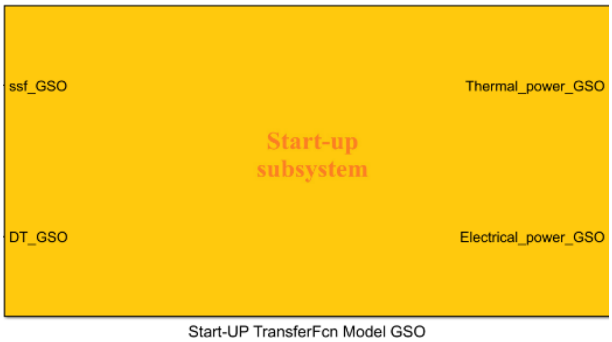

Figure 3.15 - Interface of the transfer function model for GSO with inputs on the left and outputs on the right

The internal structure of this Subsystem is similar to that shown in Figures 3.9, 3.13 and 3.14; only the inputs and the interpolated data change.

3.2 Modelling results and discussion

In this section, the results of the experiments used to develop the models, the results obtained from the execution of the models, and their discussion are presented. The thermal and electrical energies during start-up obtained from the execution of each model are compared in order to identify the model that best approximates the start-up phase, in agreement with the experimental data.

3.2.1 Results

This section presents the data used to develop the model (derived from the experimental results reported in Appendix C), their processing, and the results obtained by running the model once implemented.
For each of the three models, a graphical example of the simulation output is provided, and the thermal and electrical energies during the start-up phase are reported in order to compare them with the corresponding experimental values and evaluate how accurately the models approximate the start-up behavior.

3.2.1.1 Penalty model results

The data used to build the **ASO subsystem** are reported in Table 3.1. As with the 9 cases presented in Table 2.11, the first 9 cases in Table 3.1 are calculated as the average of the results obtained from the 27 main experiments for the three different t_{stop} values. Cases 10 to 13 correspond to the results of the 4 additional experiments conducted for higher ΔT_{sink}.
The thermal and electrical percentages represent the proportion of the steady-state power that is delivered on average during the start-up. For example, in Case 1, a thermal percentage of 0.82 indicates that the thermal power during start-up corresponds to 82% of the power actually delivered at steady-state. These values were derived from Table C.6 in Appendix C, which reports the thermal and electrical drops. They indicate the percentage by which the thermal and electrical power decreases during start-up, and are calculated as follows:

$$Power\ drop = \frac{Average\ startup\ power - Steadystate\ power}{Steadystate\ power} \times 100 \qquad (15)$$

The power drop will be a negative value, since the power during start-up is lower than at steady-state, and therefore the thermal and electrical percentages are calculated as follows:

$$Power\ percentage = 100 + Power\ drop \qquad (16)$$

Table 3.1 – Data used to build the penalty model for ASO

Case N°	Frequency	Temperature [°C]	Dtsink [°C]	Thermal transient duration [min	Electrical transient duration [min	Thermal percentage	Electrical percentage
Case 1	0.25	20	5.41	10.22	2.22	0.82	0.76
Case 2	0.25	7	4.69	23.28	2.89	0.75	0.83
Case 3	0.25	2	4.09	18.61	2.78	0.67	0.86
Case 4	0.50	20	8.76	44.00	3.67	0.79	0.65
Case 5	0.50	7	7.26	7.83	3.94	0.62	0.68
Case 6	0.50	2	6.60	14.06	4.17	0.72	0.69
Case 7	0.75	20	12.60	62.17	36.28	0.72	0.86
Case 8	0.75	7	10.26	31.61	4.72	0.79	0.63
Case 9	0.75	2	9.36	8.94	4.44	0.59	0.60
Case 10	0.5	7	14.26	11.17	5.33	0.56	0.68
Case 11	0.5	7	33.84	20.33	12.83	0.51	0.66
Case 12	0.5	20	34.98	27.50	12.83	0.59	0.66
Case 13	0.5	20	15.56	46.50	4.50	0.74	0.64

The data used to build the **GSO subsystem** are reported in Table 3.2. These data are derived from the results of the five experiments related to the GSO case. The thermal and electrical percentages are calculated in exactly the same way as for the ASO case.

Table 3.2 – Data used to build the penalty model for GSO

Test n°	Frequency	Dtsink [°C]	Thermal transient duration [min]	Electrical transient duration [min]	Thermal percentage	Electrical percentage
TEST 37	0.50	4.78	15.17	3.67	0.79	0.73
TEST 38	0.25	3.29	54.67	7.17	0.56	0.90
TEST 39	0.75	6.36	12.50	3.50	0.82	0.71
TEST 40	0.50	15.43	14.17	6.50	0.64	0.74
TEST 41	0.50	34.77	41.50	16.67	0.49	0.73

In Figure 3.16, an example is reported showing how the penalty method is applied to the thermal power (the same approach is used for the electrical power). Test 37, corresponding to the GSO case, was chosen as an example. This choice is purely arbitrary and the same test will be used for the other two models as well, so that a final comparison can be made in a single figure, highlighting the differences in the simulation results of the three models.

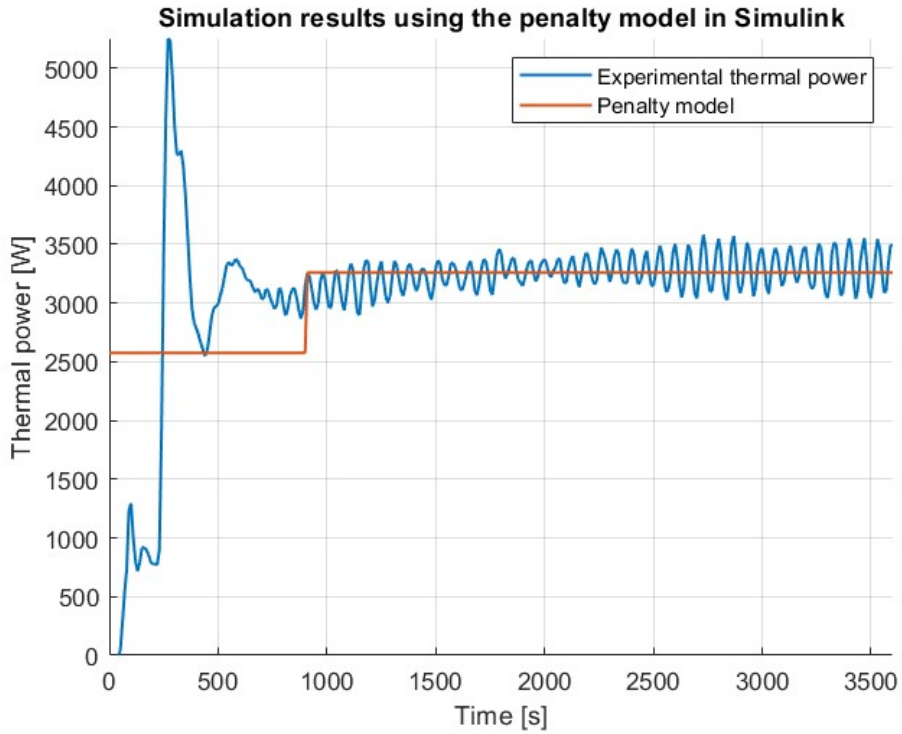

Figure 3.16 – Example of the penalty method applied to the thermal power during start-up (Test 37)

Table 3.3 reports the thermal and electrical energy during start-up obtained from the model simulations.

Table 3.3 – Thermal and electrical energy during start-up obtained from the penalty model simulations

Penalty model results																												
TEST N°	1	3	4	6	7	9	10	12	13	15	16	18	19	21	22	24	25	27	33	34	35	36	37	38	39	40	41
Thermal energy during the start-up phase [kWh]																											
	0.46	0.46	3.63	3.63	7.17	7.17	0.69	0.69	0.40	0.40	3.18	3.18	0.42	0.42	0.76	0.76	0.61	0.61	0.41	0.73	1.50	3.51	0.65	0.65	0.83	0.50	0.83
Electrical energy during the start-up phase [kWh]																											
	0.01	0.01	0.04	0.04	0.83	0.83	0.02	0.02	0.04	0.04	0.08	0.08	0.02	0.02	0.04	0.04	0.07	0.07	0.04	0.19	0.20	0.03	0.03	0.03	0.05	0.05	0.20

3.2.1.2 Polynomial equation model results

The data used to build the **ASO subsystem** are reported in Tables 3.4 and 3.5. As presented in Table 3.4, in order to simplify the model, only shut-down times of 2 and 60 minutes are considered; these data are derived from the results of the 27 main experiments and correspond to those reported in Tables 2.7 and C.4. The data in Table 3.5 are derived from the four additional experiments conducted for higher ΔT_{sink}values and correspond to those reported in Tables 2.9 and C.4.

Table 3.4 – Data used to build the polynomial equation model for ASO (different temperatures, frequencies and stop times)

TEST N°	Frequency [%]	Temperature [°C]	Time stop [min]	Thermal power in steady-state [W]	Electrical power in steady-state [W]	Thermal transient duration [min]	Electrical transient duration [min]
TEST 1	0.25	20	60	3292.74	380.22	10.17	2.67
TEST 3	0.25	20	2	3290.71	383.86	10.67	1.33
TEST 4	0.50	20	60	6257.01	882.99	45.83	3.83
TEST 6	0.50	20	2	6269.55	887.48	40.50	3.50
TEST 7	0.75	20	60	9614.09	1600.62	63.00	38.33
TEST 9	0.75	20	2	9551.50	1595.91	60.33	32.50
TEST 10	0.25	7	60	2341.45	428.83	24.33	3.00
TEST 12	0.25	7	2	2369.81	422.88	27.00	2.83
TEST 13	0.50	7	60	4943.55	905.87	8.83	4.17
TEST 15	0.50	7	2	4983.49	905.19	8.33	3.83
TEST 16	0.75	7	60	7580.16	1542.77	26.50	5.00
TEST 18	0.75	7	2	7620.95	1538.12	31.83	4.50
TEST 19	0.25	2	60	2006.07	446.54	17.50	3.00
TEST 21	0.25	2	2	2064.37	440.27	15.00	2.67
TEST 22	0.50	2	60	4444.52	905.03	14.17	4.33
TEST 24	0.50	2	2	4461.55	906.22	13.33	4.00
TEST 25	0.75	2	60	6803.32	1531.29	9.33	4.50
TEST 27	0.75	2	2	6873.05	1533.05	8.00	4.50

Table 3.5 – Data used to build the polynomial equation model for ASO (different temperatures and ΔT)

TEST N°	Frequency [%]	Temperature [°C]	Thermal power in steady-state [W]	Electrical power in steady-state [W]	Thermal transient duration [min]	Electrical transient duration [min]	Dtsink [°C]
TEST 4	0.50	20	6257.01	882.99	45.83	3.83	9.68
TEST 13	0.50	7	4943.55	905.87	8.83	4.17	8.41
TEST 33	0.50	7	5025.69	901.67	11.17	5.33	14.26
TEST 34	0.50	7	4235.88	1356.49	20.33	12.83	33.84
TEST 35	0.50	20	5537.95	1390.23	27.50	12.83	34.98
TEST 36	0.50	20	6062.21	879.50	46.50	4.50	15.56

The coefficients obtained using Equations (12) are presented in Tables 3.6 and 3.7. The coefficients a, b, c and d in Table 3.6 are obtained from the data reported in Table 3.4, while the coefficients e, f, g and h are obtained from the data in Table 3.5. Coefficients a, b, e and f refer to the thermal power, whereas coefficients c, d, g and h refer to the electrical power.

Table 3.6 – Coefficients obtained for the ASO case from the data in Table 3.4 (polynomial equation model)

a	b	c	d
-0.008849081	10.79587924	-0.014852462	4.752787901
-0.008033971	10.28348262	-0.059977865	9.596458335
-0.000827374	4.550555483	-0.016691675	7.67817029
-0.001061754	5.160126001	-0.020124246	8.452183125
-0.00067286	5.086822592	-0.000302575	1.391846728
-0.000728877	5.27707144	-0.000419699	1.636825794
-0.001098446	3.20746372	-0.013235387	4.764739229
-0.000902989	2.925685512	-0.014632391	4.975012863
-0.017598965	18.65490248	-0.014493883	7.246941467
-0.019933979	19.93397888	-0.017111256	7.871177913
-0.002998362	9.534791849	-0.017141866	10.28511984
-0.00208902	7.980054695	-0.021098975	11.39344644
-0.001819564	3.821084084	-0.013782169	4.961580823
-0.002548602	4.58748344	-0.01719786	5.503315217
-0.006151589	10.457702	-0.01338808	6.961801437
-0.006971167	11.15386719	-0.015732938	7.551810089
-0.021694264	24.29757543	-0.021005347	11.34288756
-0.029830962	28.63772388	-0.021029554	11.35595919

Table 3.7 – Coefficients obtained for the ASO case from the data in Table 3.5 (polynomial equation model)

e	f	g	h
-0.00083	4.550555	-0.01669	7.67817
-0.0176	18.6549	-0.01449	7.246941
-0.0112	15.00205	-0.00881	5.635416
-0.00285	6.944068	-0.00229	3.523354
-0.00203	6.712661	-0.00234	3.610983
-0.00078	4.345672	-0.01206	6.514779

The data used to build the **GSO subsystem** are reported in Table 3.8. These data are derived from the results of the five experiments related to the GSO case and correspond to those reported in Tables 2.10 and C.4.
The coefficients obtained using the Equations (12) are presented in Table 3.9: i and l refer to the thermal power, whereas m and n refer to the electrical power.

Table 3.8 – Data used to build the polynomial equation model for GSO

TEST N°	Frequency [%]	Thermal power in steady-state [W]	Electrical power in steady-state [W]	Thermal transient duration [min]	Electrical transient duration [min]	Dtsink [°C]
TEST 37	0.50	3259.35	662.78	15.17	3.67	4.78
TEST 38	0.25	1278.65	311.71	54.67	7.17	3.29
TEST 39	0.75	4863.54	1100.47	12.50	3.50	6.36
TEST 40	0.50	3281.22	671.13	14.17	6.50	15.43
TEST 41	0.50	2442.53	972.08	41.50	16.67	34.77

Table 3.9 – Coefficients obtained for the GSO case from the data in Table 3.8 (polynomial equation model)

i	l	m	n
-0.00394	7.163397	-0.01369	6.025288
-0.00012	0.779666	-0.00169	1.449803
-0.00865	12.96944	-0.02495	10.4807
-0.00454	7.720512	-0.00441	3.441679
-0.00039	1.961868	-0.00097	1.944153

In Figure 3.17, an example is reported showing how the polynomial equation method is applied to the thermal power (the same approach is used for the electrical power).

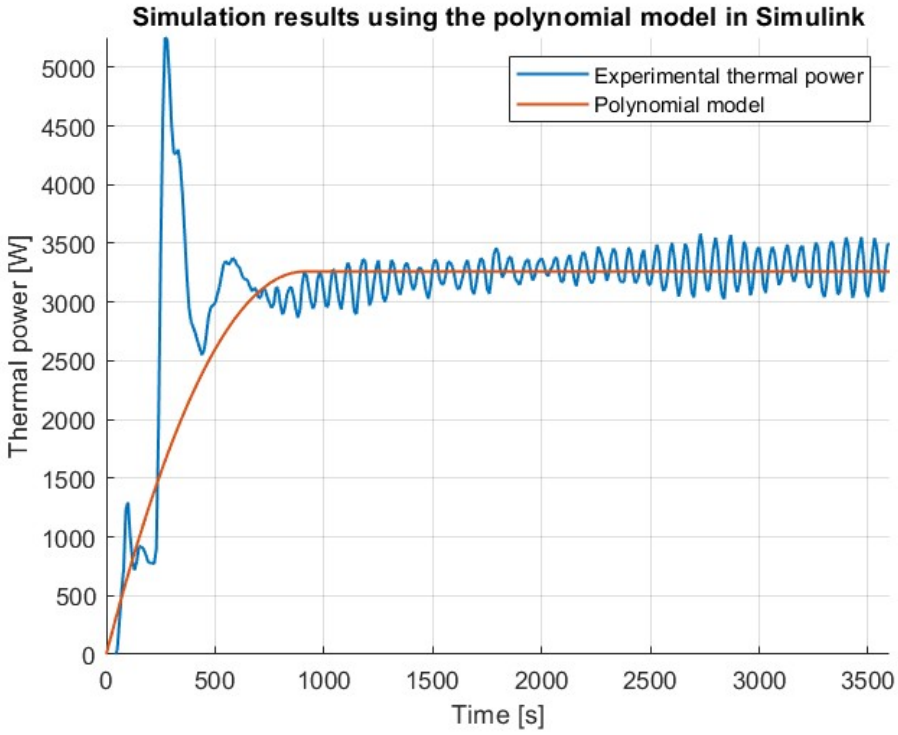

Figure 3.17 – Example of the polynomial equation method applied to the thermal power during start-up (test 37)

Table 3.10 reports the thermal and electrical energy during start-up obtained from the model simulations.

Table 3.10 – Thermal and electrical energy during start-up obtained from the polynomial equation model simulations

Polynomial equation model results																											
TEST N°	1	3	4	6	7	9	10	12	13	15	16	18	19	21	22	24	25	27	33	34	35	36	37	38	39	40	41
Thermal energy during the start-up phase [kWh]																											
	0.39	0.39	3.20	2.85	6.77	6.44	0.64	0.72	0.51	0.47	2.26	2.73	0.39	0.35	0.72	0.67	0.71	0.64	0.51	0.97	1.72	3.20	0.56	0.78	0.70	0.53	1.14
Electrical energy during the start-up phase [kWh]																											
	0.01	0.01	0.04	0.04	0.69	0.58	0.02	0.02	0.05	0.04	0.09	0.08	0.02	0.01	0.05	0.04	0.08	0.08	0.05	0.20	0.20	0.04	0.03	0.03	0.05	0.05	0.18

3.2.1.3 Transfer function model results

The data used to build the **ASO subsystem** are the same reported in Tables 3.4 and 3.5.
The coefficients obtained using the MATLAB tool "System Identification Toolbox" (presented in Appendix E) to implement Equation (13) are reported in Tables 3.11 and 3.12.

Table 3.11 – Coefficients obtained for the ASO case from the data in Table 3.4 (transfer function model)

a (thermal power)	b (thermal power)	c (thermal power)	d (electrical power)	e (electrical power)	f (electrical power)
0.006514	1	0.006514	0.03343	1	0.03337
0.01483	1	0.01472	0.05326	1	0.05329
0.002351	1	0.002548	0.01331	1	0.01328
0.0079	1	0.008718	0.015	1	0.01497
0.0008379	1	0.000832	0.006629	1	0.006816
0.001044	1	0.00106	0.008788	1	0.008981
0.002405	1	0.002444	0.03722	1	0.03722
0.006659	1	0.007136	0.03754	1	0.03745
0.003874	1	0.003822	0.01223	1	0.0122
0.006518	1	0.006497	0.01457	1	0.01454
0.003112	1	0.003145	0.008617	1	0.008571
0.004276	1	0.004443	0.01012	1	0.01008
0.001362	1	0.001253	0.02899	1	0.02895
0.009999	1	0.01007	0.06417	1	0.06396
0.003906	1	0.003878	0.01264	1	0.01261
0.005207	1	0.005207	0.01367	1	0.01364
0.003893	1	0.003849	0.009203	1	0.009172
0.004859	1	0.004805	0.009959	1	0.00992

Table 3.12 – Coefficients obtained for the ASO case from the data in Table 3.5 (transfer function model)

g (thermal power)	h (thermal power)	i (thermal power)	l (electrical power)	m (electrical power)	n (electrical power)
0.002351	1	0.002548	0.01331	1	0.01328
0.003874	1	0.003822	0.01223	1	0.0122
0.003226	1	0.003187	0.01033	1	0.01031
0.001438	1	0.001371	0.003816	1	0.003813
0.001213	1	0.001128	0.003798	1	0.003789
0.001429	1	0.00147	0.01031	1	0.01027

These coefficients are used in Equation (13) in combination with the step functions to obtain the outputs. Coefficients a, b, c, g, h and i are used to approximate the thermal power, while coefficients d, e, f, l, m and n are used to approximate the electrical power.
The data used to build the **GSO subsystem** are the same reported in Table 3.8.
The coefficients used to implement Equation (13) and obtained from the "System Identification Toolbox" are presented in Table 3.13: o, p and q refer to the thermal power, whereas r, s and t refer to the electrical power.

Table 3.13 – Coefficients obtained for the GSO case from the data in Table 3.8 (transfer function model)

o (thermal power)	p (thermal power)	q (thermal power)	r (electrical power)	s (electrical power)	t (electrical power)
0.005809	1.00	0.005796	0.02144	1	0.02143
0.0004227	1.00	0.0003233	0.04193	1	0.04201
0.009112	1.00	0.009131	0.01817	1	0.01812
0.002887	1.00	0.002836	0.01357	1	0.01363
0.0003905	1.00	0.0001202	0.004036	1	0.004079

In Figure 3.18, an example is reported showing how the penalty method is applied to the thermal power (the same approach is used for the electrical power).

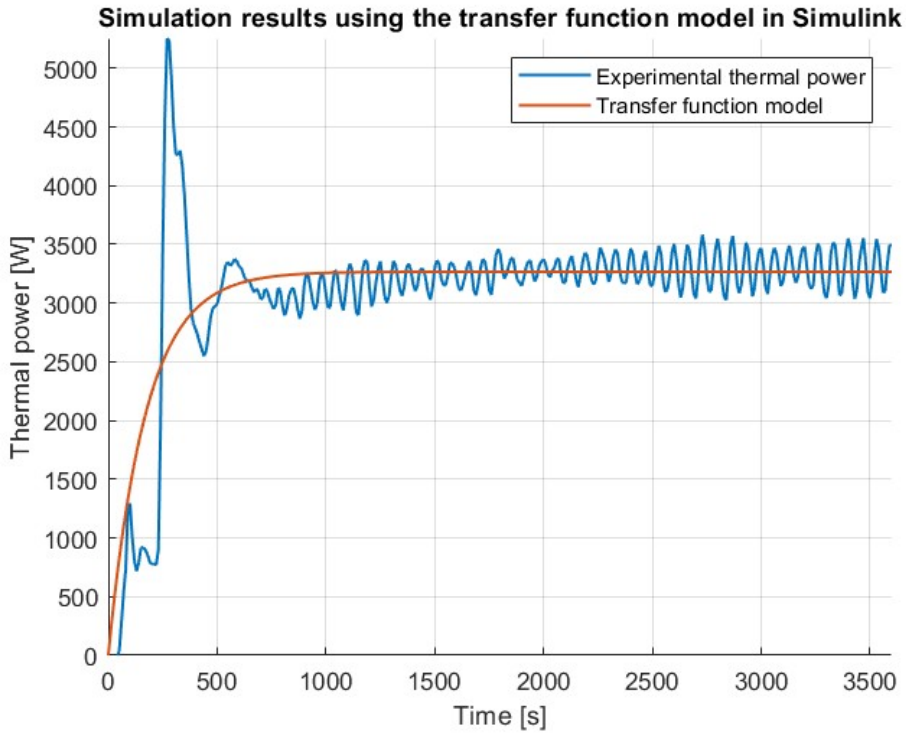

Figure 3.18 – Example of the transfer function method applied to the thermal power during start-up (Test 37)

Table 3.14 reports the thermal and electrical energy during start-up obtained from the model simulations.

Table 3.14 – Thermal and electrical energy during start-up obtained from the transfer function model simulations

Transfer function results																											
TEST N°	1	3	4	6	7	9	10	12	13	15	16	18	19	21	22	24	25	27	33	34	35	36	37	38	39	40	41
Thermal energy during the start-up phase [kWh]																											
	0.42	0.52	3.77	3.65	7.06	7.03	0.68	0.91	0.42	0.48	2.64	3.42	0.28	0.45	0.74	0.75	0.62	0.56	0.59	0.77	1.48	3.84	0.67	0.58	0.86	0.49	0.74
Electrical energy during the start-up phase [kWh]																											
	0.01	0.01	0.04	0.03	0.93	0.80	0.02	0.02	0.04	0.04	0.08	0.07	0.02	0.02	0.05	0.04	0.07	0.07	0.06	0.19	0.20	0.05	0.03	0.03	0.05	0.06	0.20

3.2.2 Discussion

In this section, the results obtained in Section 3.2.1 will be compared and discussed.
The results provided by the three different models are graphically compared in Figure 3.19. It can be clearly observed that, for the results of the polynomial model, the thermal power curve during start-up (in yellow) lies almost always below the actual thermal power obtained experimentally (in blue). This indicates that the polynomial model poorly approximates the start-up phase.
To determine which of the three developed models performs best, simulations can be carried out and the thermal and electrical energy during start-up can be analyzed, comparing them with the values obtained from the experimental analysis.
Table 3.15 reports the thermal and electrical energy during the start-up for the experiments and for the three developed models.

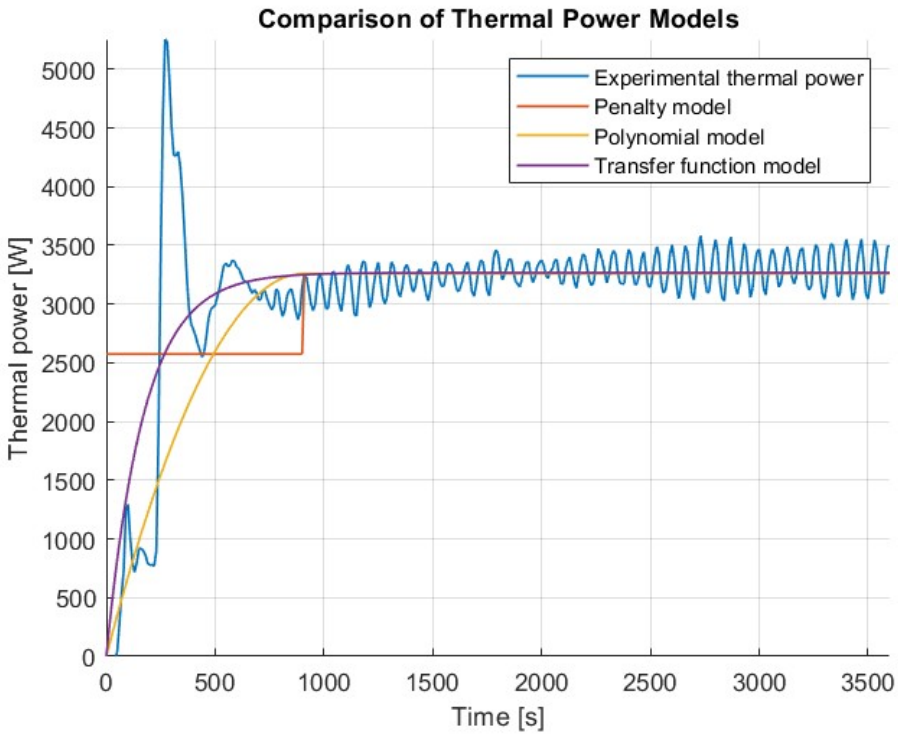

Figure 3.19 – Comparison of the results of the three different models applied to the thermal power during start-up (Test 37)

Table 3.15 - Thermal and electrical energy during the start-up for the experiments and for the three developed models

Thermal energy during the start-up phase [kWh]					Electrical energy during the start-up phase [kWh]				
TEST N°	Experiments	Penalty	Polynomial	Transfer FCN	TEST N°	Experiments	Penalty	Polynomial	Transfer FCN
TEST 1	**0.41**	**0.46**	**0.39**	**0.42**	TEST 1	**0.01**	**0.01**	**0.01**	**0.01**
TEST 3	**0.54**	**0.46**	**0.39**	**0.52**	TEST 3	**0.01**	**0.01**	**0.01**	**0.01**
TEST 4	**3.73**	**3.63**	**3.20**	**3.77**	TEST 4	**0.04**	**0.04**	**0.04**	**0.04**
TEST 6	**3.44**	**3.63**	**2.85**	**3.65**	TEST 6	**0.04**	**0.04**	**0.04**	**0.03**
TEST 7	**7.16**	**7.17**	**6.77**	**7.06**	TEST 7	**0.88**	**0.83**	**0.69**	**0.93**
TEST 9	**7.12**	**7.17**	**6.44**	**7.03**	TEST 9	**0.76**	**0.83**	**0.58**	**0.80**
TEST 10	**0.65**	**0.69**	**0.64**	**0.68**	TEST 10	**0.02**	**0.02**	**0.02**	**0.02**
TEST 12	**0.81**	**0.69**	**0.72**	**0.91**	TEST 12	**0.02**	**0.02**	**0.02**	**0.02**
TEST 13	**0.40**	**0.40**	**0.51**	**0.42**	TEST 13	**0.04**	**0.04**	**0.05**	**0.04**
TEST 15	**0.47**	**0.40**	**0.47**	**0.48**	TEST 15	**0.04**	**0.04**	**0.04**	**0.04**
TEST 16	**2.58**	**3.18**	**2.26**	**2.64**	TEST 16	**0.08**	**0.08**	**0.09**	**0.08**
TEST 18	**3.28**	**3.18**	**2.73**	**3.42**	TEST 18	**0.08**	**0.08**	**0.08**	**0.07**
TEST 19	**0.26**	**0.42**	**0.39**	**0.28**	TEST 19	**0.02**	**0.02**	**0.02**	**0.02**
TEST 21	**0.44**	**0.42**	**0.35**	**0.45**	TEST 21	**0.02**	**0.02**	**0.01**	**0.02**
TEST 22	**0.74**	**0.76**	**0.72**	**0.74**	TEST 22	**0.05**	**0.04**	**0.05**	**0.05**
TEST 24	**0.73**	**0.76**	**0.67**	**0.75**	TEST 24	**0.04**	**0.04**	**0.04**	**0.04**
TEST 25	**0.59**	**0.61**	**0.71**	**0.62**	TEST 25	**0.07**	**0.07**	**0.08**	**0.07**
TEST 27	**0.55**	**0.61**	**0.64**	**0.56**	TEST 27	**0.07**	**0.07**	**0.08**	**0.07**
TEST 33	**0.53**	**0.41**	**0.51**	**0.59**	TEST 33	**0.06**	**0.04**	**0.05**	**0.06**
TEST 34	**0.73**	**0.73**	**0.97**	**0.77**	TEST 34	**0.19**	**0.19**	**0.20**	**0.19**
TEST 35	**1.51**	**1.50**	**1.72**	**1.48**	TEST 35	**0.20**	**0.20**	**0.20**	**0.20**
TEST 36	**3.48**	**3.51**	**3.20**	**3.84**	TEST 36	**0.04**	**0.03**	**0.04**	**0.05**
TEST 37	**0.66**	**0.65**	**0.56**	**0.67**	TEST 37	**0.03**	**0.03**	**0.03**	**0.03**
TEST 38	**0.65**	**0.65**	**0.78**	**0.58**	TEST 38	**0.03**	**0.03**	**0.03**	**0.03**
TEST 39	**0.84**	**0.83**	**0.70**	**0.86**	TEST 39	**0.05**	**0.05**	**0.05**	**0.05**
TEST 40	**0.50**	**0.50**	**0.53**	**0.49**	TEST 40	**0.06**	**0.05**	**0.05**	**0.06**
TEST 41	**0.84**	**0.83**	**1.14**	**0.74**	TEST 41	**0.20**	**0.20**	**0.18**	**0.20**

To compare the three models and determine which one best approximates the start-up phase, the Root Mean Square Error (RMSE) can be computed for each model.
The RMSE is a statistical metric used to quantify the difference between predicted values and the corresponding experimental values. It is used to evaluate the accuracy of a model: a lower RMSE indicates better agreement between the model predictions and the experimental data, and therefore a better approximation of the phenomenon under investigation. The RMSE is defined as follows:

$$RMSE = \sqrt{\frac{1}{n} \cdot \sum_{i=1}^{n} (y_i - \hat{y}_i)^2} \tag{17}$$

where y_i is the predicted value (in this case from the model) and $\hat{y}_i$ is the expected value (in this case obtained from the experiments).

By plotting the RMSE obtained for each model in Figure 3.20, it can be observed that the transfer function model results are closer to the experimental data than those of the penalty and polynomial models. Among the three models, the polynomial one deviates most from the experimental results, as expected.
Both the penalty and the transfer function models perform well; the difference lies in their modelling approach: the transfer function model includes an additional input in the ASO case, which increases its accuracy by accounting for the heat pump shutdown time. The penalty model does not consider the shutdown time, which also explains the repeated results in the table (see Tests 1 and 3, 4 and 6, etc.).

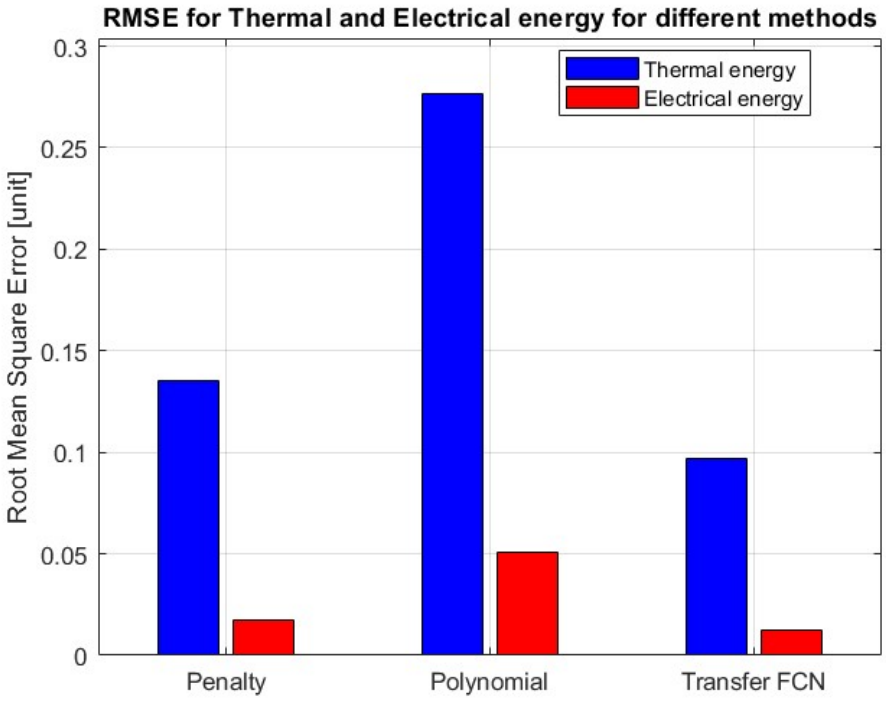

Figure 3.20 - RMSE for Thermal and Electrical energy for different methods

Among the three models, the least reliable is clearly the polynomial equation model. The choice should therefore be made between the penalty model and the transfer function model. Both models are reliable and consistent; however, their modeling approaches differ.
The penalty model requires the thermal and electrical power at steady state as inputs, whereas the transfer function model does not: it directly calculates the thermal and electrical power at steady state instead of receiving them as inputs, as in the penalty model. In addition, the penalty model does not account for the shutdown time, which makes it less precise than the transfer function model.
It is worth noting that the penalty model was originally developed to be implemented on a pre-existing heat pump model, which provides thermal and electrical power at steady state but does not consider start-up. This is why the penalty model does not automatically calculate the steady-state powers. Furthermore, the decision not to include the machine's shutdown time as a parameter was made to simplify the model as much as possible, thereby minimizing potential errors.
In Figure 3.21, the two models are compared, highlighting their advantages:

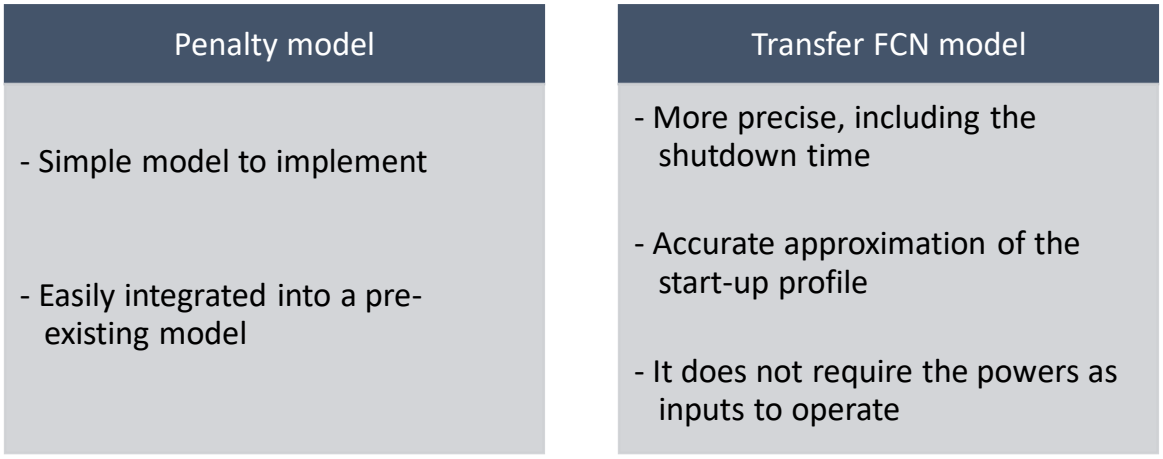

Figure 3.21 - Comparison of advantages for the penalty model and the transfer function model

In conclusion, the transfer function model is more accurate and immediate, providing a good approximation of the slope of the thermal or electrical power during start-up. For this reason, the recommended choice is this model.

The models can be modified and updated if higher accuracy is required. In all models, the distinction between heating production and domestic hot water production is rather approximate; this is due to the lack of sufficient data to extend the start-up time as a function of ΔT over the entire operating range. A possible future approach could be to collect new experimental data while ignoring the shutdown time, which, as observed in the experiments, has little impact, and instead focusing on ΔT. Of course, it is recommended that these new measurements be performed only after resolving the anomalous behavior of the expansion valves, which in some cases cause excessively slow or unstable start-ups.

Chapter 4:
Conclusions

4.1 Conclusion based on experimental results

This study analyzed the start-up phenomenon (start-up transient) of a prototype dual-source (air–ground) heat pump, manufactured by ratiotherm GmbH & Co. KG and installed at the Technische Hochschule Ingolstadt.
A total of 41 experiments were carried out: 36 using air as the source and 5 using the ground as the source. According to the literature presented in Section 1.4, the start-up phenomenon is influenced by four variables: T_{ext}, ssf, t_{stop} and ΔT_{sink}.
For the air-source operation (ASO), 27 experiments were carried out varying T_{ext}, ssf and t_{stop}, 5 experiments with a greater variation of t_{stop} and 4 experiments varying ΔT_{sink}.
For the ground-source operation (GSO), 5 experiments were carried out varying only ssf and ΔT_{sink}, since T_{ext} is almost constant throughout the year in the ground and because the influence of t_{stop} would require dynamic simulations of the ground, which were not conducted in this study.

The **results for ASO** are:

- The thermal start-up is always longer than the electrical start-up.
- The influence of t_{stop} is negligible.
- The PID controller of the expansion valve has a crucial role in the start-up phenomenon.
- High ΔT_{sink} leads to longer electrical start-up times.

The result that the thermal start-up is always longer than the electrical start-up is in accordance with the literature [13] presented in Section 1.4.
Longer t_{stop} was expected to lead to longer start-up times due to the migration of the refrigerant between the evaporator and the condenser caused by the pressure difference. However, this phenomenon is not observable because the expansion valve automatically opens when the heat pump is shut down. For this dual-source heat pump, the influence of the shutdown time is therefore negligible.
The PID controller of the expansion valve has a crucial role in the start-up phenomenon: it leads to longer thermal and electrical start-up times for high external temperatures and high ssf, in contrast with the literature [14] [16] in Section 1.4. Furthermore, the PID sometimes causes anomalous oscillations in the thermal power, making it difficult to detect the start-up time.
High ΔT_{sink} leads to longer electrical start-up times, but not necessarily to a longer thermal start-up due to the action of the PID controller.

The **results for GSO** are:

- The thermal start-up is always longer than the electrical start-up.
- The PID controller of the expansion valve has a crucial role in the start-up phenomenon.
- High ΔT_{sink} leads to longer electrical start-up times.

As for the ASO case, the experimental results show that the thermal start-up is always longer than the electrical start-up, and that the electrical start-up increases as ΔT_{sink} increases.

Also in the GSO case, the PID controller plays a crucial role in the start-up phenomenon: anomalous oscillations lead to unusually long thermal start-up times for $ssf = 25\%$ and for $\Delta T_{sink} = 35°C$. The expansion valve is excessively open at the beginning due to the PID controller, resulting in the absence of superheating during the initial phase. Moreover, the valve closes too slowly, causing the superheating to stabilize only after a long period, when the correct valve opening is finally reached and proper superheating can be established.

The **final conclusions** are that the electrical start-up time is always shorter than the thermal start-up time, and that the electrical start-up time increases as ΔT_{sink} increases.
The PID controller for the dual-source heat pump analyzed should be improved. Its current configuration leads to anomalous oscillations, which negatively affect the heat pump's efficiency. Moreover, the PID configuration leads to longer start-up times at high external temperatures and high ssf, resulting in reduced efficiency of the heat pump during the summer to produce domestic hot water.

4.2 Conclusion based on the execution of the models

The results collected from the experiments were used to develop three different Simulink models that approximate the start-up behavior. Three different approaches were adopted:

- The penalty approach generates a step function with a single vertical jump from the start-up power level to the steady-state power level, representing the two stages of power during the start-up phase.
- The polynomial equation approach generates a second-degree equation that reaches its maximum at the start-up time, after which a straight line represents the steady-state.
- The transfer function approach directly approximates the power behavior using a transfer function, capturing the dynamic response without explicitly separating start-up and steady-state.

The three models were developed and subsequently executed, and the obtained results were compared with the experimental results. For each of the three models, the thermal and electrical energies during the start-up phase were calculated in order to compare them with the corresponding experimental values and evaluate how accurately the models approximate the start-up behavior.
The results obtained from the executions of the three models are:

- The polynomial equation model is not accurate.
- Both the penalty model and the transfer function model are consistent and accurate.
- The transfer function model is more accurate than the penalty model because it also considers the shutdown time.
- The transfer function model approximates not only the transient behavior but also the steady-state. This makes the model self-sufficient and directly ready for use.
- The penalty model is the simplest model.
- The penalty model avoids possible errors because it is more approximate and does not take the shutdown time into account.
- The penalty model is the easiest to implement in a pre-existing model.

In conclusion, several suggestions for potential improvements to the prototype and to the simulation model are provided below.

First, in order to minimize the efficiency loss due to the start-up transient, it is necessary to improve the PID controller of the expansion valve. After this improvement, new experiments could be carried out to verify the correct operation of the PID controller.
In future experiments, the shutdown time could be neglected if the expansion valve automatically opens after the heat pump is shut down. The focus should then be placed more on ΔT_{sink}, by carrying out additional experiments in which this variable is varied.
Once the PID controller has been improved, the new results could be used to develop an updated model. The recommended approach is the transfer function model, as it is self-sufficient and provides an accurate approximation of the transient behavior, as well as a clear graphical representation of the transient.
With additional experiments varying ΔT_{sink}, it would be possible to use this parameter as a new variable instead of t_{stop}; in this way, the distinction within the model between heating production and domestic hot water production could be eliminated, making the model more sensitive and accurate with respect to ΔT_{sink}.

Appendix A:
Results for Code A and Code B

Appendix A reports all experimental results for ASO using Code A and Code B.

Table A.1 – Experimental results for 36 tests using Code A

TEST N°	ssf [%]	Text [°C]	t_{stop} [min]	Thermal transient duration [min:sec]	Electrical transient duration [min:sec]
TEST 1	25%	20	60	6:10	2:40
TEST 2	25%	20	10	3:20	2:40
TEST 3	25%	20	2	2:50	1:20
TEST 4	50%	20	60	41:20	3:50
TEST 5	50%	20	10	40:50	3:40
TEST 6	50%	20	2	35:00	3:30
TEST 7	75%	20	60	58:00	38:20
TEST 8	75%	20	10	58:00	38:00
TEST 9	75%	20	2	56:00	32:30
TEST 10	25%	7	60	27:10	3:00
TEST 11	25%	7	10	25:30	2:50
TEST 12	25%	7	2	28:10	2:50
TEST 13	50%	7	60	18:00	4:10
TEST 14	50%	7	10	11:30	3:50
TEST 15	50%	7	2	20:40	3:50
TEST 16	75%	7	60	24:10	5:00
TEST 17	75%	7	10	33:20	4:40
TEST 18	75%	7	2	28:20	4:30
TEST 19	25%	2	60	17:30	3:00
TEST 20	25%	2	10	49:40	2:40
TEST 21	25%	2	2	15:30	2:40
TEST 22	50%	2	60	19:20	4:20
TEST 23	50%	2	10	19:10	4:10
TEST 24	50%	2	2	12:10	4:00
TEST 25	75%	2	60	38:00	4:30
TEST 26	75%	2	10	10:10	4:20
TEST 27	75%	2	2	12:10	4:30
TEST 28	50%	20	180	44:40	4:10
TEST 29	25%	20	3600	36:40	4:50
TEST 30	50%	20	3600	43:30	5:00
TEST 31	50%	20	3600	44:10	5:50
TEST 32	75%	20	3600	58:10	38:50
TEST 33	50%	7	60	20:00	5:20
TEST 34	50%	7	60	36:00	12:50
TEST 35	50%	20	60	21:30	12:50
TEST 36	50%	20	60	42:30	4:30

Table A.2 - Experimental results for 36 tests using Code B

TEST N°	ssf [%]	Text [°C]	t_{stop} [min]	Thermal transient duration [min:sec]	Electrical transient duration [min:sec]
TEST 1	25%	20	60	6:10	2:40
TEST 2	25%	20	10	3:20	2:40
TEST 3	25%	20	2	2:50	1:20
TEST 4	50%	20	60	41:20	3:50
TEST 5	50%	20	10	40:50	3:40
TEST 6	50%	20	2	35:00	3:30
TEST 7	75%	20	60	58:00	38:20
TEST 8	75%	20	10	58:00	38:00
TEST 9	75%	20	2	56:00	32:30
TEST 10	25%	7	60	27:20	3:00
TEST 11	25%	7	10	12:40	2:50
TEST 12	25%	7	2	28:20	2:50
TEST 13	50%	7	60	11:20	4:10
TEST 14	50%	7	10	10:30	3:50
TEST 15	50%	7	2	11:10	3:50
TEST 16	75%	7	60	24:10	5:00
TEST 17	75%	7	10	33:20	4:40
TEST 18	75%	7	2	28:20	4:30
TEST 19	25%	2	60	17:30	3:00
TEST 20	25%	2	10	50:20	2:40
TEST 21	25%	2	2	2:40	2:40
TEST 22	50%	2	60	11:10	4:20
TEST 23	50%	2	10	10:40	4:10
TEST 24	50%	2	2	11:10	4:00
TEST 25	75%	2	60	11:40	4:30
TEST 26	75%	2	10	10:50	4:20
TEST 27	75%	2	2	12:10	4:30
TEST 28	50%	20	180	44:40	4:10
TEST 29	25%	20	3600	18:30	4:50
TEST 30	50%	20	3600	43:30	5:00
TEST 31	50%	20	3600	44:10	5:50
TEST 32	75%	20	3600	58:10	38:50
TEST 33	50%	7	60	12:20	5:20
TEST 34	50%	7	60	15:10	12:50
TEST 35	50%	20	60	21:40	12:50
TEST 36	50%	20	60	42:30	4:30

Appendix B:
MATLAB “Code C”

The following MATLAB code was used to determine the thermal and electrical start-up times, the thermal and electrical power, and the COP during both start-up and steady-state conditions.

```
%% Input data

fprintf(2, ['For the correct execution of the code, keep in mind ' ...
'that the startup start row is taken as the first ' ...
'row where the frequency is different from zero, while ' ...
'the startup end row is taken as the last row where ' ...
'the frequency is equal to the set value.\n']);

% Extraction of timetable times
Time = timeofday(measurementair.Uhrzeit);
% Frequency extraction
Frequencies = measurementair.VerdichterLuftWP0_10V;
% Extraction of climatic chamber temperatures
Climatic_chamber_temperature = measurementair.T_ist;
% Extraction of evaporation pressure
P_eva = measurementair.NiederdruckLuftWP;
% Extraction of condensation pressure
P_cond = measurementair.HochdruckLuftWP;
% Extraction of electrical power data
Electrical_power = measurementair.VerdichterleistungLuft;
% Extraction of thermal power data
Thermal_power = measurementair.P_heat;
% Extraction of COP data
COP = measurementair.COP;

% Input to enter: time corresponding to the start of the startup
Hour = input('Startup start time (example - 16:36:40): ','s');

% Find the row corresponding to the start of the startup
X = find(Hour == Time);

% Find compressor frequency
Frequency = measurementair.VerdichterLuftWP0_10V(X+30);

Method = input('Do you want to stop the experiment at 60 min? (if you want press
enter, otherwise type "no"): ','s');

if strcmpi(Method,'no')

% Search for the row corresponding to the end of the experiment
for i = X : length(Frequencies)
    if Frequencies(i) == 0
        Y = i;
        break
    end
end

    while Frequencies(Y) ~= Frequency
    Y = Y-1;
    end
```

```
else

% Row corresponding to the end of the experiment (60 min)
Y = X + 360;
if Frequencies(Y) ~= Frequency
    while Frequencies(Y) ~= Frequency
    Y = Y-1;
    end
end
end

% Sampling interval [s]
deltaT_sec = 10;
interval_5min = 30;
interval_10min = 60;

%% Electrical power

Averaged_electrical_power = Electrical_power;
Averaged_electrical_power(X:Y) = movmean(Electrical_power(X:Y),interval_5min);
last_window_E = mean(Averaged_electrical_power(Y-interval_10min:Y));

for i = X:Y
    Value_E = Averaged_electrical_power(i);
          if Value_E > last_window_E*0.95
             electrical_row = i;
          break
          end
end

Electrical_power_stabilization_time_sec = (electrical_row - X)*deltaT_sec;
Electrical_power_stabilization_time_min =
Electrical_power_stabilization_time_sec/60;
Average_electrical_power_startup_Watt = mean(Electrical_power(X:electrical_row));
Electrical_energy_startup_Joule = sum(Electrical_power(X:electrical_row)) *
deltaT_sec;
Electrical_power_steady_state_Watt = mean(Electrical_power(electrical_row:Y));

%% Thermal power

Averaged_P_eva = P_eva;
Averaged_P_eva(X:Y) = movmean(P_eva(X:Y),interval_10min);
Averaged_P_cond = P_cond;
Averaged_P_cond(X:Y) = movmean(P_cond(X:Y),interval_10min);
thermal_row_eva = NaN;
thermal_row_cond = NaN;

last_window_T = mean(Averaged_P_eva(Y-interval_10min:Y));
first_window_T = mean(Averaged_P_eva(X:X+interval_10min));
if last_window_T < first_window_T
    for i = Y : -1 : X
        index_T = max(X, i - interval_10min);
        move_window_T = mean(Averaged_P_eva(i: -1 :index_T));
          if move_window_T > last_window_T*1.05
             thermal_row_eva = i;
          break
          end
    end
```

```
else
     for i = Y : -1 : X
         index_T = max(X, i - interval_10min);
         move_window_T = mean(Averaged_P_eva(i: -1 :index_T));
          if move_window_T < last_window_T*0.95
             thermal_row_eva = i;
          break
          end
     end
end

last_window_T = mean(Averaged_P_cond(Y-interval_10min:Y));
first_window_T = mean(Averaged_P_cond(X:X+interval_10min));
if last_window_T < first_window_T
    for i = Y : -1 : X
        index_T = max(X, i - interval_10min);
        move_window_T = mean(Averaged_P_cond(i: -1 :index_T));
          if move_window_T > last_window_T*1.05
             thermal_row_cond = i;
          break
          end
    end
else
     for i = Y : -1 : X
         index_T = max(X, i - interval_10min);
         move_window_T = mean(Averaged_P_cond(i: -1 :index_T));
          if move_window_T < last_window_T*0.95
             thermal_row_cond = i;
          break
          end
     end
end

thermal_row = max(thermal_row_eva,thermal_row_cond);
Thermal_power_stabilization_time_sec = (thermal_row - X)*deltaT_sec;
Thermal_power_stabilization_time_min = Thermal_power_stabilization_time_sec/60;
Average_thermal_power_startup_Watt = mean(Thermal_power(X:thermal_row));
Thermal_energy_startup_Joule = sum(Thermal_power(X:thermal_row)) * deltaT_sec;
Thermal_power_steady_state_Watt = mean(Thermal_power(thermal_row:Y));

%% COP

COP_row = max(electrical_row,thermal_row);
Average_COP_startup = mean(COP(X:COP_row));
COP_steady_state = mean(COP(COP_row:Y));

%% Average temperature in the climatic chamber

T_ext = mean(Climatic_chamber_temperature(X:Y));

%% Find initial temperature of sink Tsink_0 and setpoint temperature Tsink

% Extraction of sink's temperatures
Sink_data = measurementair.K2ST2;

Tsink_0 = Sink_data(X-1);
Tsink = mean(Sink_data(Y-30:Y));

%% Graphs
```

```
save_name = strrep(Hour, ':', '_');

figure(1)
Time_sec = seconds(measurementair.Uhrzeit(X:Y) - measurementair.Uhrzeit(X));
Time_min = Time_sec/60;
yyaxis left
plot(Time_min, Thermal_power(X:Y), 'b')
ylabel('Thermal power [W]')
ylim([0 max(Thermal_power(X:Y))])
ax = gca;
ax.YColor = 'b';
hold on
yyaxis right
plot(Time_min, Electrical_power(X:Y), 'r')
ylabel('Electrical power [W]')
ylim([0 2000])
ax = gca;
ax.YColor = 'r';
xline((thermal_row - X)*deltaT_sec/60, '--b');
xline((electrical_row - X)*deltaT_sec/60, '--r');
xlabel('Time [min]')
legend('Thermal power','Electrical power','Location','southeast')
title('Thermal and electrical power of the HP over time at startup')
grid on
hold off
saveas(gcf, ['Grafico_potenze_' save_name '.jpg'])

figure(2)
plot(Time_min, P_cond(X:Y))
hold on
plot(Time_min, P_eva(X:Y))
xlabel('Time [min]')
ylabel('Pressure [bar]')
legend('Condensation pressure', 'Evaporation pressure','Location','southeast')
title('Condensation and evaporation pressures of the HP over time at startup')
grid on
hold off

figure(3)
plot(Time_min, measurementair.Ex_VentilPWM(X:Y))
ylim([0 50])
grid on
xlabel('Time [min]')
ylabel('Expansion valve opening percentage [%]')
title('Expansion valve operation')
legend('Expansion valve','Location','southeast')
saveas(gcf, ['Grafico_apertura_valvola' save_name '.jpg'])

%% Saving results to Excel

StartUpTime = max([Thermal_power_stabilization_time_min,
Electrical_power_stabilization_time_min]);

COP_drop = ((Average_COP_startup - COP_steady_state) / COP_steady_state)*100;

Thermal_drop = ((Average_thermal_power_startup_Watt -
Thermal_power_steady_state_Watt) / Thermal_power_steady_state_Watt)*100;
```

```
Electrical_drop = ((Average_electrical_power_startup_Watt -
Electrical_power_steady_state_Watt) / Electrical_power_steady_state_Watt)*100;

DTsink = Tsink - Tsink_0;

filename = ['Risultati_startup_' save_name '.xlsx'];

headers = { ...
    'Start-up time [min]', ...
    'Average thermal power during start-up [W]', ...
    'Thermal power in steady-state', ...
    'Average electrical power during start-up [W]', ...
    'Electrical power in steady-state', ...
    'Average COP during start-up [/]', ...
    'Average climate chamber''s temperature [°C]', ...
    'Thermal transient duration [min]', ...
    'Electrical transient duration [min]', ...
    'COP steady-state [/]', 'COP drop [%]', ...
    'Thermal power drop [%]', 'Electrical power drop [%]', ...
    'T0 sink [°C]', 'Tsetpoint sink [°C]', 'DTsink [°C]', ...
    'Thermal energy start-up [J]', ...
    'Electrical energy start-up [J]'};

values = { ...
    StartUpTime, ...
    Average_thermal_power_startup_Watt, ...
    Thermal_power_steady_state_Watt, ...
    Average_electrical_power_startup_Watt, ...
    Electrical_power_steady_state_Watt, ...
    Average_COP_startup, ...
    T_ext, ...
    Thermal_power_stabilization_time_min, ...
    Electrical_power_stabilization_time_min, ...
    COP_steady_state, COP_drop, ...
    Thermal_drop, Electrical_drop, ...
    Tsink_0, Tsink, DTsink, ...
    Thermal_energy_startup_Joule, ...
    Electrical_energy_startup_Joule};

excelData = [headers; values];

writecell(excelData, filename);

%% Saving measurementair to Excel

writetimetable(measurementair, 'measurementair.xlsx');
```

Appendix C:
Complete set of experimental results for Code C

Appendix C includes the complete set of experimental results for Code C: Table C.1 provides the legend for the tabulated data, Table C.2 presents the durations of the thermal and electrical transients, Table C.3 lists the experimental conditions for all test cases, Table C.4 reports the steady-state thermal power, electrical power, and COP, Table C.5 gives the average thermal power, electrical power, and COP during start-up, and Table C.6 shows the thermal power, electrical power, and COP drops from steady-state conditions during start-up.

Table C.1 - Legend of the tabulated experimental data

Data:	**Meaning:**
Δtsink [°C]	*Difference between the temperature of the water at the setpoint and the temperature of the water at time 0 in the sink system*
Average climate chamber's temperature [°C]	*Measured average temperature in the climate chamber during the experiment*
Average COP during start-up [/]	*Average value of the COP during start-up*
Average electrical power during start-up [W]	*Average value of the electrical power during start-up*
Average thermal power during start-up [W]	*Average value of the thermal power during start-up*
COP drop [%]	*COP reduction relative to steady-state during start-up*
COP steady-state [/]	*COP under steady-state conditions*
Electrical power drop [%]	*Electrical power reduction relative to steady-state during start-up*
Electrical power in steady-state [W]	*Electrical power under steady-state conditions*
Electrical transient duration [min:sec]	*Duration of the electrical transient (electrical start-up time)*
Experiment duration [min]	*Operating time of the heat pump for data acquisition*
ssf [%]	*Percentage of the frequency of the inverter*
T0 sink [°C]	*Water temperature at time 0 in the sink system*
TEST N°	*Number of the experiment*
T_{ext} [°C]	*Target temperature in the climate chamber during the experiment*
Thermal power drop [%]	*Thermal power reduction relative to steady-state during start-up*
Thermal power in steady-state [W]	*Thermal power under steady-state conditions*
Thermal transient duration [min:sec]	*Duration of the thermal transient (thermal start-up time)*
T out Sink [°C]	*Inlet water temperature inside the HSHX*
Tsetpoint sink [°C]	*Water temperature at steady-state in the sink system (setpoint)*
t_{stop} [min]	*Time between the initial shutdown and the start of the experiment*
Voume flow heat sink [l/h]	*Volume flow rate of the heat sink*

Table C.2 - Thermal and electrical transient duration for all test cases

TEST N°	ssf [%]	Text [°C]	t_{stop} [min]	Thermal transient duration [min:sec]	Electrical transient duration [min:sec]
Air Source Operation					
TEST 1	25%	20	60	10:10	2:40
TEST 2	25%	20	10	9:50	2:40
TEST 3	25%	20	2	10:40	1:20
TEST 4	50%	20	60	45:50	3:50
TEST 5	50%	20	10	45:40	3:40
TEST 6	50%	20	2	40:30	3:30
TEST 7	75%	20	60	63:00	38:20
TEST 8	75%	20	10	63:10	38:00
TEST 9	75%	20	2	60:20	32:30
TEST 10	25%	7	60	24:20	3:00
TEST 11	25%	7	10	18:30	2:50
TEST 12	25%	7	2	27:00	2:50
TEST 13	50%	7	60	8:50	4:10
TEST 14	50%	7	10	6:20	3:50
TEST 15	50%	7	2	8:20	3:50
TEST 16	75%	7	60	26:30	5:00
TEST 17	75%	7	10	36:30	4:40
TEST 18	75%	7	2	31:50	4:30
TEST 19	25%	2	60	17:30	3:00
TEST 20	25%	2	10	23:20	2:40
TEST 21	25%	2	2	15:00	2:40
TEST 22	50%	2	60	14:10	4:20
TEST 23	50%	2	10	14:40	4:10
TEST 24	50%	2	2	13:20	4:00
TEST 25	75%	2	60	9:20	4:30
TEST 26	75%	2	10	9:30	4:20
TEST 27	75%	2	2	8:00	4:30
TEST 28	50%	20	180	49:00	4:10
TEST 29	25%	20	3600	12:10	4:50
TEST 30	50%	20	3600	47:30	5:00
TEST 31	50%	20	3600	51:00	5:50
TEST 32	75%	20	3600	63:00	38:50
TEST 33	50%	7	60	11:10	5:20
TEST 34	50%	7	60	20:20	12:50
TEST 35	50%	20	60	27:30	12:50
TEST 36	50%	20	60	46:30	4:30
Ground Source Operation					
TEST 37	50%	5	10	15:10	3:40
TEST 38	25%	5	10	54:40	7:10
TEST 39	75%	5	10	12:30	3:30
TEST 40	50%	5	10	14:10	6:30
TEST 41	50%	5	10	41:30	16:40

Table C.3 - Experimental conditions for all test cases

TEST N°	Volume flow heat sink [l/h]	T out Sink [°C]	Average climate chamber's temperature [°C]	T0 sink [°C]	Tsetpoint sink [°C]	Δtsink [°C]	Experiment duration [min]
Air Source Operation							
TEST 1	950	30	19.38	26.16	33.07	6.91	60
TEST 2	950	30	19.25	28.16	33.03	4.88	60
TEST 3	950	30	19.28	28.56	33.02	4.46	60
TEST 4	950	30	19.92	26.00	35.68	9.68	60
TEST 5	950	30	19.66	27.27	35.72	8.45	60
TEST 6	950	30	19.48	27.61	35.76	8.14	60
TEST 7	950	30	18.37	25.36	38.84	13.48	104
TEST 8	950	30	18.50	26.74	38.82	12.08	110
TEST 9	950	30	17.94	26.51	38.75	12.23	94
TEST 10	950	30	6.97	26.15	32.32	6.18	60
TEST 11	950	30	7.07	28.11	32.30	4.19	60
TEST 12	950	30	7.03	28.67	32.38	3.71	60
TEST 13	950	30	6.67	26.03	34.44	8.41	60
TEST 14	950	30	7.02	27.92	34.69	6.76	60
TEST 15	950	30	7.00	28.03	34.63	6.60	60
TEST 16	950	30	6.15	25.63	36.92	11.29	60
TEST 17	950	30	6.65	27.12	37.00	9.88	60
TEST 18	950	30	6.46	27.38	36.98	9.60	60
TEST 19	950	30	1.98	26.14	32.01	5.86	60
TEST 20	950	30	1.95	28.41	32.11	3.70	60
TEST 21	950	30	1.92	28.99	31.71	2.72	60
TEST 22	950	30	2.03	25.90	33.92	8.02	60
TEST 23	950	30	2.02	27.90	33.90	6.00	60
TEST 24	950	30	2.00	28.14	33.90	5.76	60
TEST 25	950	30	2.00	25.57	36.42	10.85	60
TEST 26	950	30	1.93	27.38	36.34	8.96	60
TEST 27	950	30	1.96	28.14	36.41	8.27	60
TEST 28	950	30	19.96	24.00	35.80	11.80	60
TEST 29	950	30	18.97	18.32	32.99	14.66	60
TEST 30	950	30	19.47	17.74	35.73	17.99	60
TEST 31	950	30	18.80	13.12	35.88	22.77	60
TEST 32	950	30	18.94	14.97	38.92	23.95	98
TEST 33	950	30	6.91	20.23	34.49	14.26	60
TEST 34	950	50	7.17	20.09	53.93	33.84	60
TEST 35	950	50	18.37	20.14	55.12	34.98	60
TEST 36	950	30	18.58	19.97	35.54	15.56	60
Ground Source Operation							
TEST 37	950	30	/	28.23	33.01	4.78	60
TEST 38	950	30	/	27.91	31.20	3.29	60
TEST 39	950	30	/	28.07	34.43	6.36	60
TEST 40	950	30	/	17.60	33.04	15.43	60
TEST 41	950	50	/	17.54	52.31	34.77	60

Table C.4 – Steady-state thermal power, electrical power, and COP

TEST N°	Thermal power in steady-state [W]	Electrical power in steady-state [W]	COP steady-state [/]
Air Source Operation			
TEST 1	3292.74	380.22	8.72
TEST 2	3287.99	379.62	8.70
TEST 3	3290.71	383.86	8.65
TEST 4	6257.01	882.99	7.18
TEST 5	6285.85	885.23	7.21
TEST 6	6269.55	887.48	7.18
TEST 7	9614.09	1600.62	5.95
TEST 8	9650.68	1599.77	5.97
TEST 9	9551.50	1595.91	5.92
TEST 10	2341.45	428.83	5.45
TEST 11	2428.31	422.34	5.67
TEST 12	2369.81	422.88	5.53
TEST 13	4943.55	905.87	5.46
TEST 14	4918.04	905.35	5.44
TEST 15	4983.49	905.19	5.52
TEST 16	7580.16	1542.77	4.85
TEST 17	7648.90	1527.75	4.89
TEST 18	7620.95	1538.12	4.88
TEST 19	2006.07	446.54	4.52
TEST 20	1999.76	441.28	4.48
TEST 21	2064.37	440.27	4.69
TEST 22	4444.52	905.03	4.89
TEST 23	4447.32	906.53	4.89
TEST 24	4461.55	906.22	4.91
TEST 25	6803.32	1531.29	4.45
TEST 26	6848.79	1530.15	4.48
TEST 27	6873.05	1533.05	4.49
TEST 28	6288.22	880.86	7.23
TEST 29	3196.34	387.39	8.34
TEST 30	6229.93	877.46	7.14
TEST 31	6356.52	880.38	7.37
TEST 32	9687.05	1599.74	6.00
TEST 33	5025.69	901.67	5.57
TEST 34	4235.88	1356.49	3.12
TEST 35	5537.95	1390.23	3.97
TEST 36	6062.21	879.50	6.93
Ground Source Operation			
TEST 37	3259.35	662.78	4.90
TEST 38	1278.65	311.71	3.93
TEST 39	4863.54	1100.47	4.42
TEST 40	3281.22	671.13	4.89
TEST 41	2442.53	972.08	2.53

Table C.5 – Average thermal power, electrical power, and COP during start-up

TEST N°	Average thermal power during start-up [W]	Average electrical power during start-up [W]	Average COP during start-up [/]
Air Source Operation			
TEST 1	2384.14	299.21	6.07
TEST 2	2788.69	329.21	7.12
TEST 3	2965.74	237.39	7.32
TEST 4	4865.57	581.87	5.56
TEST 5	4897.43	570.98	5.56
TEST 6	5081.87	582.52	5.73
TEST 7	6802.18	1370.79	4.55
TEST 8	6921.85	1379.45	4.62
TEST 9	7057.23	1392.63	4.62
TEST 10	1589.54	338.42	3.73
TEST 11	1971.48	368.58	4.80
TEST 12	1791.12	349.78	4.30
TEST 13	2666.34	593.75	2.99
TEST 14	3250.04	634.94	3.53
TEST 15	3309.38	618.17	3.65
TEST 16	5801.83	956.52	3.82
TEST 17	6064.41	969.93	4.06
TEST 18	6148.63	979.48	4.07
TEST 19	880.04	342.95	1.87
TEST 20	1480.71	400.54	3.44
TEST 21	1724.92	402.14	3.93
TEST 22	3079.02	617.18	3.48
TEST 23	3316.43	635.75	3.70
TEST 24	3235.10	617.79	3.62
TEST 25	3727.72	896.52	2.47
TEST 26	4304.90	922.41	2.86
TEST 27	4029.71	956.79	2.61
TEST 28	4619.51	534.52	5.24
TEST 29	1742.31	222.11	4.27
TEST 30	4493.60	534.16	5.31
TEST 31	4527.01	544.31	5.32
TEST 32	6543.60	1328.16	4.45
TEST 33	2816.93	615.58	3.36
TEST 34	2149.66	894.80	1.89
TEST 35	3270.59	917.17	2.79
TEST 36	4478.24	558.53	5.25
Ground Source Operation			
TEST 37	2573.97	485.30	4.18
TEST 38	716.08	279.91	2.35
TEST 39	3970.83	777.95	3.90
TEST 40	2091.12	499.95	3.46
TEST 41	1202.96	710.22	1.45

Table C.6 - Thermal power, electrical power, and COP drops from steady-state conditions during start-up

TEST N°	Thermal power drop [%]	Electrical power drop [%]	COP drop [%]
Air Source Operation			
TEST 1	-27.59	-21.31	-30.43
TEST 2	-15.19	-13.28	-18.07
TEST 3	-9.88	-38.16	-15.37
TEST 4	-22.24	-34.10	-22.48
TEST 5	-22.09	-35.50	-22.91
TEST 6	-18.94	-34.36	-20.12
TEST 7	-29.25	-14.36	-23.51
TEST 8	-28.28	-13.77	-22.59
TEST 9	-26.11	-12.74	-21.91
TEST 10	-32.11	-21.08	-31.52
TEST 11	-18.81	-12.73	-15.38
TEST 12	-24.42	-17.29	-22.26
TEST 13	-46.06	-34.46	-45.34
TEST 14	-33.92	-29.87	-35.10
TEST 15	-33.59	-31.71	-33.88
TEST 16	-23.46	-38.00	-21.23
TEST 17	-20.72	-36.51	-17.01
TEST 18	-19.32	-36.32	-16.62
TEST 19	-56.13	-23.20	-58.62
TEST 20	-25.96	-9.23	-23.20
TEST 21	-16.44	-8.66	-16.23
TEST 22	-30.72	-31.81	-28.89
TEST 23	-25.43	-29.87	-24.40
TEST 24	-27.49	-31.83	-26.33
TEST 25	-45.21	-41.45	-44.39
TEST 26	-37.14	-39.72	-36.25
TEST 27	-41.37	-37.59	-41.77
TEST 28	-26.54	-39.32	-27.54
TEST 29	-45.49	-42.67	-48.77
TEST 30	-27.87	-39.12	-25.67
TEST 31	-28.78	-38.17	-27.83
TEST 32	-32.45	-16.98	-25.77
TEST 33	-43.95	-31.73	-39.64
TEST 34	-49.25	-34.04	-39.42
TEST 35	-40.94	-34.03	-29.77
TEST 36	-26.13	-36.49	-24.34
Ground Source Operation			
TEST 37	-21.03	-26.78	-14.79
TEST 38	-44.00	-10.20	-40.30
TEST 39	-18.36	-29.31	-11.68
TEST 40	-36.27	-25.51	-29.22
TEST 41	-50.75	-26.94	-42.73

Appendix D:
Thermal and Electrical Power Profiles over Time for Each Experiment

Appendix D provides all the thermal and electrical power profiles for the 41 tests described in Chapter 2. The blue and red vertical dashed lines represent, respectively, the end of the thermal and electrical transients.

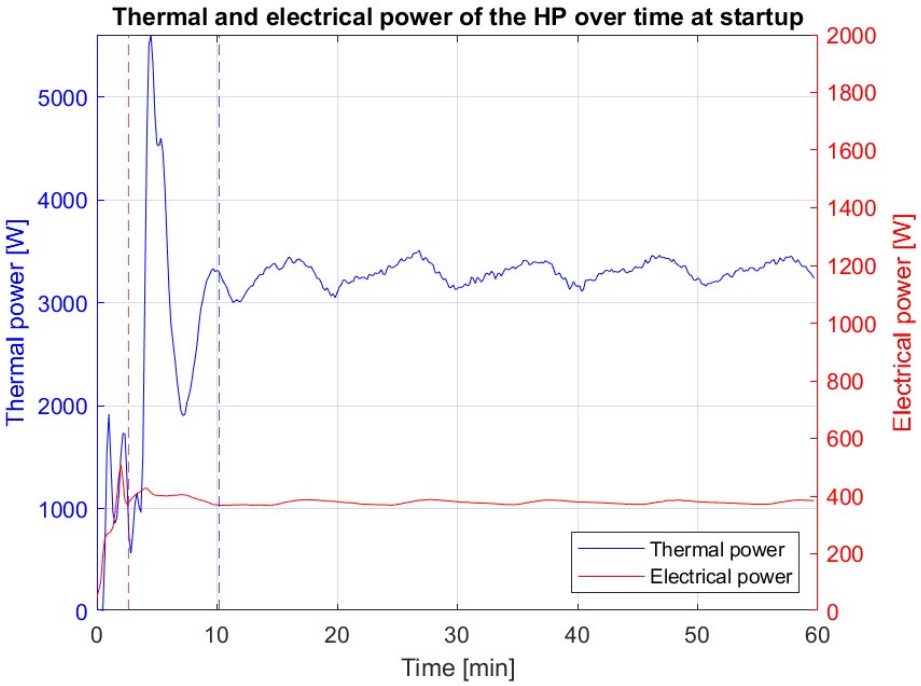

Figure D.1 – Thermal and electrical power profiles over time for TEST 1

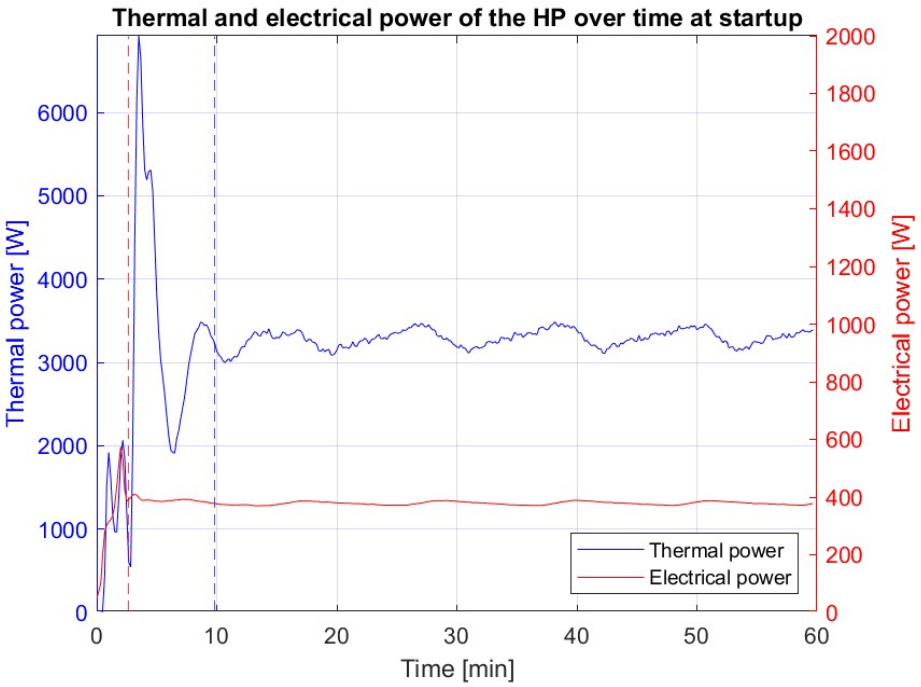

Figure D.2 – Thermal and electrical power profiles over time for TEST 2

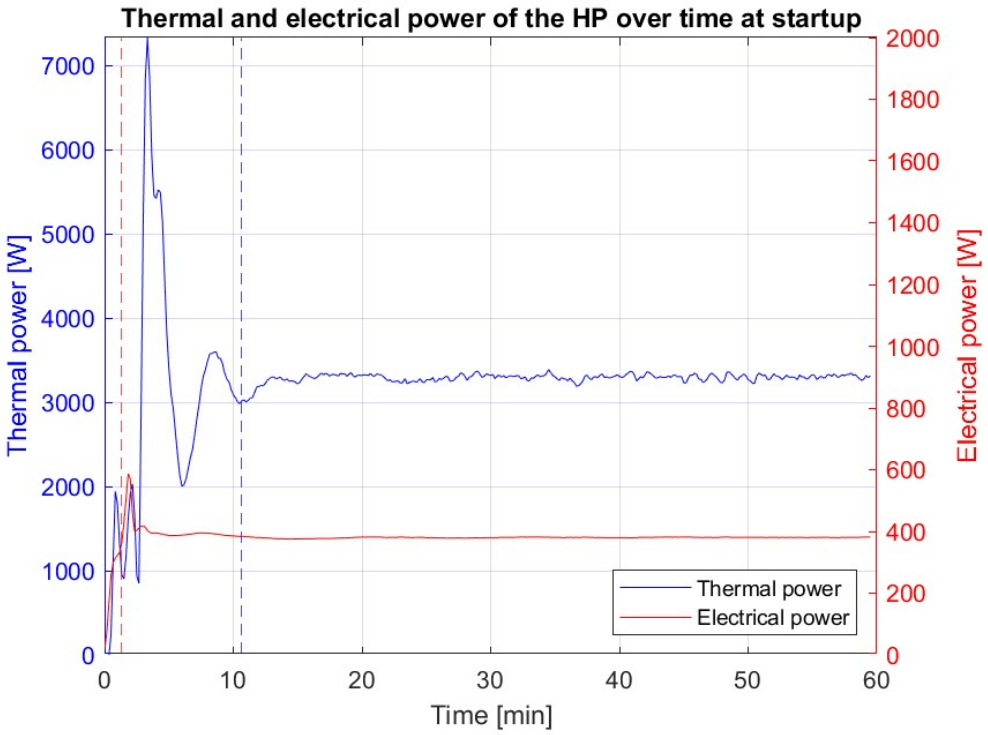

Figure D.3 – Thermal and electrical power profiles over time for TEST 3

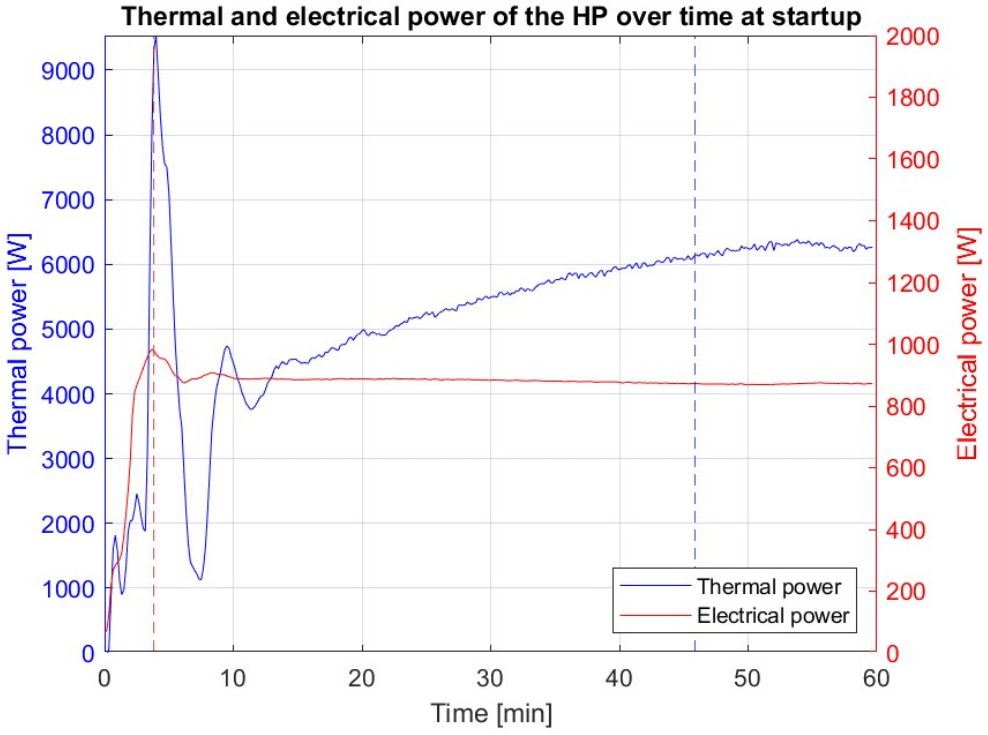

Figure D.4 – Thermal and electrical power profiles over time for TEST 4

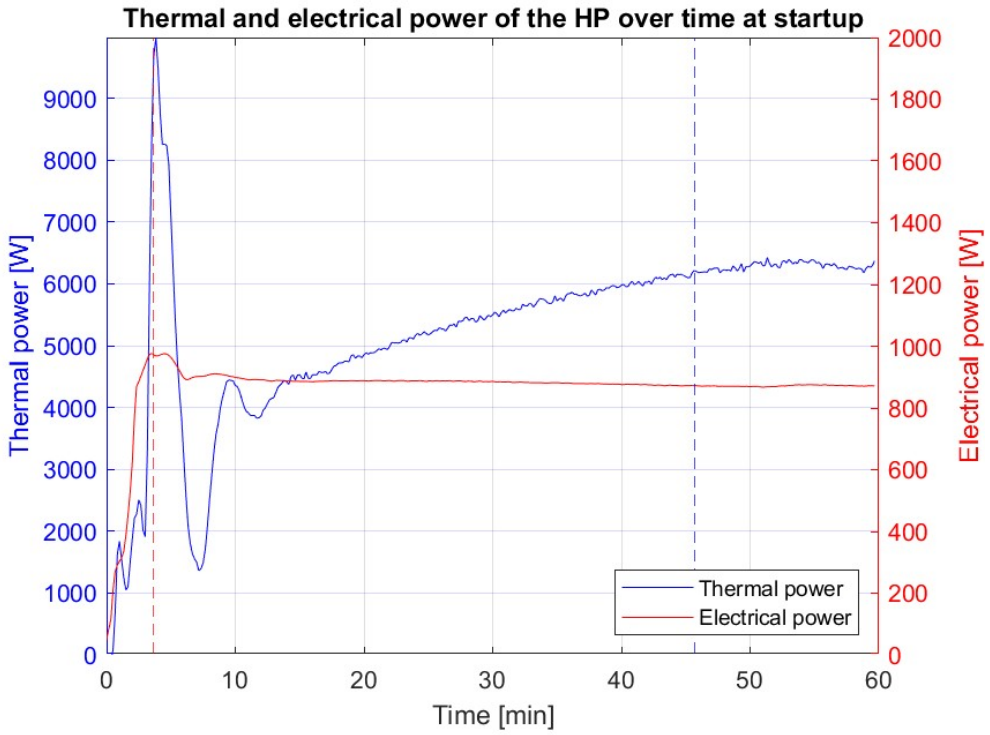

Figure D.5 – Thermal and electrical power profiles over time for TEST 5

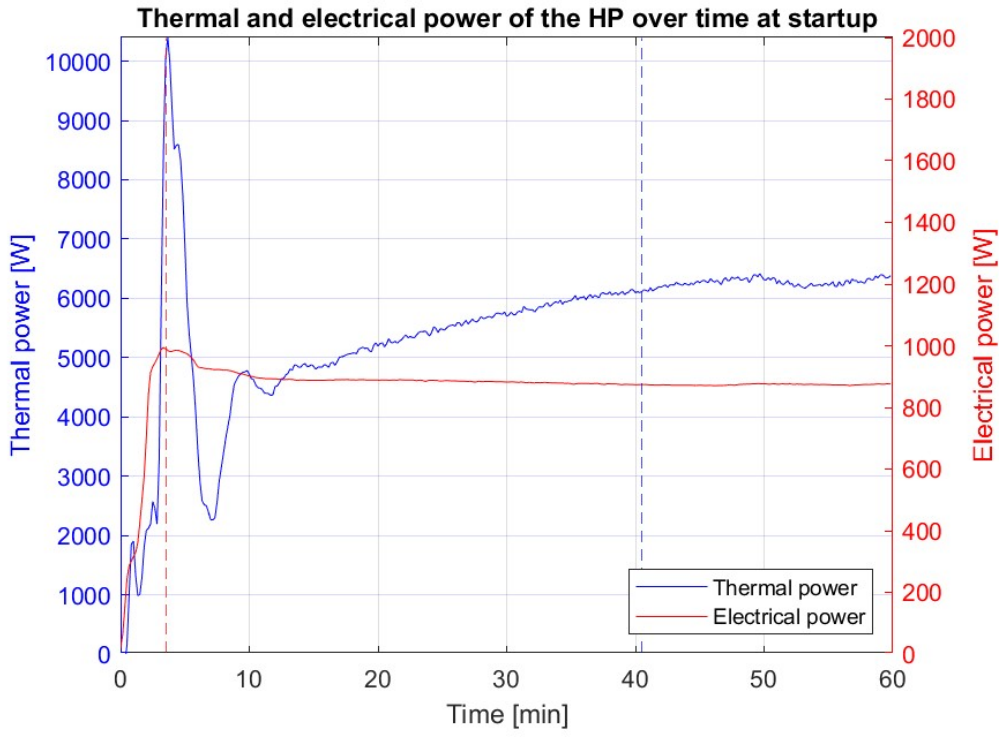

Figure D.6 – Thermal and electrical power profiles over time for TEST 6

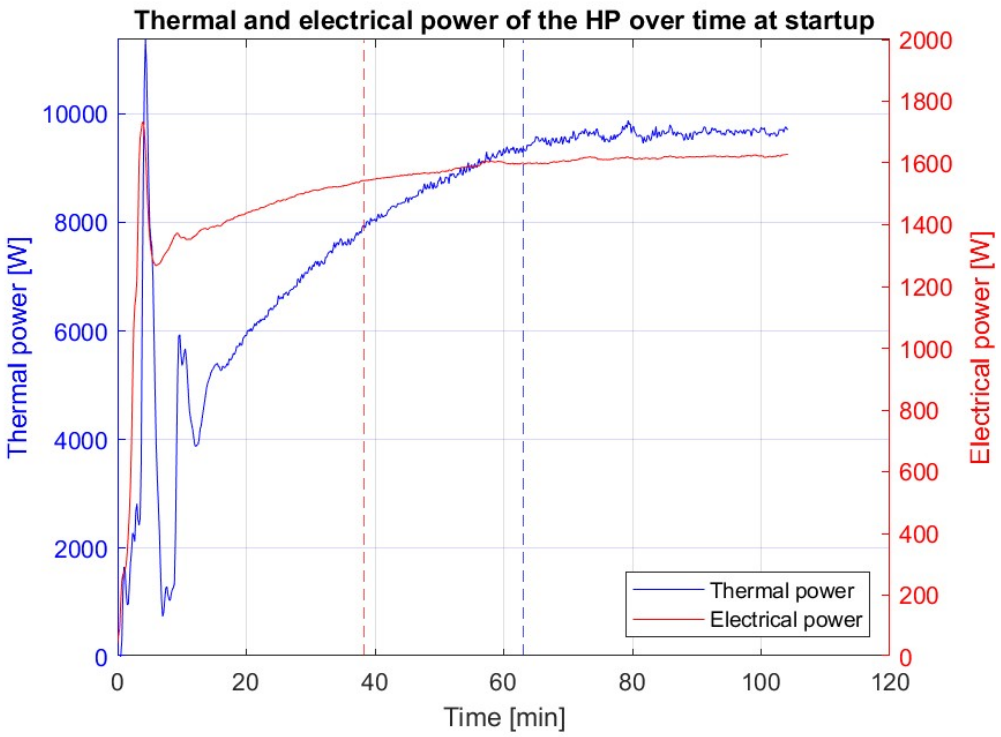

Figure D.7 – Thermal and electrical power profiles over time for TEST 7

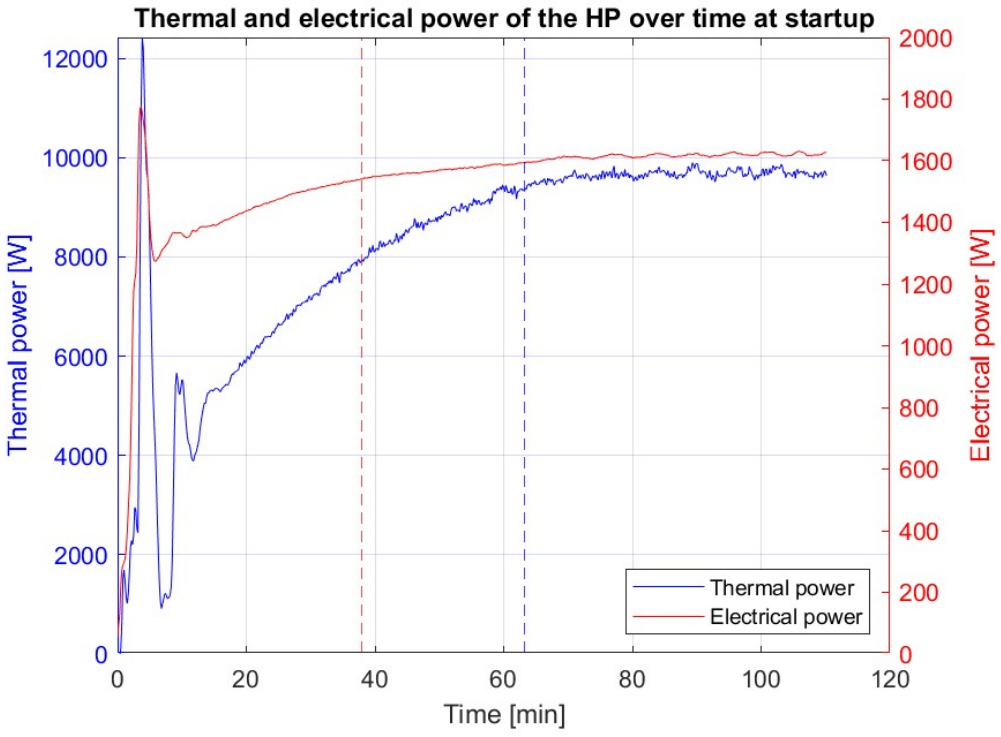

Figure D.8 – Thermal and electrical power profiles over time for TEST 8

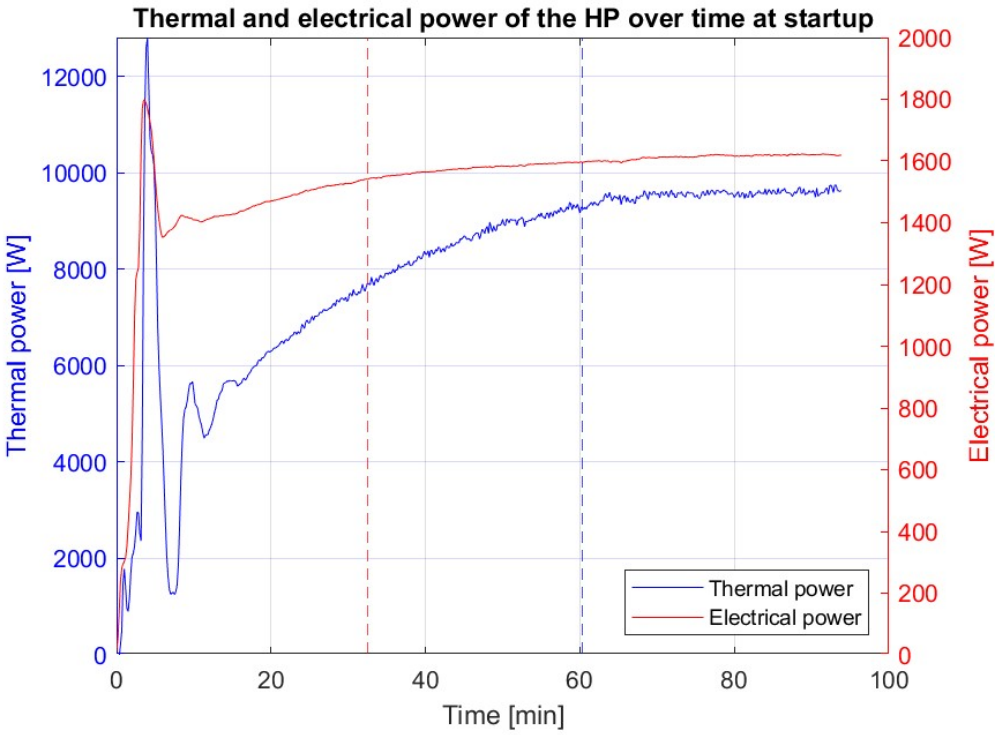

Figure D.9 – Thermal and electrical power profiles over time for TEST 9

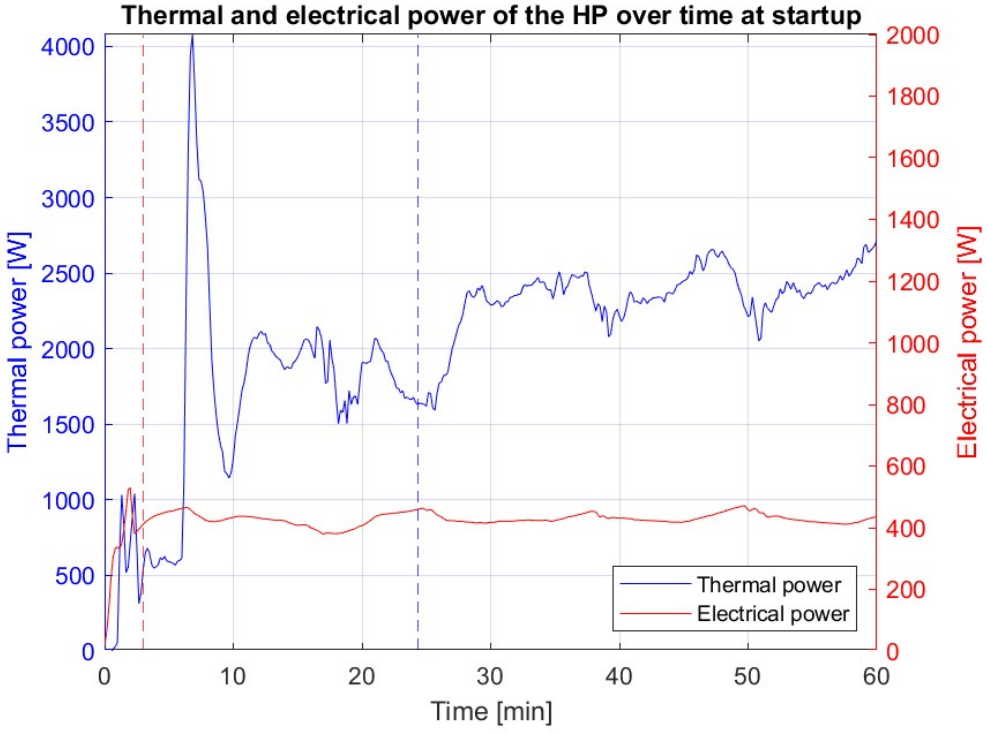

Figure D.10 – Thermal and electrical power profiles over time for TEST 10

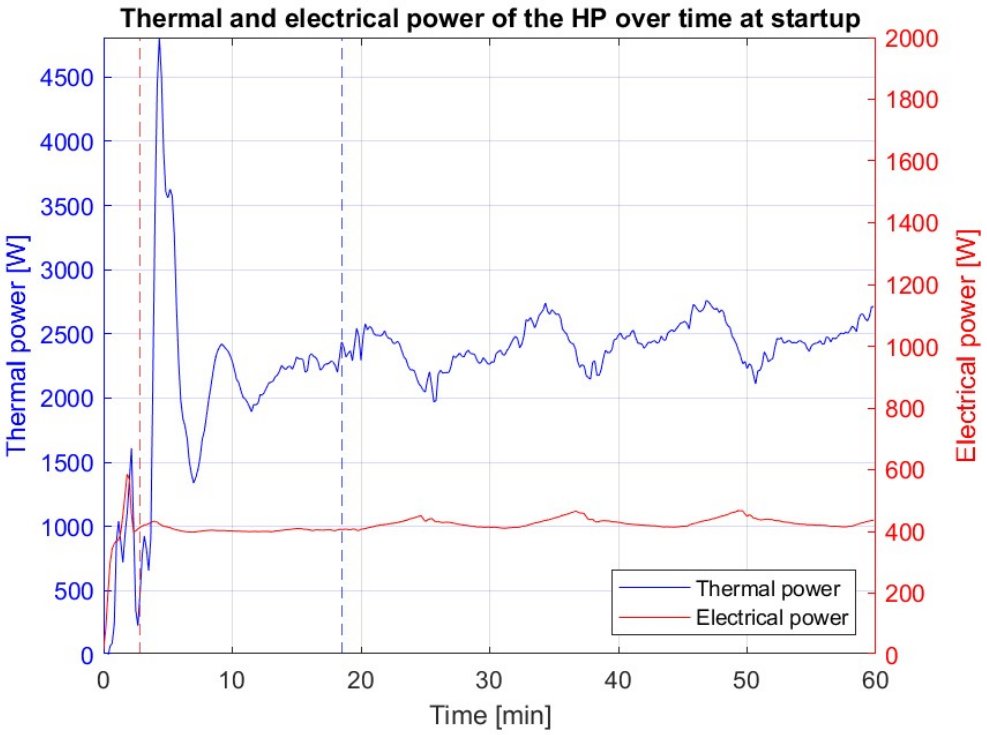

Figure D.11 – Thermal and electrical power profiles over time for TEST 11

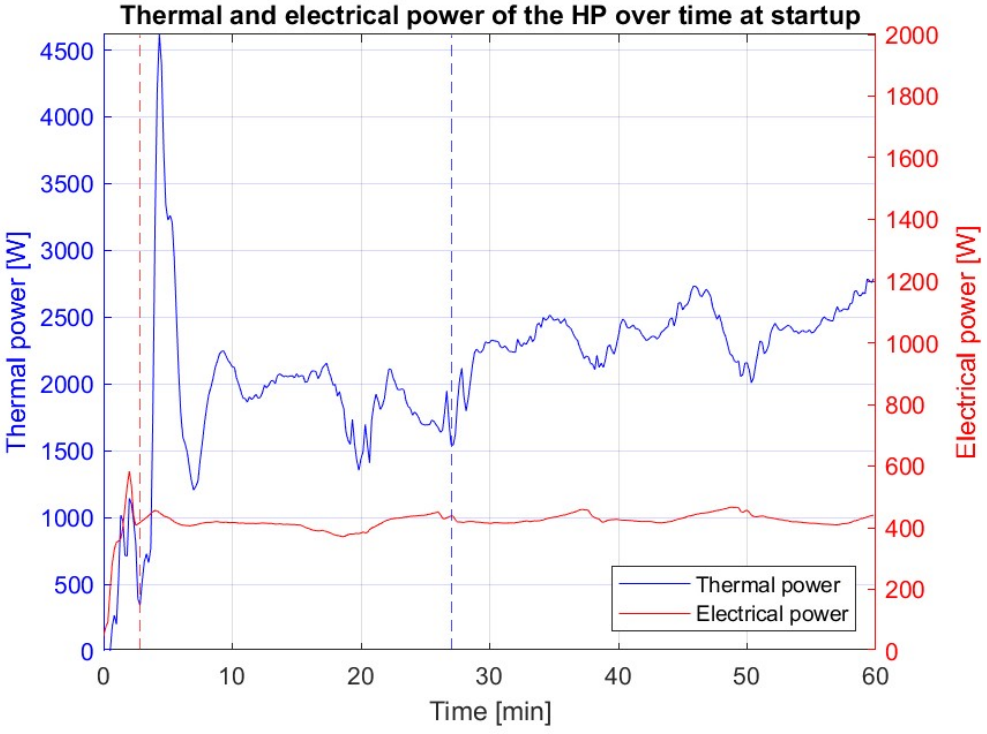

Figure D.12 – Thermal and electrical power profiles over time for TEST 12

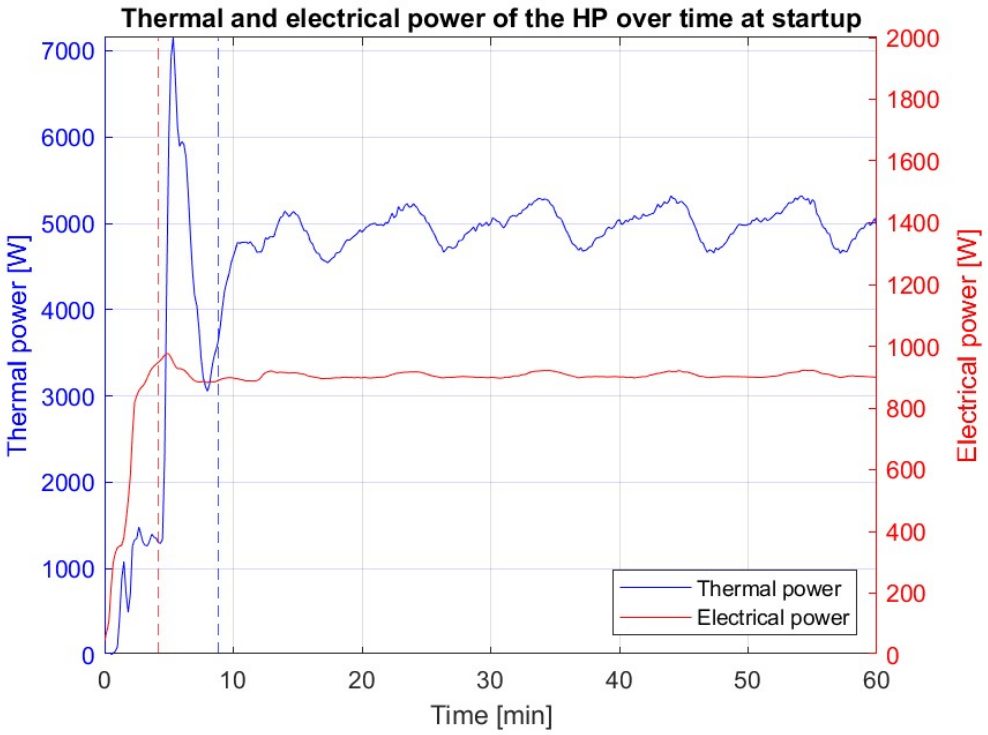

Figure D.13 – Thermal and electrical power profiles over time for TEST 13

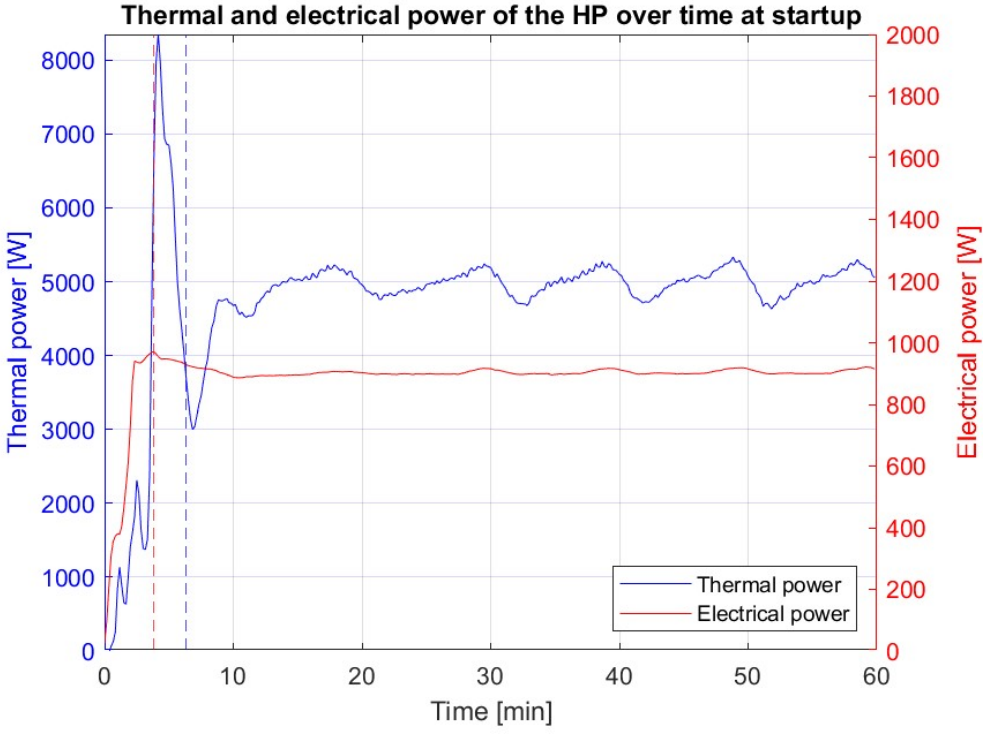

Figure D.14 – Thermal and electrical power profiles over time for TEST 14

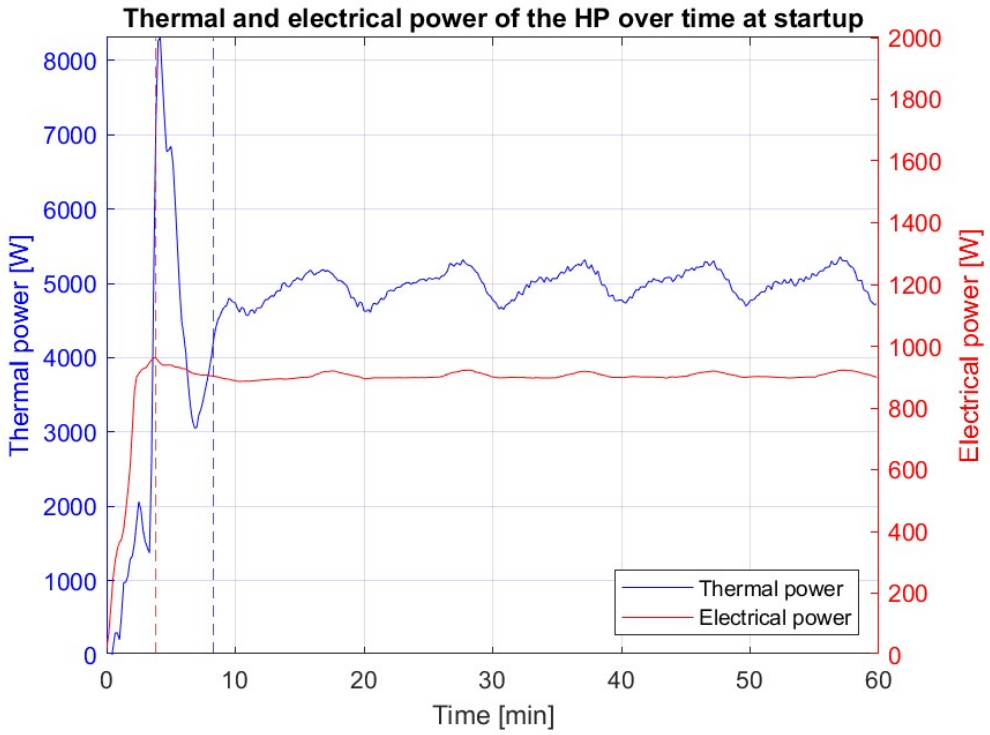

Figure D.15 – Thermal and electrical power profiles over time for TEST 15

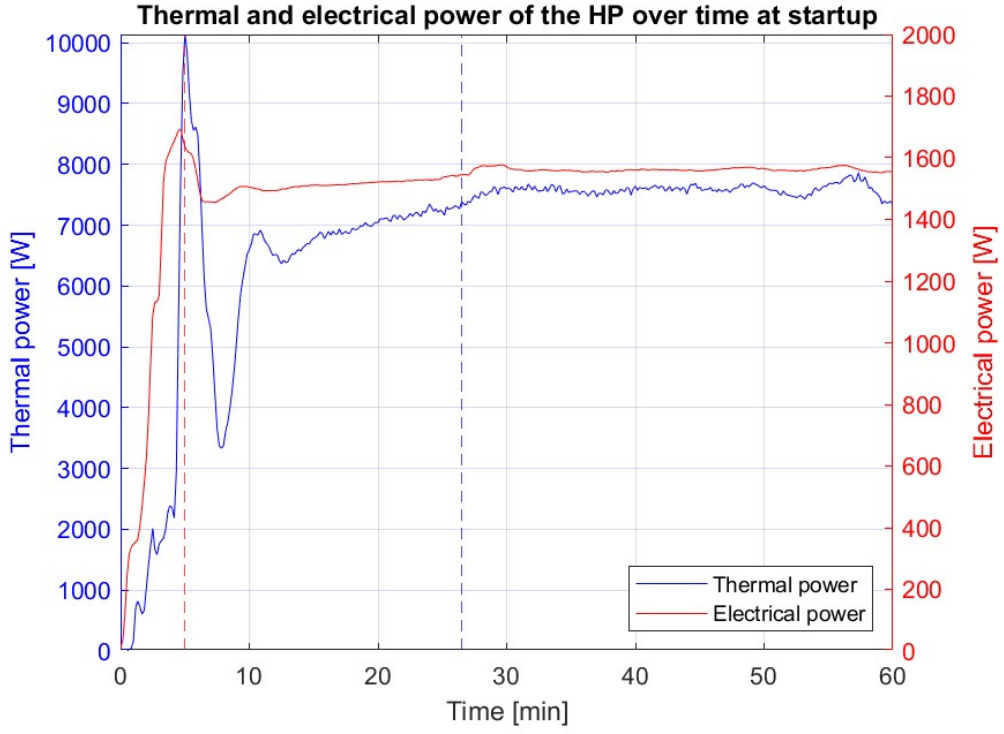

Figure D.16 – Thermal and electrical power profiles over time for TEST 16

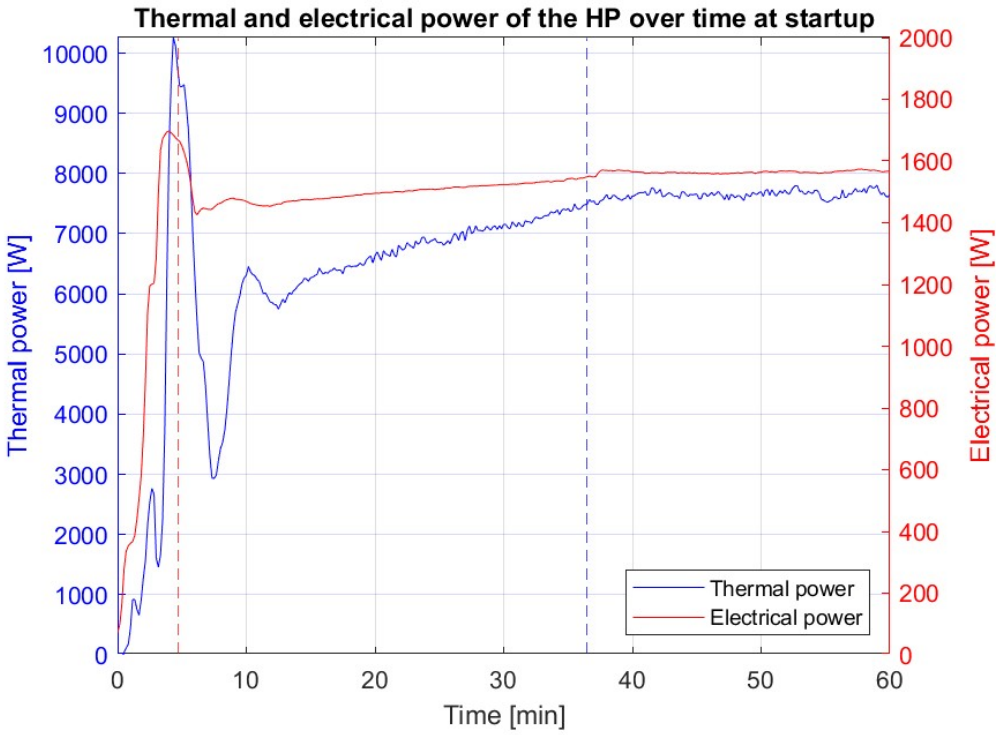

Figure D.17 – Thermal and electrical power profiles over time for TEST 17

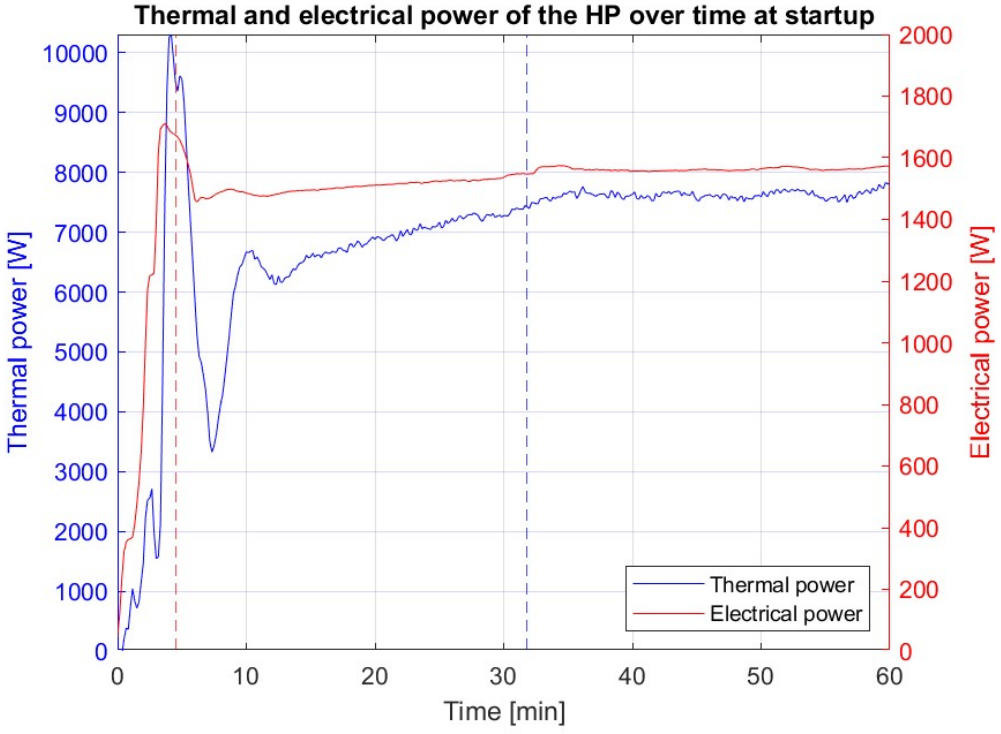

Figure D.18 – Thermal and electrical power profiles over time for TEST 18

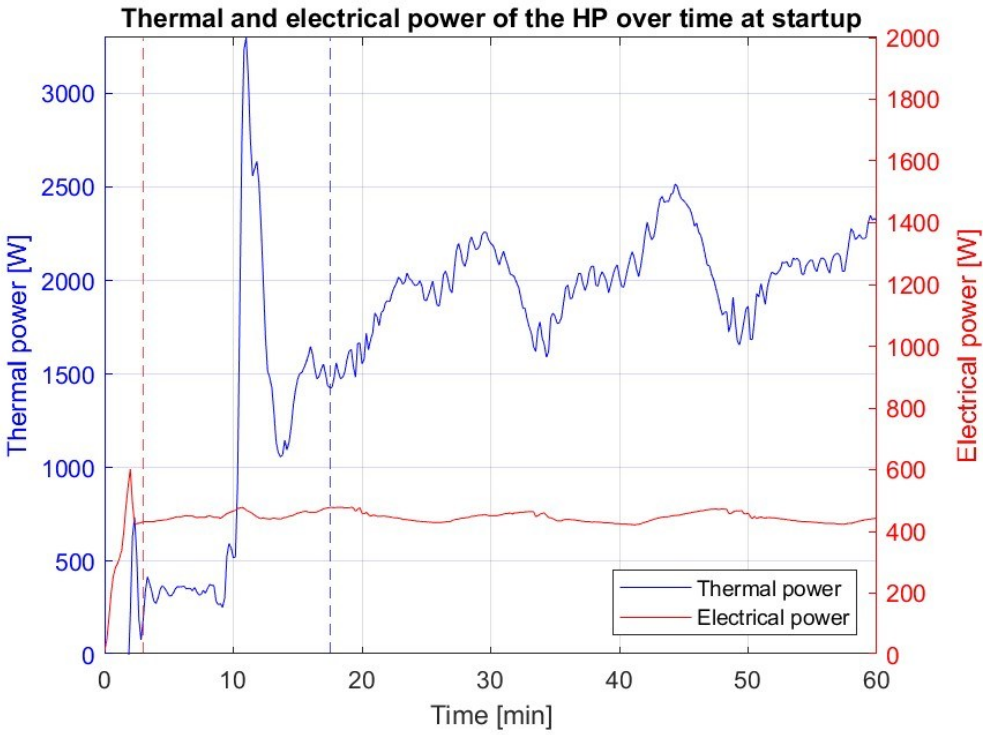

Figure D.19 – Thermal and electrical power profiles over time for TEST 19

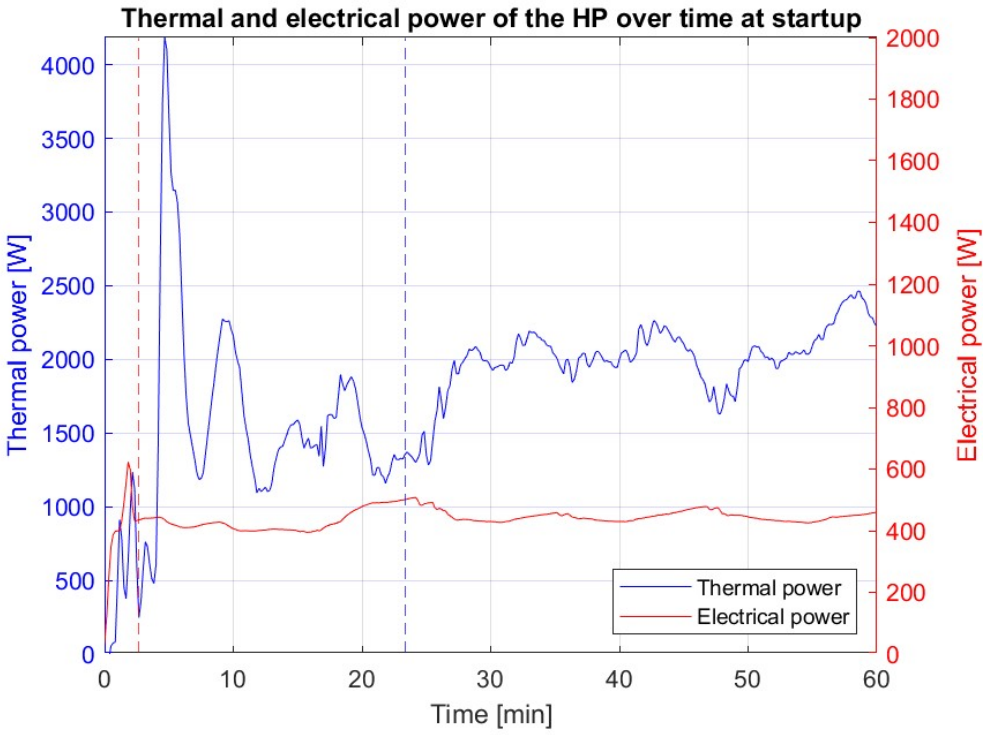

Figure D.20 – Thermal and electrical power profiles over time for TEST 20

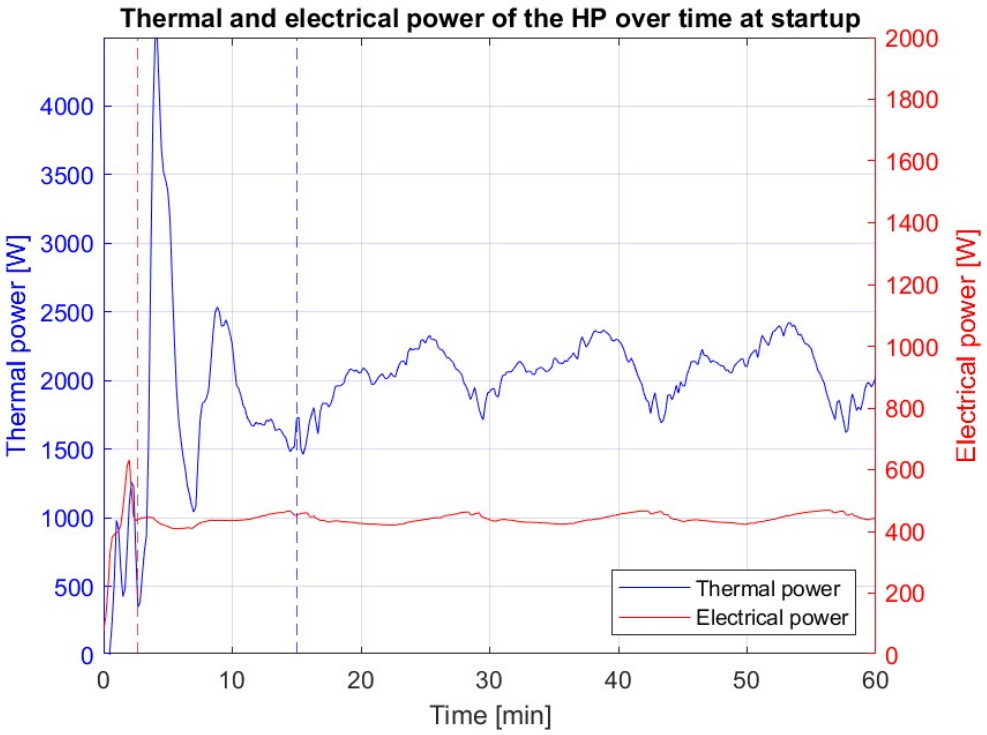

Figure D.21 – Thermal and electrical power profiles over time for TEST 21

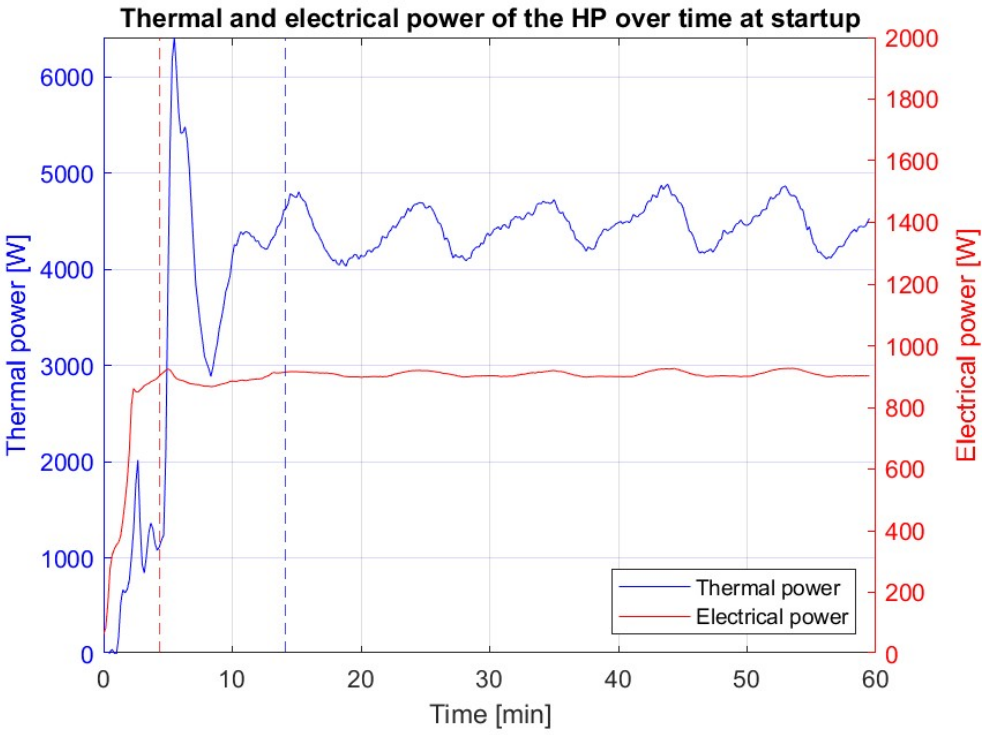

Figure D.22 – Thermal and electrical power profiles over time for TEST 22

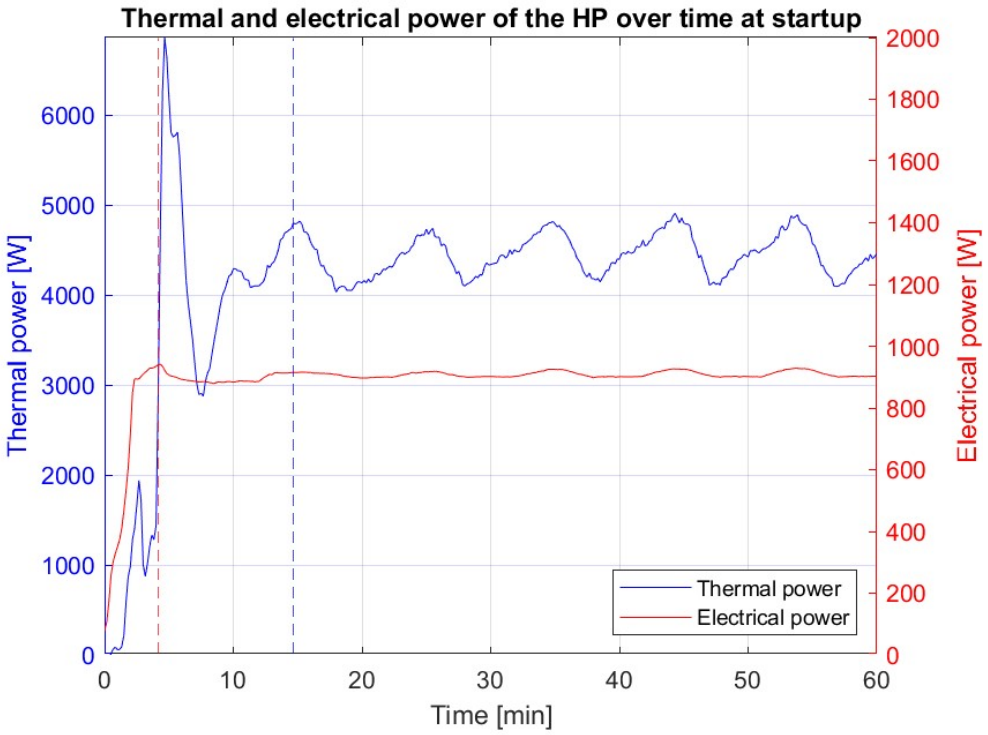

Figure D.23 – Thermal and electrical power profiles over time for TEST 23

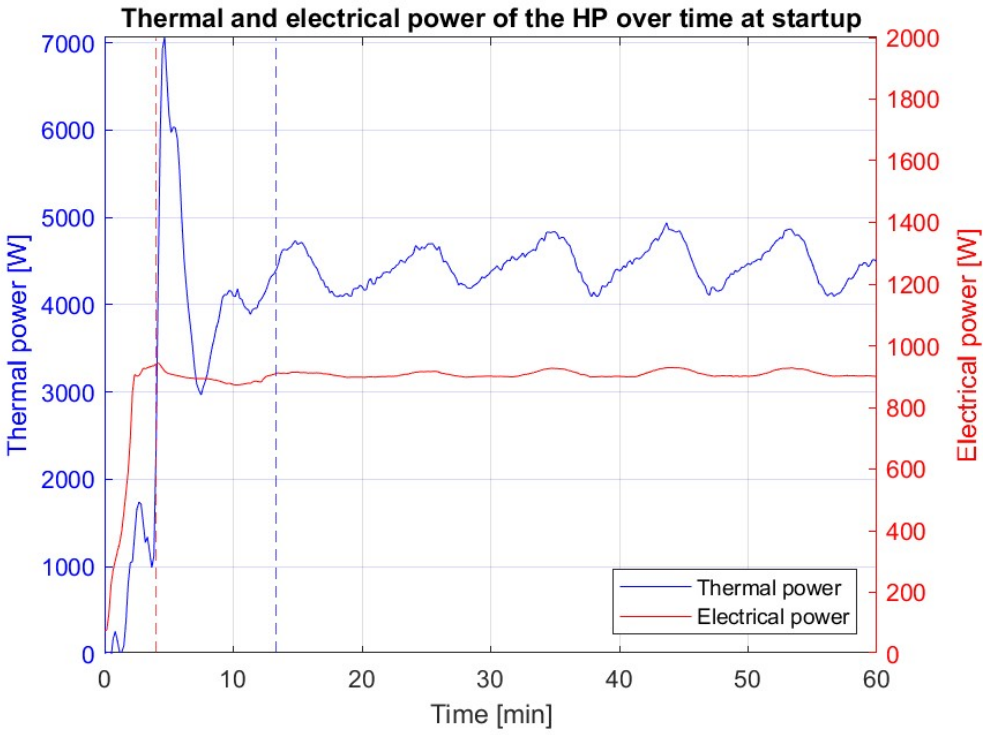

Figure D.24 – Thermal and electrical power profiles over time for TEST 24

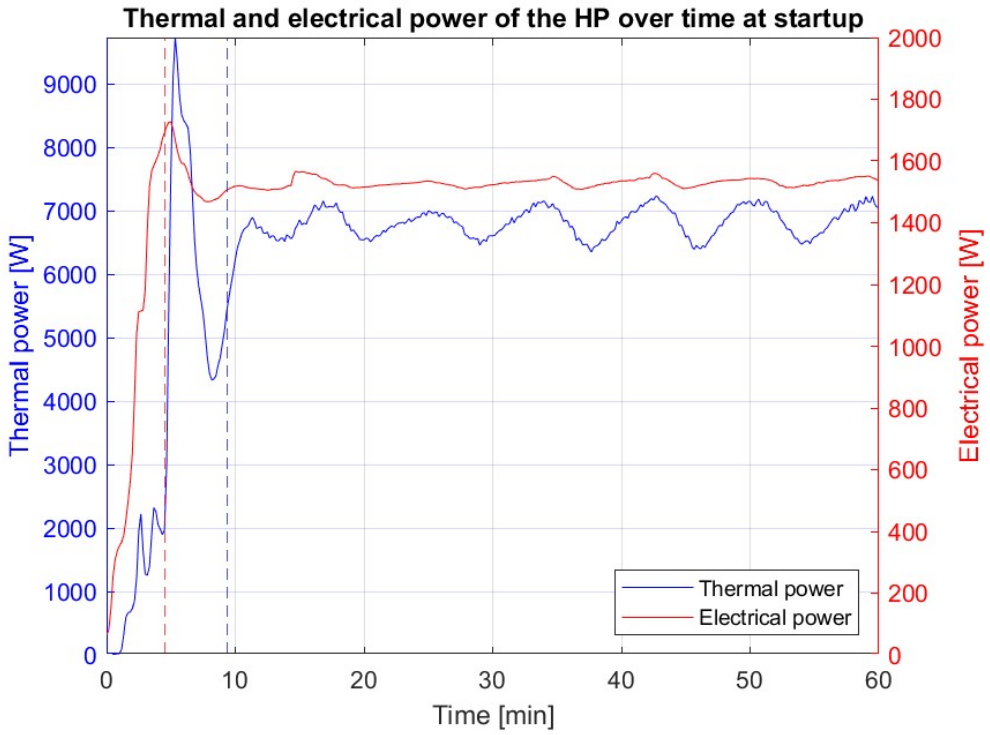

Figure D.25 – Thermal and electrical power profiles over time for TEST 25

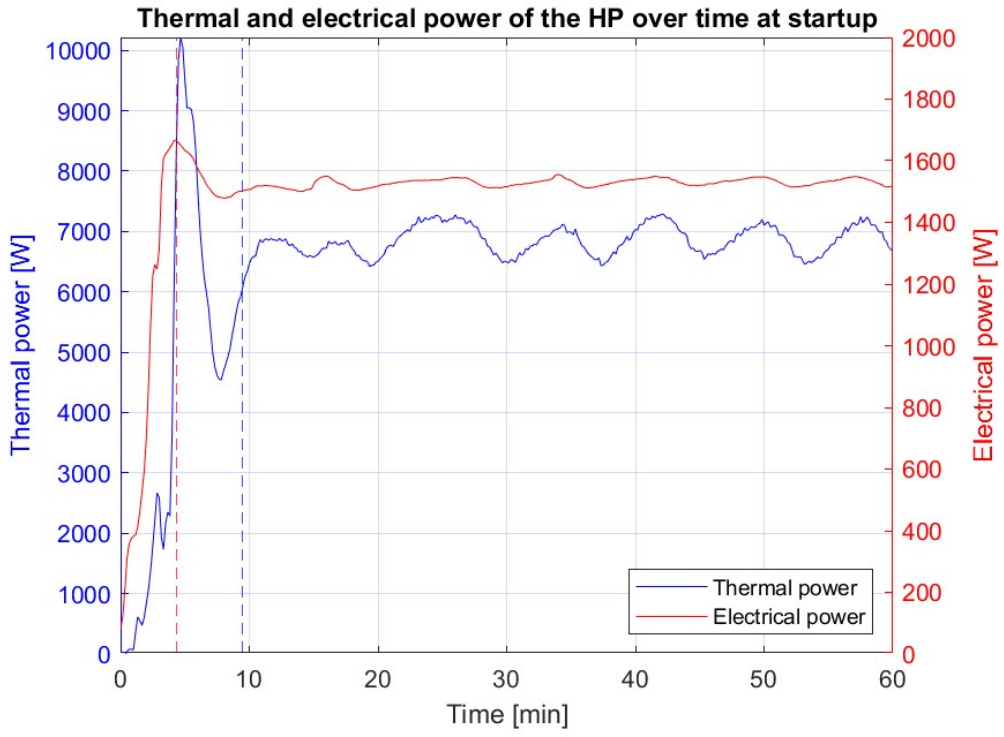

Figure D.26 – Thermal and electrical power profiles over time for TEST 26

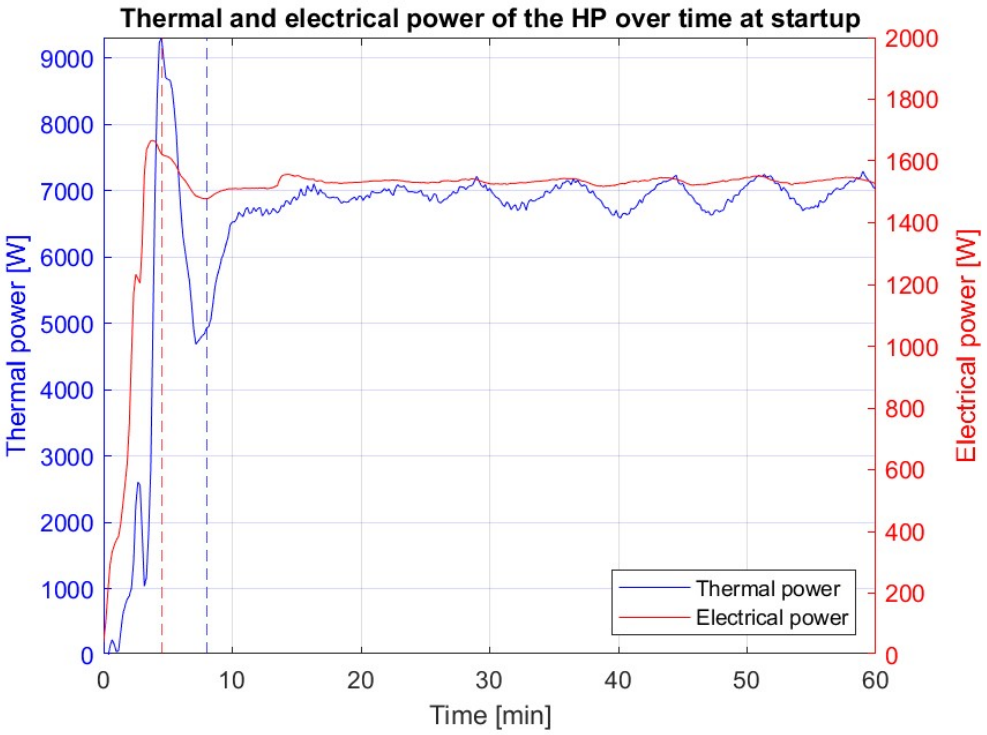

Figure D.27 – Thermal and electrical power profiles over time for TEST 27

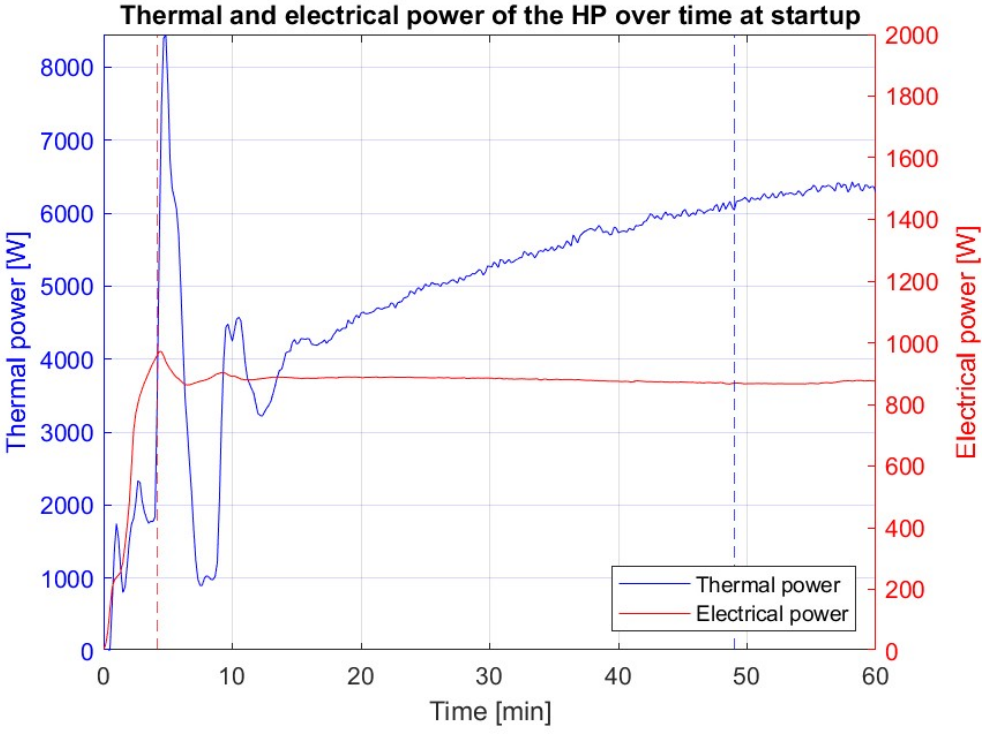

Figure D.28 – Thermal and electrical power profiles over time for TEST 28

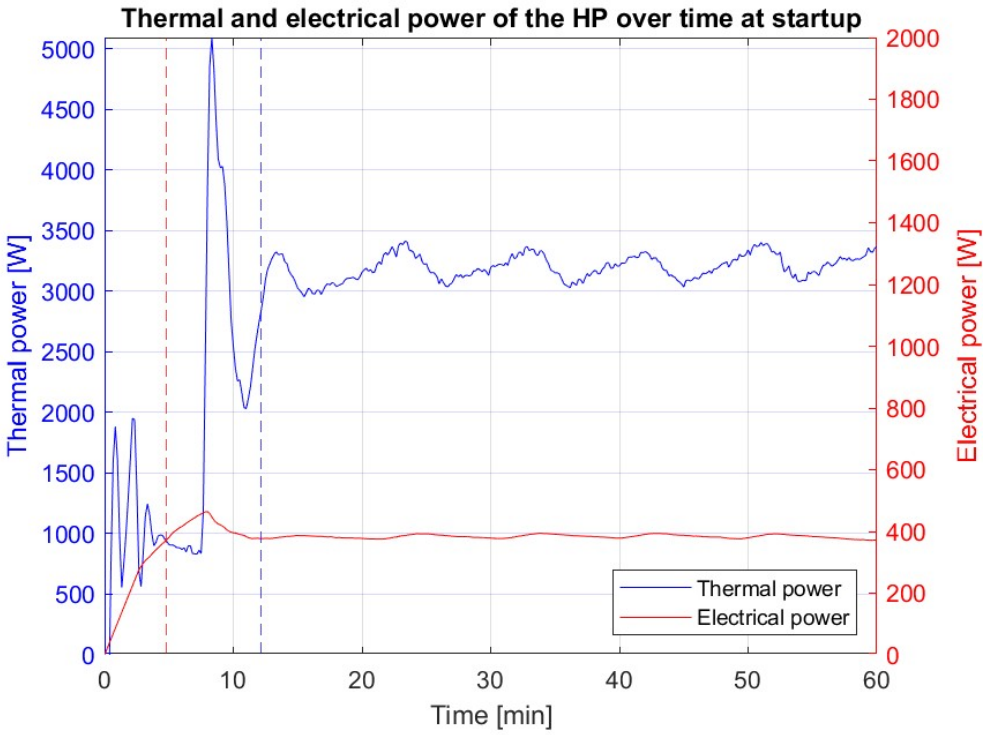

Figure D.29 – Thermal and electrical power profiles over time for TEST 29

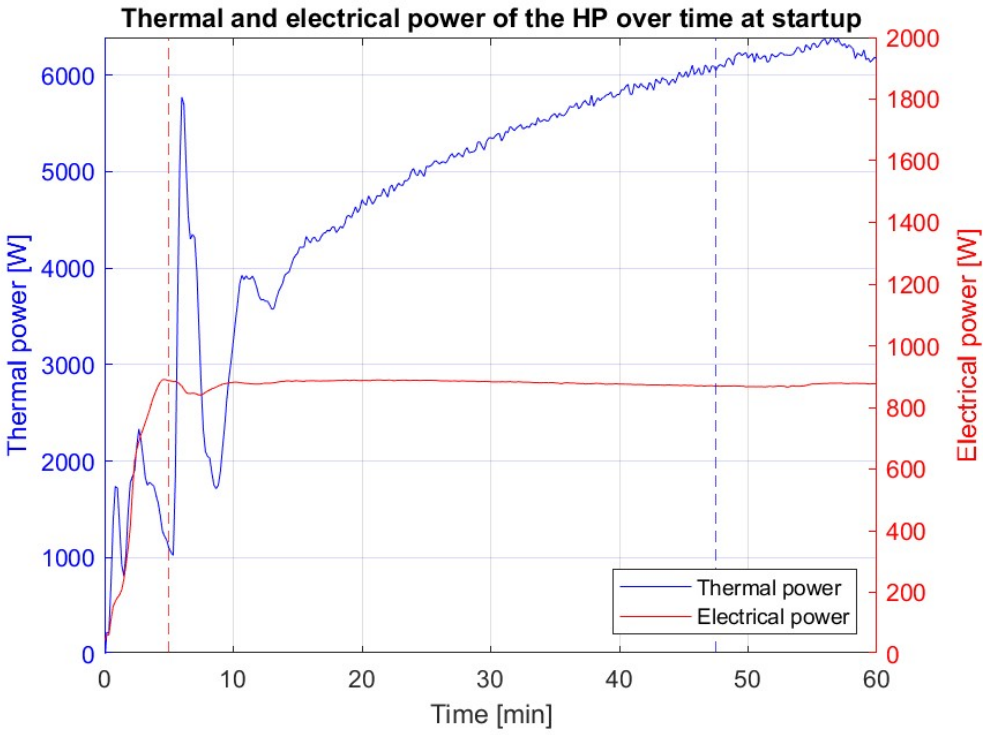

Figure D.30 – Thermal and electrical power profiles over time for TEST 30

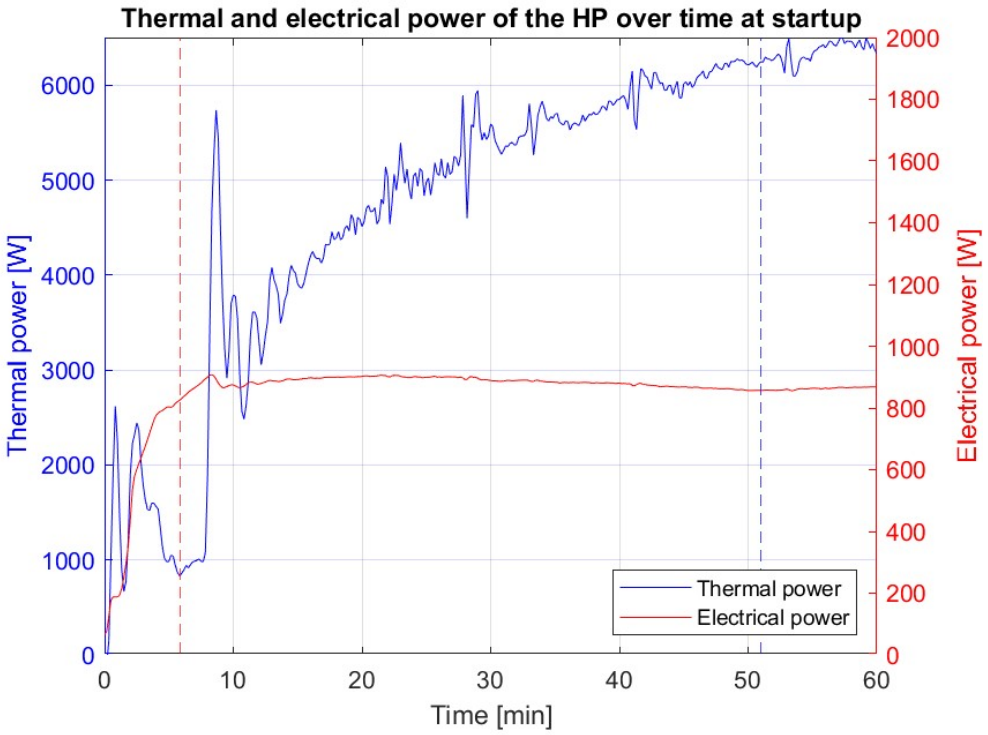

Figure D.31 – Thermal and electrical power profiles over time for TEST 31

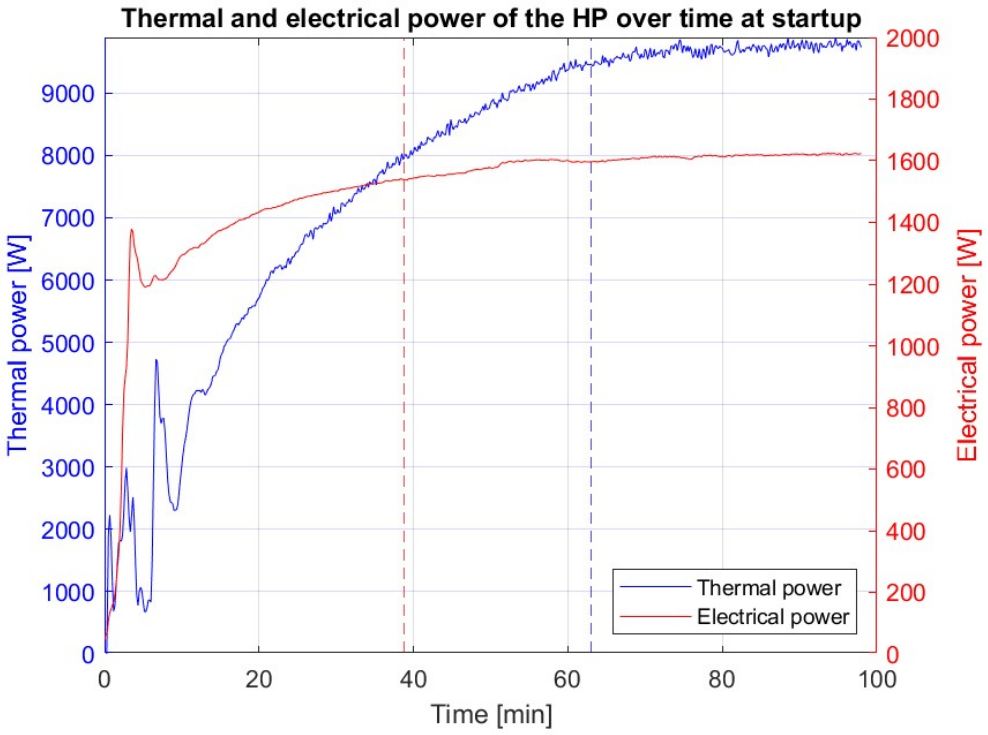

Figure D.32 – Thermal and electrical power profiles over time for TEST 32

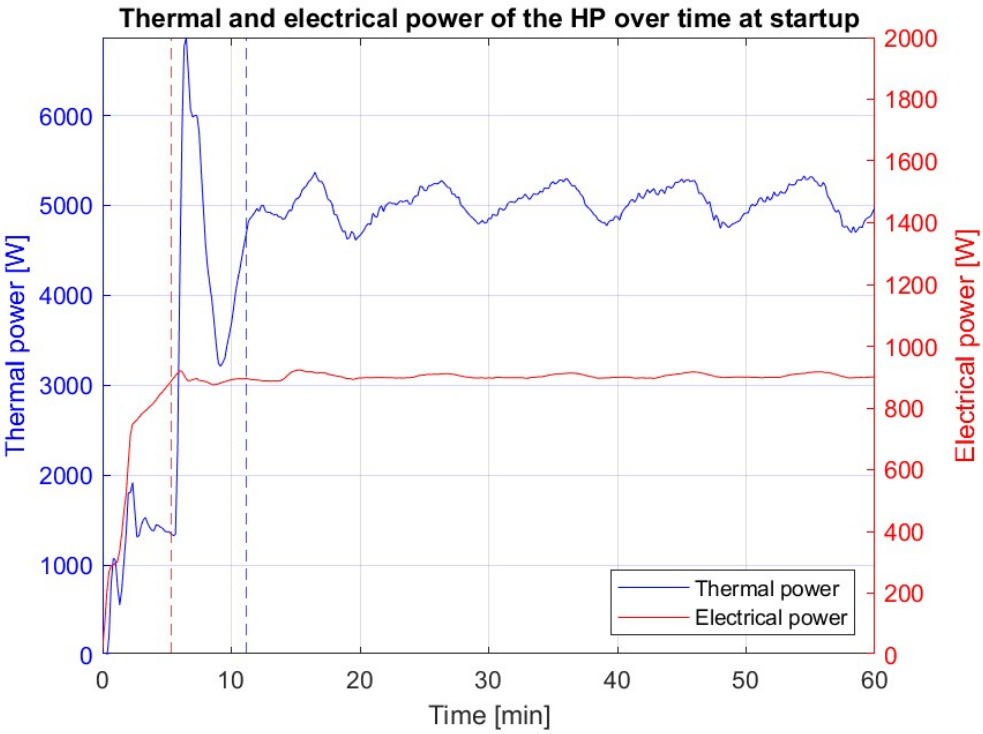

10

Figure D.33 – Thermal and electrical power profiles over time for TEST 33

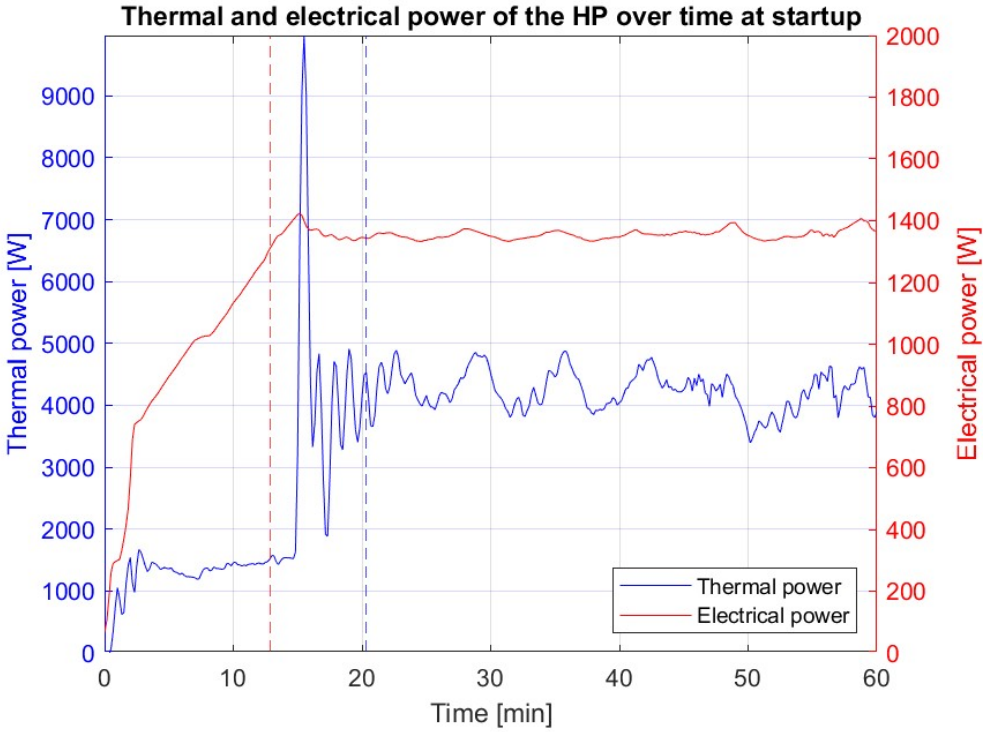

Figure D.34 – Thermal and electrical power profiles over time for TEST 34

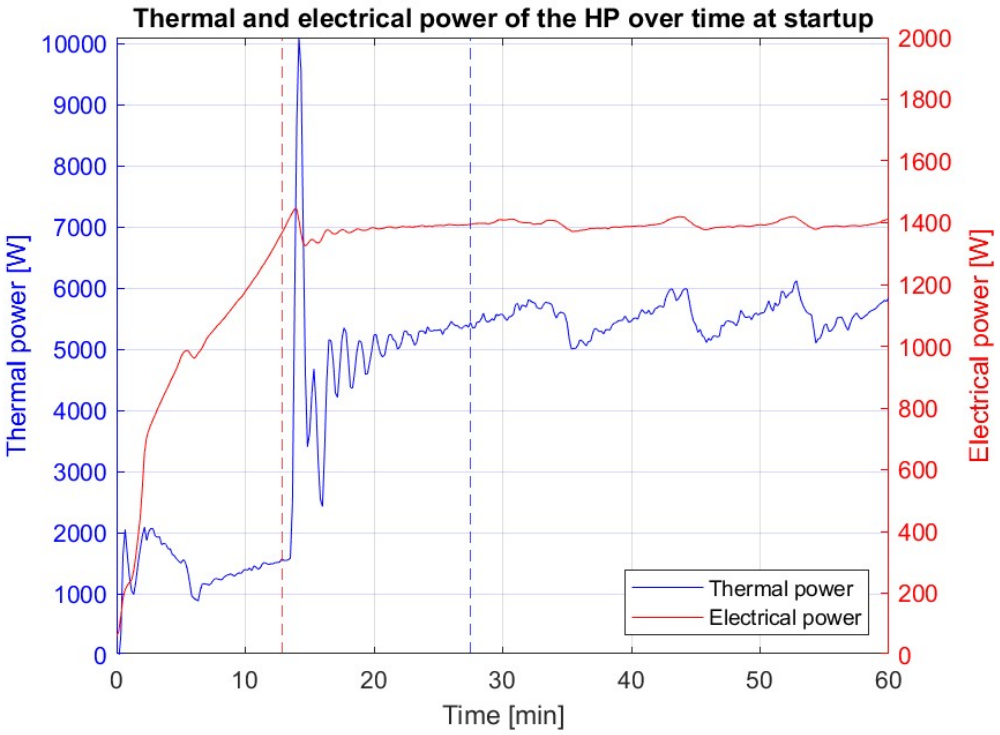

Figure D.35 – Thermal and electrical power profiles over time for TEST 35

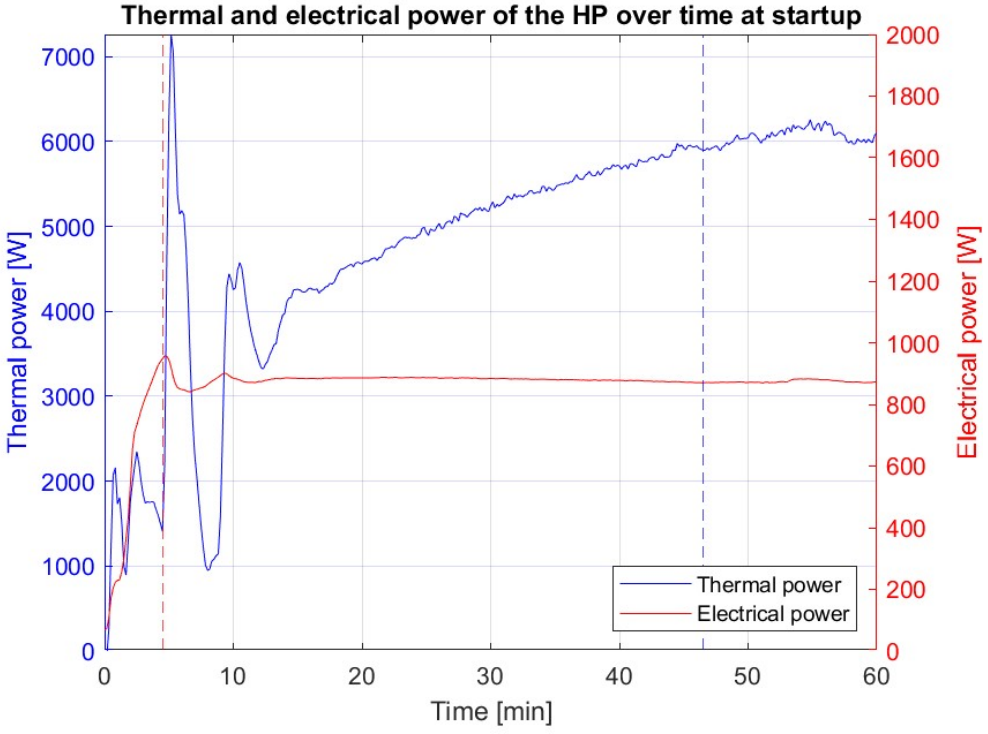

Figure D.36 – Thermal and electrical power profiles over time for TEST 36

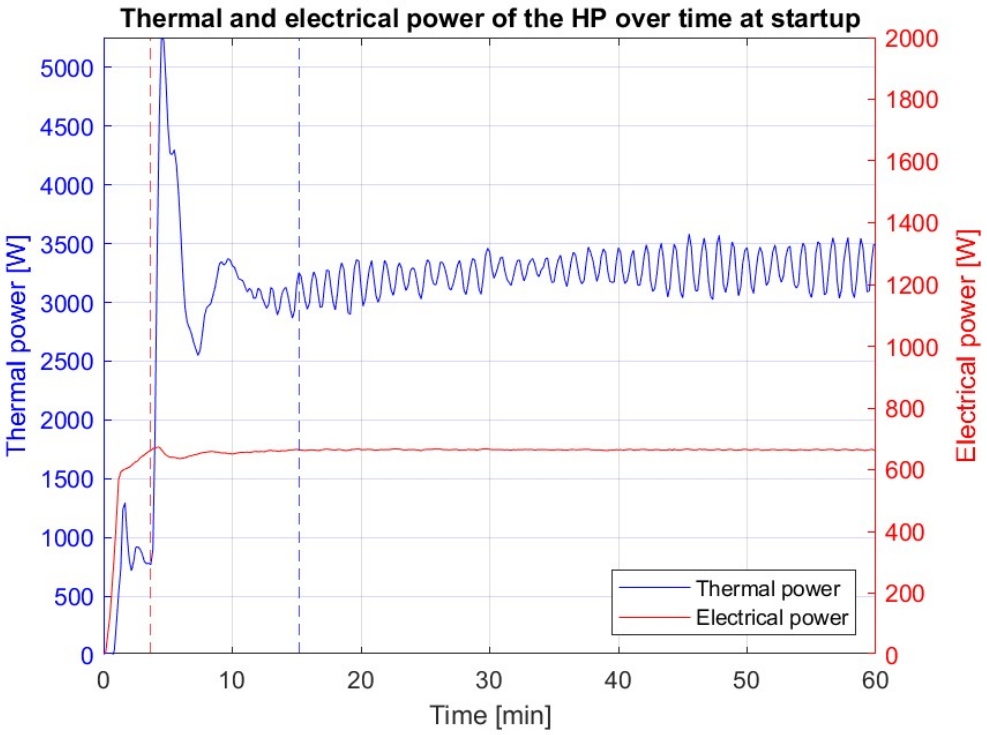

Figure D.37 – Thermal and electrical power profiles over time for TEST 37

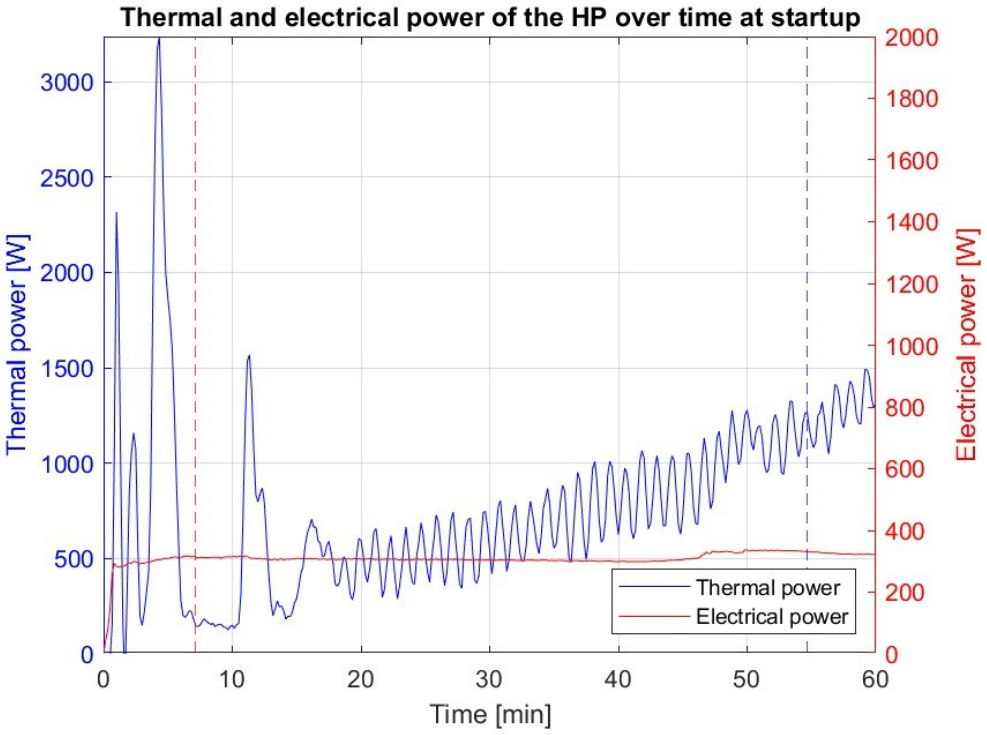

Figure D.38 – Thermal and electrical power profiles over time for TEST 38

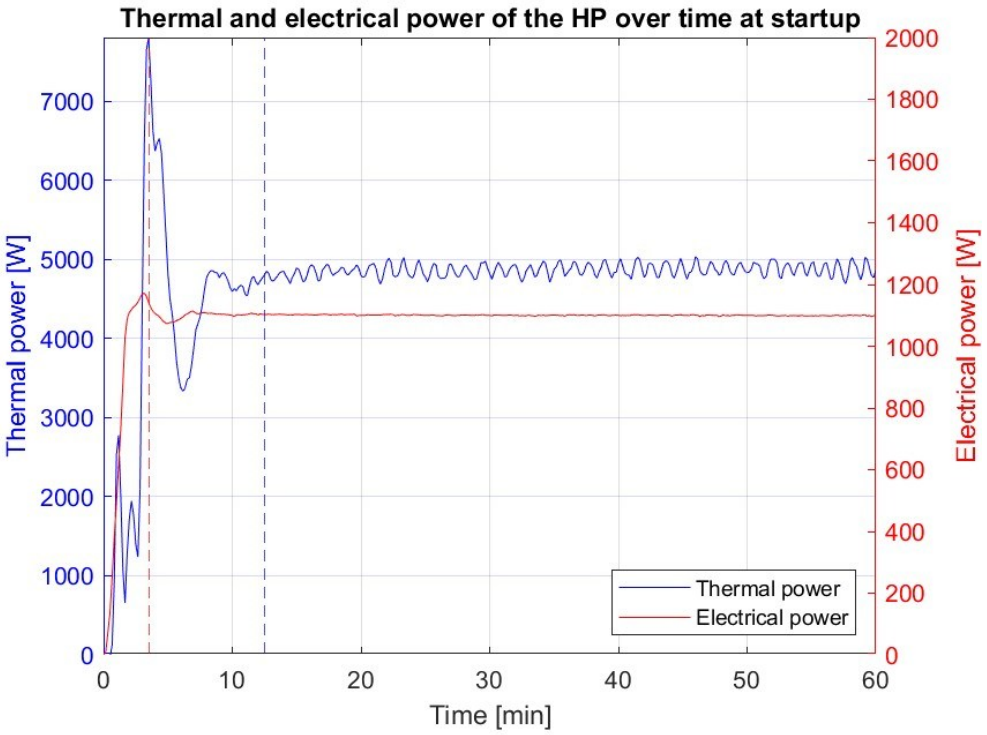

Figure D.39 – Thermal and electrical power profiles over time for TEST 39

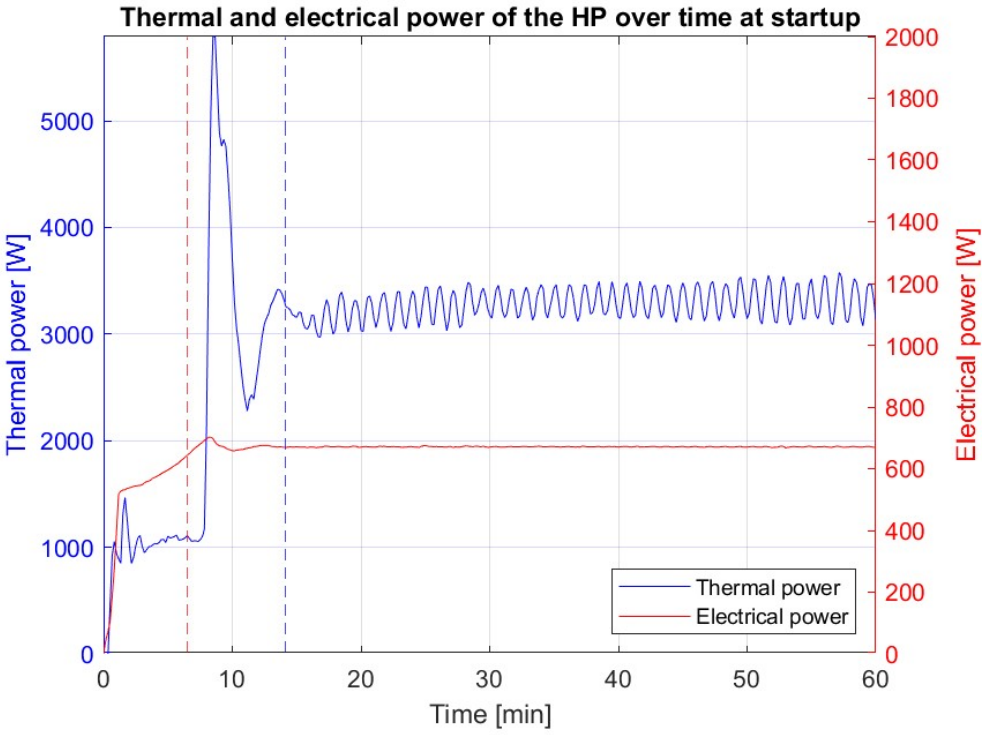

Figure D.40 – Thermal and electrical power profiles over time for TEST 40

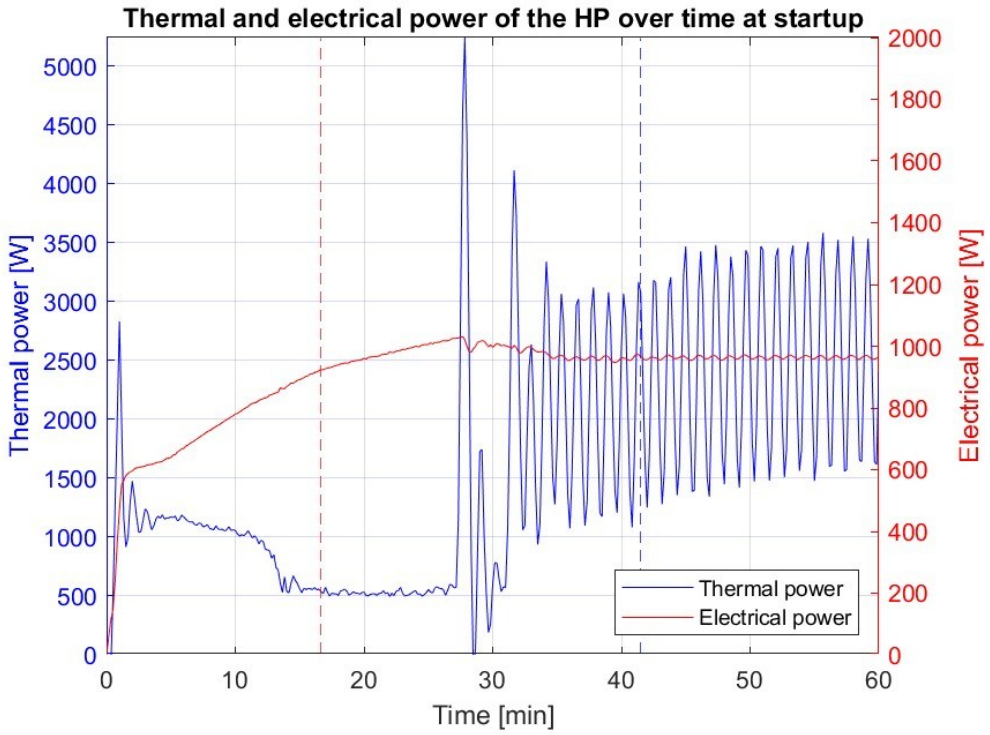

Figure D.41 – Thermal and electrical power profiles over time for TEST 41

Appendix E: scatteredInterpolant command and System Identification Toolbox

Appendix E complements Chapter 3 by illustrating how to use the MATLAB scatteredInterpolant command to interpolate the data and how to use the System Identification Toolbox to obtain transfer functions for the Simulink model presented in Section 3.1.3.

scatteredInterpolant

The MATLAB scatteredInterpolant command is used to interpolate data defined at irregularly distributed points in two or three dimensions. Unlike methods that require data on a regular grid, this function works directly with scattered datasets, making it suitable for experimental data where measurements are not evenly spaced.

The command creates an interpolant object that describes how the output depends on the input variables. Once created, this object can be evaluated at any new input condition to estimate the corresponding output. When the input values are within the range of the experimental data, the output is obtained by interpolation; when the input values are outside this range, the output is obtained by extrapolation. For both interpolation and extrapolation, two methods can be used: linear and nearest. Linear interpolation estimates the output by connecting data points with straight lines, producing smooth changes. Nearest interpolation assigns to each new point the value of the closest data point, giving a more stable but less smooth output.

The following is an example of how to use the scatteredInterpolant command to create an interpolant object and how to use it to obtain an output value:

```
d_int = scatteredInterpolant(a, b, c, d, 'linear', 'nearest');
```

In this case, a, b, c, and d are vectors with the same number of elements. The goal is to interpolate d as a function of the inputs a, b, and c. The methods linear and nearest refer respectively to interpolation and extrapolation; using 'nearest' for extrapolation is reasonable to avoid unrealistic results.

The resulting interpolant object is d_int, and the output can be obtained as follows:

```
output = d_int(input1, input2, input3);
```

The output corresponds to the interpolated or extrapolated value of d for the given input combination.

System Identification Toolbox

The System Identification Toolbox in MATLAB provides tools to create dynamic models from measured input–output data. It can identify both linear and nonlinear system behavior and generate transfer functions, state-space models, or other types of models from experimental data, which can then be used for simulation, prediction, and control design.

Within this toolbox, the App System Identification offers a user-friendly interface to perform system identification interactively. In this work, the app was used to estimate transfer functions directly from the experimental data.

The app can be launched directly from MATLAB and provides the interface shown in Figure E.1. In red is highlighted the area for imported data, corresponding to the experimental measurements to be used for estimation, in green is the section where the estimation method

is selected (transfer function model, polynomial model, etc.), in yellow are displayed the data that are about to be estimated and in blue the resulting models are shown.

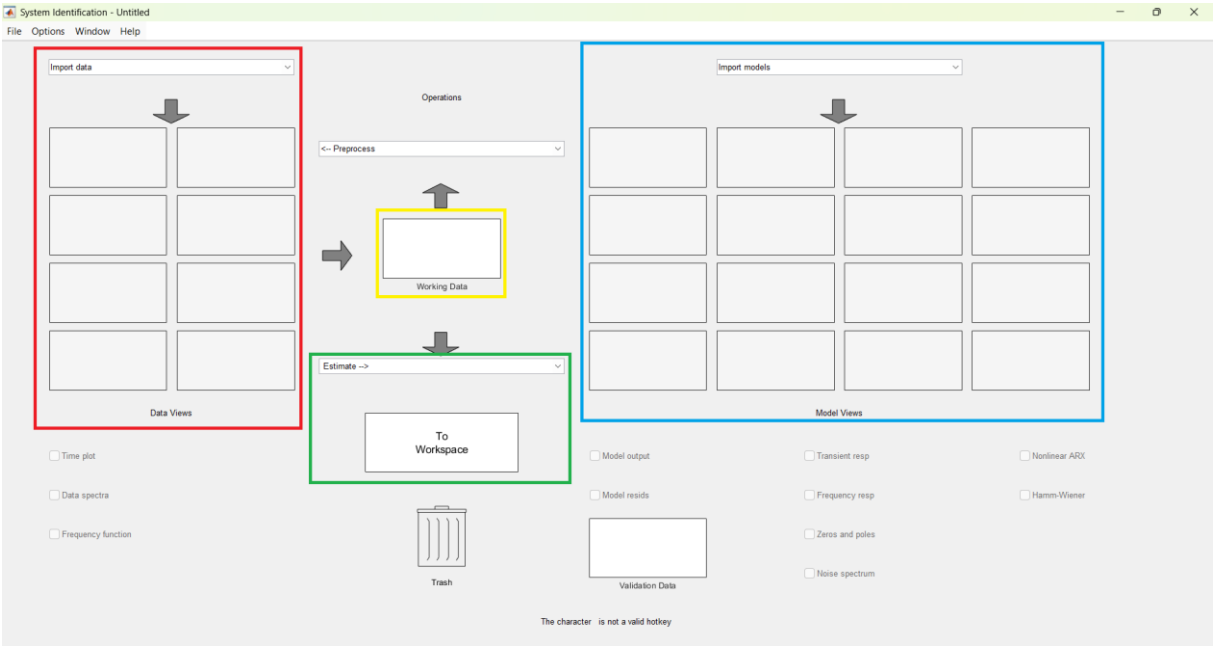

Figure E.1 - System Identification App interface in MATLAB

The following is an example of how a transfer function is generated from the thermal power signal. The thermal power, called "thp", is recorded over one hour with measurements every 10 seconds, while the step input, which transitions from 0 to the steady-state value of the thermal power, is called "step". The goal is to obtain a transfer function that approximates the behavior of the thermal power, using the step input as excitation.
By clicking "Import Data," it is possible to select "Time Domain Data," since the thermal power is a function of time. This opens the interface shown in Figure E.2, where the input (step) and output (thp) can be specified. The sample time is set to 10, corresponding to the 10-second measurement interval. Clicking "Import" loads the thermal power data into the app.

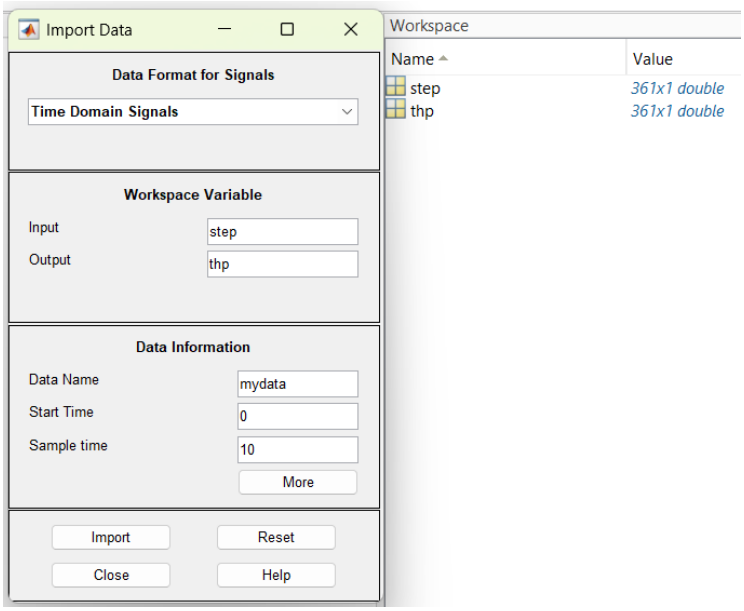

Figure E.2 – Import Data in System Identification App

Next, clicking “Estimate” allows choosing the estimation method. In this case, “Transfer Function Models” is selected, opening the screen shown in Figure E.3, where the number of poles and zeros can be defined. By clicking “Estimation Options,” the initial condition can be set to zero, so that the model starts from 0.

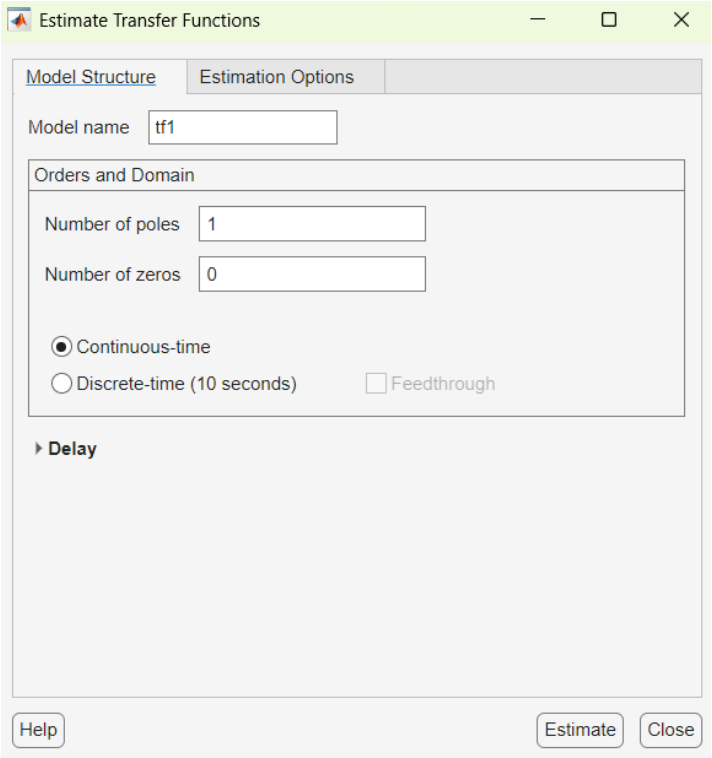

Figure E.3 – Estimate Transfer Functions in System Identification App

Clicking “Estimate” generates the transfer function model, as shown in Figure E.4.

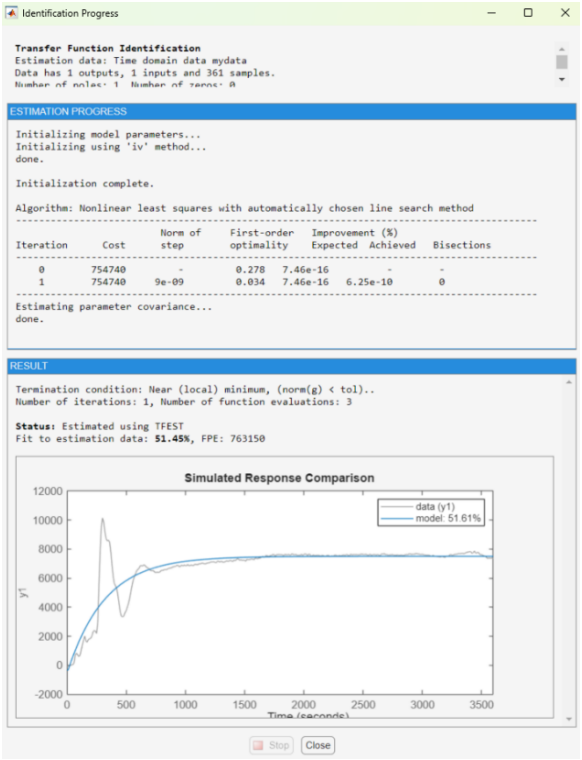

Figure E.4 – Estimated transfer function model in the System Identification App

At this point, the screen appears as in Figure E.5. By double-clicking on the transfer function tf1, the window shown in Figure E.6 opens, displaying the transfer function in red.

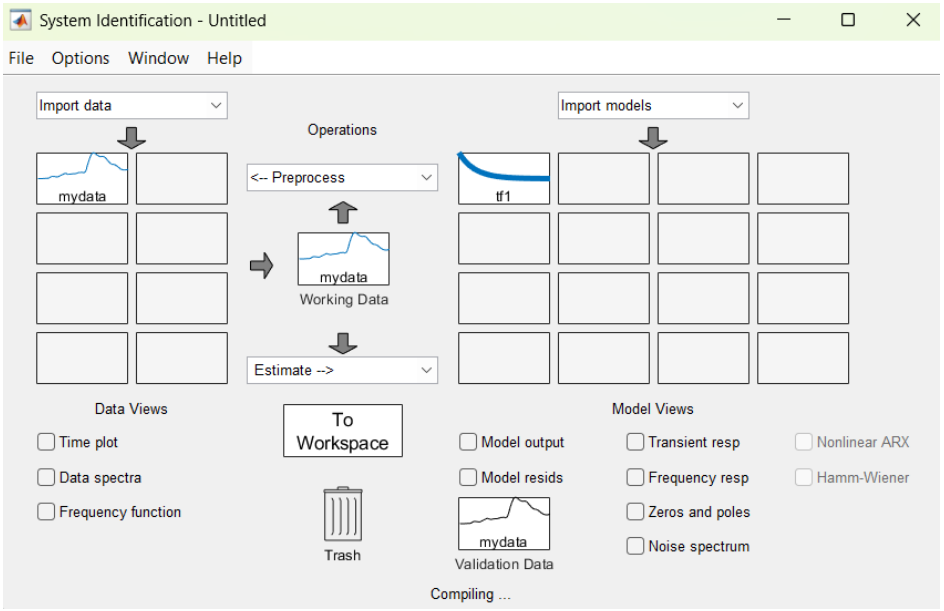

Figure E.5 - System Identification App interface showing the imported input and output data

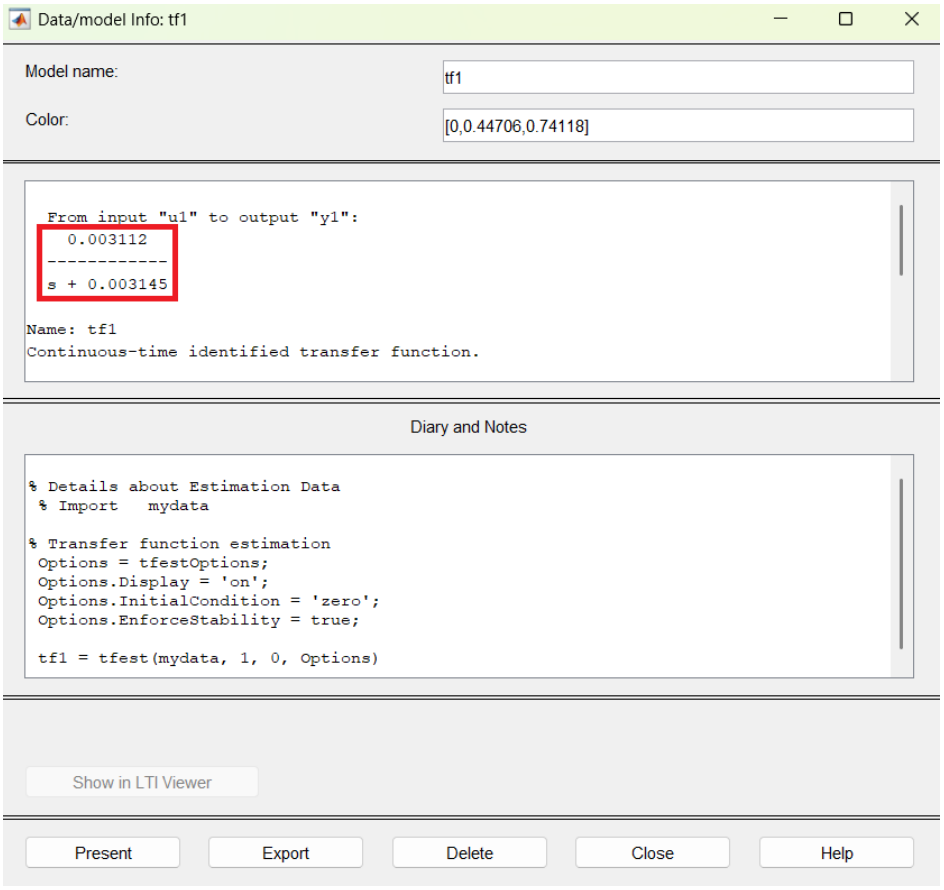

Figure E.6 – Transfer function displayed in the System Identification App

References

[1] "REGULATION (EU) 2021/1119 OF THE EUROPEAN PARLIAMENT AND OF THE COUNCIL of 30 June 2021," *Official Journal of the European Union*, Jul. 2021, Available: https://eur-lex.europa.eu/legal-content/EN/TXT/?uri=CELEX%3A32021R1119

[2] European Commission, "The European Green Deal. Brussels," 2019. Available: https://commission.europa.eu/index_en

[3] "Annual European Union greenhouse gas inventory 1990-2023 and inventory document 2025," *European Environment Agency's Home Page*, Apr. 16, 2025. Available: https://www.eea.europa.eu/en/analysis/publications/annual-european-union-greenhouse-gas-inventory-2025

[4] A. Cesarano and P. Mazzei, *Elementi di termodinamica applicata*. 1987.

[5] R. M. Mastrullo, P. Mazzei, and R. Vanoli, *Termodinamica per ingegneri. Applicazioni*. 1996.

[6] T. Reum, T. Summ, M. Ehrenwirth, and T. Schrag, "Experimental Investigation of a Novel Hybrid Heat Pump," *EuroSun2022*, Jan. 2022, doi: 10.18086/eurosun.2022.08.11. Available: https://doi.org/10.18086/eurosun.2022.08.11

[7] T. Reum, D. Schmitt, T. Summ, C. Trinkl, F. Ochs, and T. Schrag, "Experimental Analysis of Parallel Operation of Two Heat Sources in a Dual-Source Heat Pump incorporating Two Compressors," *International Journal of Refrigeration*, vol. 171, pp. 124–138, Dec. 2024, doi: 10.1016/j.ijrefrig.2024.12.013. Available: https://doi.org/10.1016/j.ijrefrig.2024.12.013

[8] T. Reum, D. Schmitt, T. Summ, and T. Schrag, "Energetic potential of parallel operation of two heat sources in a Dual-Source heat pump," *International Sustainable Energy Conference - Proceedings*, vol. 1, Apr. 2024, doi: 10.52825/isec.v1i.1158. Available: https://doi.org/10.52825/isec.v1i.1158

[9] I. Grossi, M. Dongellini, A. Piazzi, and G. L. Morini, "Dynamic modelling and energy performance analysis of an innovative dual-source heat pump system," *Applied Thermal Engineering*, vol. 142, pp. 745–759, Jul. 2018, doi:

10.1016/j.applthermaleng.2018.07.022. Available: https://doi.org/10.1016/j.applthermaleng.2018.07.022

[10] C. Natale, C. Naldi, M. Dongellini, and G. L. Morini, “Dynamic modelling of a dual-source heat pump system through a Simulink tool,” *Journal of Physics Conference Series*, vol. 2385, no. 1, p. 012090, Dec. 2022, doi: 10.1088/1742-6596/2385/1/012090. Available: https://doi.org/10.1088/1742-6596/2385/1/012090

[11] C. Natale, M. Dongellini, C. Naldi, and G. L. Morini, “Experimental study on a Dual-Source Heat Pump in ground mode to assess the soil thermal response by means of a Distributed Temperature Sensing system,” *Journal of Physics Conference Series*, vol. 2685, no. 1, p. 012036, Jan. 2024, doi: 10.1088/1742-6596/2685/1/012036. Available: https://doi.org/10.1088/1742-6596/2685/1/012036

[12] C. Natale, M. Dongellini, C. Naldi, and G. L. Morini, “Evaluation of the seasonal energy performance of a Dual-Source heat pump through dynamic experimental tests,” *Energies*, vol. 18, no. 10, p. 2532, May 2025, doi: 10.3390/en18102532. Available: https://doi.org/10.3390/en18102532

[13] S. Katipamula, “A Study of Transient Behavior During Start-Up of Residential Heat Pumps,” 1989. Available: http://oaktrust.library.tamu.edu/handle/1969.1/6424

[14] Z. Xu *et al.*, “Investigation on the efficiency degradation characterization of low ambient temperature air source heat pump under partial load operation,” *International Journal of Refrigeration*, vol. 133, pp. 99–110, Oct. 2021, doi: 10.1016/j.ijrefrig.2021.10.002. Available: https://doi.org/10.1016/j.ijrefrig.2021.10.002

[15] M. Uhlmann and S. S. Bertsch, Eds., *DYNAMIC MODELING OF HEAT PUMPS*. 2011. Available: https://heatpumpingtechnologies.org/publications/dynamic-modeling-of-heat-pumps/

[16] E. Roccatello, A. Prada, P. Baggio, and M. Baratieri, “Impact of startup and defrosting on the modeling of hybrid systems in building energy simulations,” *Journal of Building Engineering*, vol. 65, p. 105767, Dec. 2022, doi: 10.1016/j.jobe.2022.105767. Available: https://doi.org/10.1016/j.jobe.2022.105767

[17] M. Dongellini and G. L. Morini, “On-off cycling losses of reversible air-to-water heat pump systems as a function of the unit power modulation capacity,” *Energy Conversion and Management*, vol. 196, pp. 966–978, Jun. 2019, doi: 10.1016/j.enconman.2019.06.022. Available: https://doi.org/10.1016/j.enconman.2019.06.022